AD-A146 261 LAMINAR AND TURBULENT BOUNDARY LAYERS IN A PLANE OF SYMMETRY(U) IOWA INST OF HYDRAULIC RESEARCH IOWA CITY J H BAEK ET AL. JUL 84 IIHR-278 AFOSR-80-0148 1/1

UNCLASSIFIED F/G 20/4 NL

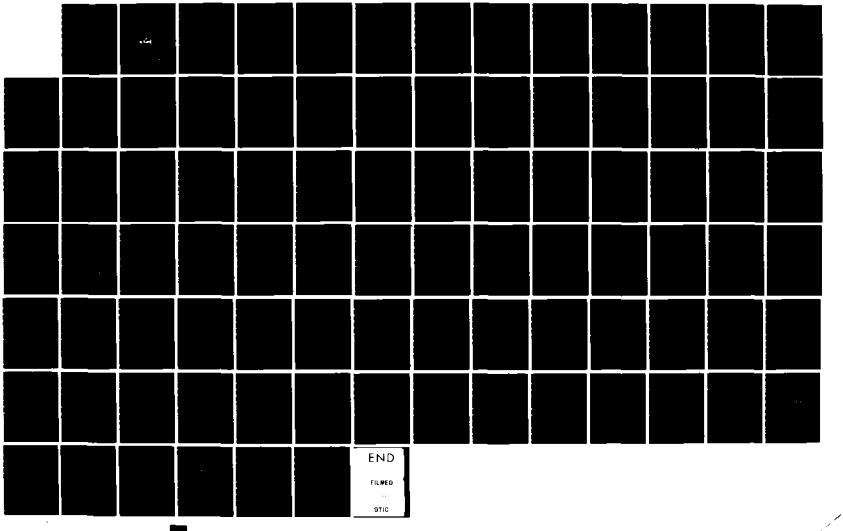

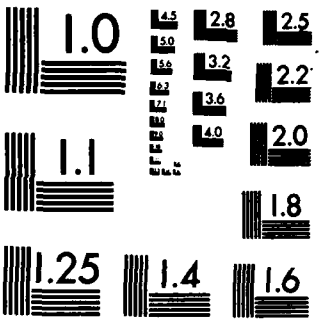

LAMINAR AND TURBULENT BOUNDARY LAYERS IN A PLANE OF SYMMETRY

by

J. H. Baek and V. C. Patel

Sponsored by
U.S. Army Research Office
and
U.S. Air Force Office of Scientific Research
Grant No. AFOSR-80-0148

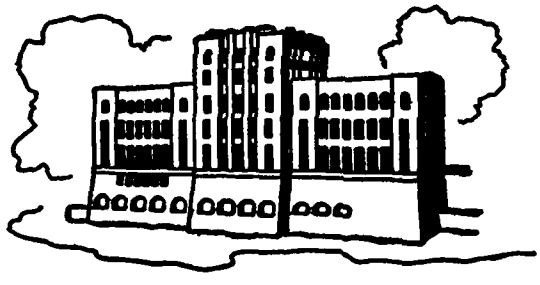

IIHR Report No. 278

Iowa Institute of Hydraulic Research
The University of Iowa
Iowa City, Iowa 52242

July 1984

50272-101

REPORT DOCUMENTATION PAGE	1. REPORT NO. No. 278	2.	3. Recipient's Accession No.

4. Title and Subtitle

Laminar and Turbulent Boundary Layers in a Plane of Symmetry

5. Report Date: July, 1984

6.

7. Author(s): J.H. Baek & V.C. Patel

8. Performing Organization Rept. No. No. 278

9. Performing Organization Name and Address

Iowa Institute of Hydraulic Research
The University of Iowa
Iowa City, Iowa 52242

10. Project/Task/Work Unit No.

11. Contract(C) or Grant(G) No.

(C)

(G) AFOSR-80-0148

12. Sponsoring Organization Name and Address

U.S. Army Research Office & U.S. Air Force Office of Scientific Research

13. Type of Report & Period Covered

14.

15. Supplementary Notes

16. Abstract (Limit: 200 words)

Detailed mean-flow and turbulence measurements have been made in the boundary layer in the plane of symmetry of a body of revolution at incidence. These data and the somewhat limited information available from previous experiments are utilized, together with extensive plane-of-symmetry boundary-layer calculations in laminar and turbulent flows, to demonstrate the most important effects of mean-flow convergence and divergence.

17. Document Analysis a. Descriptors

Boundary Layers; Laminar; Turbulent; Transition; Convergent Flow; Divergent Flow; Separation; Viscous-Inviscid Interaction

b. Identifiers/Open-Ended Terms

c. COSATI Field/Group

18. Availability Statement: Release Unlimited	19. Security Class (This Report) Unclassified	21. No. of Pages 85
	20. Security Class (This Page)	22. Price

(See ANSI-Z39.18) See Instructions on Reverse

OPTIONAL FORM 272 (4-77)
(Formerly NTIS-35)
Department of Commerce

DO NOT PRINT THESE INSTRUCTIONS AS A PAGE IN A REPORT

INSTRUCTIONS

Optional Form 272, Report Documentation Page is based on Guidelines for Format and Production of Scientific and Technical Reports, ANSI Z39.18–1974 available from American National Standards Institute, 1430 Broadway, New York, New York 10018. Each separately bound report—for example, each volume in a multivolume set—shall have its unique Report Documentation Page.

1. Report Number. Each individually bound report shall carry a unique alphanumeric designation assigned by the performing organization or provided by the sponsoring organization in accordance with American National Standard ANSI Z39.23–1974, Technical Report Number (STRN). For registration of report code, contact NTIS Report Number Clearinghouse, Springfield, VA 22161. Use uppercase letters, Arabic numerals, slashes, and hyphens only, as in the following examples: FASEB/NS–75/87 and FAA/RD–75/09.
2. Leave blank.
3. Recipient's Accession Number. Reserved for use by each report recipient.
4. Title and Subtitle. Title should indicate clearly and briefly the subject coverage of the report, subordinate subtitle to the main title. When a report is prepared in more than one volume, repeat the primary title, add volume number and include subtitle for the specific volume.
5. Report Date. Each report shall carry a date indicating at least month and year. Indicate the basis on which it was selected (e.g., date of issue, date of approval, date of preparation, date published).
6. Sponsoring Agency Code. Leave blank.
7. Author(s). Give name(s) in conventional order (e.g., John R. Doe, or J. Robert Doe). List author's affiliation if it differs from the performing organization.
8. Performing Organization Report Number. Insert if performing organization wishes to assign this number.
9. Performing Organization Name and Mailing Address. Give name, street, city, state, and ZIP code. List no more than two levels of an organizational hierarchy. Display the name of the organization exactly as it should appear in Government indexes such as Government Reports Announcements & Index (GRA & I).
10. Project/Task/Work Unit Number. Use the project, task and work unit numbers under which the report was prepared.
11. Contract/Grant Number. Insert contract or grant number under which report was prepared.
12. Sponsoring Agency Name and Mailing Address. Include ZIP code. Cite main sponsors.
13. Type of Report and Period Covered. State interim, final, etc., and, if applicable, inclusive dates.
14. Performing Organization Code. Leave blank.
15. Supplementary Notes. Enter information not included elsewhere but useful, such as: Prepared in cooperation with . . . Translation of . . . Presented at conference of . . . To be published in . . . When a report is revised, include a statement whether the new report supersedes or supplements the older report.
16. Abstract. Include a brief (200 words or less) factual summary of the most significant information contained in the report. If the report contains a significant bibliography or literature survey, mention it here.
17. Document Analysis. (a). Descriptors. Select from the Thesaurus of Engineering and Scientific Terms the proper authorized terms that identify the major concept of the research and are sufficiently specific and precise to be used as index entries for cataloging.

    (b). Identifiers and Open-Ended Terms. Use identifiers for project names, code names, equipment designators, etc. Use open-ended terms written in descriptor form for those subjects for which no descriptor exists.

    (c). COSATI Field/Group. Field and Group assignments are to be taken from the 1964 COSATI Subject Category List. Since the majority of documents are multidisciplinary in nature, the primary Field/Group assignment(s) will be the specific discipline, area of human endeavor, or type of physical object. The application(s) will be cross-referenced with secondary Field/Group assignments that will follow the primary posting(s).
18. Distribution Statement. Denote public releasability, for example "Release unlimited", or limitation for reasons other than security. Cite any availability to the public, with address, order number and price, if known.
19. & 20. Security Classification. Enter U.S. Security Classification in accordance with U.S. Security Regulations (i.e., UNCLASSIFIED).
21. Number of pages. Insert the total number of pages, including introductory pages, but excluding distribution list, if any.
22. Price. Enter price in paper copy (PC) and/or microfiche (MF) if known.

☆U.S. Government Printing Office: 1978—261-647/2308

LAMINAR AND TURBULENT BOUNDARY LAYERS IN A PLANE OF SYMMETRY

by

J. H. Baek and V. C. Patel

Sponsored by
U.S. Army Research Office
and
U.S. Air Force Office of Scientific Research
Grant No. AFOSR-80-0148

IIHR Report No. 278

Iowa Institute of Hydraulic Research
The University of Iowa
Iowa City, Iowa 52242

July 1984

ABSTRACT

Detailed mean-flow and turbulence measurements have been made in the boundary layer in the plane of symmetry of a body of revolution at incidence. These data and the somewhat limited information available from previous experiments are utilized, together with extensive plane-of-symmetry boundary-layer calculations in laminar and turbulent flows, to demonstrate the most important effects of mean-flow convergence and divergence.

I. INTRODUCTION

The boundary layer along a plane of symmetry is considered. For three-dimensional bodies, such as ship hulls and aircraft fuselages, the flow in the plane of symmetry provides the boundary conditions to be satisfied by the flow on either side of it and consequently dictates the behavior of the boundary layer over the entire body. The complexity of the plane-of-symmetry boundary layer is intermediate to that of the idealized two-dimensional boundary layer, on the one hand, and the fully three-dimensional boundary layer, on the other. It differs from the former in the presence of lateral flow convergence or divergence and from the latter in the absence of a crossflow. It is of interest to study this rather special boundary layer for several reasons. First, its development can be calculated independently of the flow elsewhere on the body and therefore the results can be used to provide the boundary conditions for the calculation of the three-dimensional boundary layer on the body. Alternatively, the independent calculations can be used to provide a check on the performance of methods which include the planes of symmetry in the solution procedure. Secondly, the plane-of-symmetry boundary layer offers the opportunity to isolate and study the influence of flow convergence and divergence in the absence of a crossflow. Divergence of flow out of a plane of symmetry retards the local growth of the boundary layer and therefore delays transition from laminar to turbulent flow and separation. Conversely, convergence leads to a thickening of the boundary layer and earlier transition. Calculations and experiments, however, indicate that prolonged convergence of the external streamlines leads to a zone of divergent flow near the surface and this provides a mechanism for separation on the body. Thirdly, the turbulent boundary layer in the plane of symmetry provides a simple but effective test of the ability of turbulence closure models to account for the extra straining of the turbulence due to mean-flow convergence and divergence. Fourthly, since measurements in nominally two-dimensional boundary layers are usually made in the plane of symmetry of models and ducts of finite and often small aspect ratio, such data usually contain undocumented influence of convergence or divergence.

Very few experimental or theoretical studies explicitly devoted to plane-of-symmetry boundary layers have been reported. For laminar flow, Wang (1969, 1974) carried out systematic calculations of boundary-layer development in the

symmetry plane of a prolate spheroid at various incidences and showed that the solutions admit a variety of separation patterns on the body although the issues of definition and prediction of separation still remain unsettled. Similar calculations have been reported recently by Schneider (1983). Experimental information in laminar flow is rather limited and, as will be discussed later, comes from the measurements of Meier, Kreplin and others (Meier et al. 1980, 1981; Kreplin et al. 1980, 1982) on a spheroid at incidence. In turbulent flow, experiments in three-dimensional boundary layers involving planes of symmetry have been carried out by Hornung and Joubert (1963), East and Hoxey (1969), Dechow and Felsch (1977), Krogstad (1979) and Pierce and McAllister (1980). All of these considered the boundary layer ahead of a symmetrical obstacle mounted on flat surfaces so that the flow in the plane of symmetry is divergent throughout and separates (with zero skin friction) at a saddle point in the wall streamlines just ahead of the obstacle. Measurements in the boundary layer along ship keels (Larsson, 1974; Hoffmann, 1976) and the body of revolution experiments of Meier, Kreplin and others, and Ramaprian, Patel and Choi (1981) also provide some data in the plane of symmetry. However, turbulence measurements were not made in these experiments and therefore the information necessary to validate turbulence models is not available. Calculations of turbulent boundary layers using integral and differential methods have been reported by many authors but comparisons with experiments are limited to the mean flow and, in most instances, to planes of symmetry with flow divergence.

From the foregoing brief review it is clear that data on plane-of-symmetry boundary layers subjected to mean-flow convergence, or simultaneous convergence and divergence, is quite limited and practically no information is available on the influence of either convergence or divergence on the turbulence. Extensive previous work in nominally two-dimensional boundary layers has indicated a very strong influence of extra rates of strain (in addition to the primary strain rate) due, for example, to surface curvature, rotation and buoyancy (see Bradshaw, 1973) on the turbulence structure. Similar extra strain rates are present in the plane-of-symmetry boundary layer due to the mean-flow convergence and divergence. Turbulence measurements in these flows are therefore of fundamental interest in the study of turbulent shear flows, in general, and three-dimensional boundary layers, in particular.

A body of revolution at incidence is perhaps the simplest configuration which can be used to study all aspects of plane-of-symmetry boundary layers. The potential-flow streamlines (outside the boundary layer) diverge out of the windward plane of symmetry and converge into the leeward plane. Thus, the boundary layer on the windward plane is subjected to a divergent external flow. The convergence of the external streamlines into the leeward plane initially subjects the flow in the entire boundary layer to convergence but, further downstream, the boundary layer experiences divergence near the wall and convergence in the outer part. The flow in the plane of symmetry of bodies at incidence is therefore the focus of the present study. However, the results and conclusions are of more general interest.

Detailed mean-flow and turbulence measurements have been made in the boundary layer on the windward and leeward planes of symmetry of the body of revolution used earlier in the experiments of Ramaprian, Patel and Choi. The results of these experiments and data from some previous experiments are then used, in conjunction with a calculation method, to illustrate the important features of laminar, transitional and turbulent plane-of-symmetry boundary layers.

Figure 1 shows the coordinates and notation used in the experiments and calculations. The length of the body is L, and X is the distance measured along the axis from the nose. The boundary layer is measured and calculated in the orthogonal surface coordinates (x,y,θ); x and y being, respectively, along and normal to the body surface; θ = 0° and 180° correspond to the windward and leeward generators, respectively. The mean and fluctuating velocity components in the (x,y,θ) directions are denoted by (U,V,W) and (u,v,w).

II. EXPERIMENTS IN TURBULENT FLOW

The experiments were conducted in the large wind tunnel of the Institute of Hydraulic Research on the model described in detail by Choi (1978) and Ramaprian, Patel and Choi (1981) at a nominal incidence of 15 degrees. Since the surface pressure distribution and mean-velocity profiles had been measured in the previous experiments, these could have been supplemented simply by making the corresponding turbulence measurements. However, in order to obtain

a complete and self-consistent set of data, it was decided to repeat the previous measurements. Small but systematic differences between the new and previous data were observed. Although the reasons for these are not entirely clear, it is believed that they may be due to small differences in the model alignment or the effectiveness of the trip wire used to promote turbulence. Only the new data are reported here.

The experimental procedures used for the measurement of the pressure distribution on the body and the mean-velocity profiles by pitot probes were essentially the same as those in the previous experiments. Although a simple pitot tube would have sufficed for the measurement of mean velocity in the plane of symmetry, a three-hole yaw probe was used in order to ascertain the degree of flow symmetry and to measure the variation of static pressure across the boundary layer. The latter was accomplished by a probe calibration procedure somewhat different from that used in the previous experiments.

Standard x-type (DISA 55P51) hot-wire probes were employed for the turbulence measurements. The difficulty of making reliable turbulence measurements in a three-dimensional flow (by triple wires or laser anemometers) is well known. However, measurements in the plane of symmetry can be made with some confidence using conventional cross-wire probes due to the absence of a crossflow. Thus, these data serve the additional purpose of providing a check on measurements made elsewhere on the body by other means. The anemometer voltages were processed digitally by using a Preston A-D converter and the HP-1000 computer. Measurements were made with the plane containing the x-wires normal to the body surface (u-v configuration) and parallel to the surface (u-w configuration) to obtain all velocity components.

Further details of all experimental procedures are given in Baek (1984). The experimental results consist of: (a) the pressure distributions measured by surface taps and pressure variation across the boundary layer obtained with the yaw probe; (b) distributions of the mean-velocity components U and W measured by the yaw probe, and U,V, and W by hot-wires; (c) the Reynolds stresses $\overline{u^2}$, $\overline{v^2}$, $\overline{w^2}$, $\overline{uv}$ and $\overline{uw}$; and (d) the triple products $\overline{u^3}$, $\overline{uv^2}$, $\overline{u^2v}$, $\overline{v^3}$, $\overline{w^3}$, $\overline{uw^2}$ and $\overline{u^2w}$. It should be mentioned that some of these quantities should be zero in the plane of symmetry and therefore the data can be used to ascertain the degree of symmetry realized in the experiment. The

yaw-probe data were obtained at six stations labelled 1 to 6: X/L = 0.169, 0.234, 0.326, 0.419, 0.530 and 0.641, but due to the limitations of the internal traverse mechanism and differences in the probe lengths, hot-wire data could be obtained only at four intermediate stations labelled 3H to 6H: X/L = 0.291, 0.384, 0.495 and 0.606 (see Fig. 1). The nominal tunnel speed, Q_o, was kept at 21.4 m/s so that the overall Reynolds number, $Q_oL/\nu = 1.86 \times 10^6$. The uncertainties in the data have been estimated to be as follows: 0.5% of freestream dynamic head for surface pressures; 0.5 degree in angle, 0.7% of dynamic head in velocity magnitude, and 1.5% of dynamic head in local pressure for yaw-probe measurements; and 0.6% of freestream velocity for all hot-wire data.

II.1. Pressure Distribution

Figure 2 shows the pressure distributions on the body along the windward and leeward planes of symmetry. The pressure coefficient, C_p, is defined by

$$C_p = \frac{P - P_o}{\frac{1}{2}\rho Q_o^2}$$

where P is the local pressure, P_o and Q_o are the pressure and velocity, respectively, in the undisturbed stream in the tunnel and ρ is density. The measurements are compared with the potential-flow distribution calculated by the method of Landweber and Macagno (1969) at $\alpha = 15°$. The general agreement between the data and theory over the front of the body suggests that the tunnel blockage is negligible at this angle of attack, and the differences observed for X/L > 0.8 on the windward side and X/L > 0.3 on the leeward side are due to viscous-inviscid interaction.

The variations of pressure across the boundary layer measured by the yaw probe at the six axial stations are shown in Fig. 3. Also indicated there is the size of the probe and the independently measured surface pressures. The data point closest to the wall thus corresponds to the reading at the probe center with the probe resting on the wall. It is clear that the data points within distances of the order of one probe height show rather peculiar trends presumably due to interference between the wall and the probe. This is particularly noticable on the windward side where the boundary layer is rather thin. If these data are disregarded, it is seen that the pressures measured

at the wall agree reasonably well with extrapolations from those measured further away within the boundary layer.

In general, the variation of pressure across the boundary layer on the windward side is quite small ($\Delta Cp < 0.02$) and the small increase in the wall region at the first two stations indicates that the mean streamlines are convex, i.e., they follow the body contour. On the leeside, however, the variation of pressure across the boundary layer is quite significant at all stations. The pressure increase at the upstream stations is to be expected from the convex curvature of the surface but further downstream the body curvature, although convex, is quite small and, as we shall see later, the boundary layer thickness increases rapidly. Thus, if this were a two-dimensional boundary layer we would not expect the pressure to increase. However, the lateral divergence in the wall region, alluded to earlier, maintains a negative component of vertical velocity and hence a conve streamline curvature in the plane of symmetry.

On both planes of symmetry, the pressure is expected to return to freestream value ($Cp = 0$) at large distances from the body. This is not s from the present measurements since they were confined to the boundary layer and a small distance beyond it.

II.2. Mean Velocity Profiles

The component of velocity, W, in the circumferential direction should be zero in the plane of symmetry. The yaw-probe measurements indicated that the angle between the velocity vector and the geometric plane of symmetry of the body was nowhere greater than 3 degrees, i.e., $W \leq 0.05U$. This was again verified by the hot-wire measurements. Although $W = 0$, its circumferential gradient, $\partial W/\partial\theta$, is not zero. In fact, this quantity is a measure of the rate of lateral convergence or divergence of the mean flow from either side of the symmetry plane. Initially, an effort was made to measure this by using the yaw probe along body generators on either side of the symmetry plane. However, as will be discussed later, reliable data could not be obtained due to the rather small crossflow angles and the accuracy with which such data could be differentiated to obtain the required gradient.

The velocity profiles measured along the windward (θ = 0°) and leeward (θ = 180°) planes of symmetry by the yaw probe are shown in Fig. 4. The longitudinal component of mean velocity, U, measured with the cross-wire probe in the two configurations at the four axial stations is shown in Fig. 5. The hot-wire measurements also indicated that the maximum deviation of the resultant velocity vector from the plane of symmetry was of the order of 3 degrees. From Figs. 3(a) and 4(a) it is seen that the boundary layer remains thin on the windward side and consequently the hot wire data are confined to the outer part. Also, at station 6H on the leeside, the boundary layer was too thick to be measured in a single traverse of the probe. These measurements were therefore carried out in two parts after carefully realigning the probe and ensuring a large region of overlap between the two traverses. From the data presented in Fig. 5 and later, it is seen that the profiles obtained with the two probe configurations are in excellent agreement. The measurements for station 6H on the leeside (Fig. 5b) also indicate that a reasonably continuous profile is obtained in spite of the separate traverses in the inner and outer regions.

The normal component of mean velocity, V, measured by the x-wire in the u-v configuration is shown in Fig. 6. On the windward side, this is small and negative everywhere, except at station 6H. The negative values indicate a flow toward the surface as required by the strong divergence of the mean flow out of this plane of symmetry. The data on the leeside are perhaps the most interesting. The normal velocity is positive at the first station (station 3H), as would be expected from the mean-flow convergence into the symmetry plane. However, further downstream (beyond station 4H) there is a region of negative normal velocity in the inner part of the boundary layer and a region of positive velocity in the outer part. The former is associated with divergent flow near the wall.

Since the most complete mean-velocity profiles were measured with the yaw probe, these were integrated to calculate the displacement and momentum thicknesses, defined by

$$\frac{\delta_1}{\delta} = \int_0^1 \left(1 - \frac{U}{U_e}\right) d\left(\frac{y}{\delta}\right), \qquad \frac{\theta_{11}}{\delta} = \int_0^1 \frac{U}{U_e}\left(1 - \frac{U}{U_e}\right) d\left(\frac{y}{\delta}\right) \qquad (1)$$

respectively, after determining the boundary-layer thickness δ from the measured total-pressure profiles. The integrations were then performed by matching the near-wall measurements to the usual law of the wall, including the sublayer, transition layer and the logarithmic region, and using the measured value of the velocity at the edge of the boundary layer, U_e. The latter assumption obviously introduces an error in the integral thicknesses at the stations where the static pressure varies across the boundary layer. However, this error is at most of the order of 2 percent. The wall shear-stress coefficient,

$$C_f = \frac{\tau_w}{\frac{1}{2}\rho U_e^2}$$

was also determined from the yaw-probe data using the method of Clauser. The Clauser plots of the velocity profiles at the most upstream stations on the two sides, shown in Fig. 7, suggest that the flow on the windward side may not be fully developed and turbulent although that on the leeside appears to be so. The integral parameters δ_1, θ_{11} and C_f are presented and discussed together with the calculations in Section III.

II.3. Turbulence Intensities and Reynolds Stresses

The root-mean-square turbulence intensities, u', v' and w', defined by

$$u' = (\overline{u^2})^{1/2}, \quad v' = (\overline{v^2})^{1/2}, \quad w' = (\overline{w^2})^{1/2}$$

are shown in the Fig. 8. It is seen that the values of u' measured with the two configurations of the x-wire are in very good agreement, especially in the region where the boundary layer is thick enough for the probe-size effect to be negligible. On the windward side, the v' and w' components are nearly equal and somewhat smaller than u'. It is not clear whether this is significant since data in the important wall region could not be obtained. On the leeside, the relative magnitudes of the three components and the shapes of the distributions at the two upstream stations are similar to those observed in a two-dimensional boundary layer. However, at the two downstream stations (5H and 6H) major changes appear to be taking place both in the shape and relative magnitudes of the three components. By station 6H, the absolute values are greatly decreased.

The two Reynolds shear-stresses ($\overline{uv}$ and $\overline{uw}$) which were measured are shown in Fig. 9. Note that $\overline{uw}$ should be zero on the plane of symmetry. The third stress, $\overline{vw}$, which was not measured, should also be zero. It is seen that $\overline{uw}$ does not vanish everywhere. The values on the windward side (Fig. 9a) are quite significant although they are all much smaller than the primary stress, $\overline{uv}$, in the region of the measurements. The results indicate that $\overline{uw}$ decreases towards the wall whereas $\overline{uv}$ increases continuously. Although the lack of data over a large region in the inner part of the boundary layer precludes any definitive conclusions, the most probable reason for the non-zero values of $\overline{uw}$ are the effects of probe interference and alignment, rather than a lack of flow symmetry.

On the leeward side, the boundary layer is much thicker and therefore the same probe enabled measurements to be made closer to the wall, in terms of boundary-layer thickness. In this case, the decrease in $\overline{uw}$ in the near wall region is clearly seen and, by stations 5H and 6H, this is practically zero throughout the boundary layer.

The distributions of the primary shear-stress, $\overline{uv}$, suffer from similar defects on the windward side but are much more complete on the leeward side. The values of the wall shear-stress, determined independently using the method of Clauser are also indicated. It is seen that the measured distributions of $\overline{uv}$ can be extrapolated smoothly (with some uncertainty on the windward side) to the wall shear-stress values, and the resulting slopes in the wall region are compatible with the local pressure gradients which can be seen from Fig. 2. Thus, for example, on the leeward side, the increase in the Reynolds stress with wall distance at stations 3H and 4H is indicative of the adverse pressure gradient seen in Fig. 2 at those stations, while the nearly constant values at stations 5H and 6H reflect the small local pressure gradients.

Finally, from Figs. 8 and 9 we note that the general shapes of all Reynolds-stress profiles are similar to those expected in two-dimensional boundary layers everywhere except at stations 5H and 6H on the leeside. The profiles at these stations indicate inflection points in the outer part of the boundary layer which are not observed in two-dimensional flows.

II.4. Turbulent Kinetic Energy and Transport Properties

The above data have been processed to determine some commonly-used quantities in turbulence models. The distributions of the turbulent kinetic energy k, defined by

$$k = (\overline{u^2} + \overline{v^2} + \overline{w^2})/2$$

are shown in Fig. 10. Since the normal stresses were measured at different physical locations in the boundary layer by separate traverses, and $\overline{u^2}$ was measured twice, k was determined by taking an average value for $\overline{u^2}$ and interpolations in the other data. Little can be said about these distributions except to note that the turbulence levels at stations 5H and 6H on the leeside are considerably smaller than that which would be expected in a two-dimensional boundary layer under similar pressure-gradient conditions. These data are presented here to facilitate comparisons with calculations by means of turbulence models which use the turbulent kinetic-energy equation.

Figure 11 shows the so-called structure parameter

$$a_1 = -\overline{uv}/k$$

which is known to demonstrate a degree of universality in turbulent shear flows. A commonly accepted value for a_1 is 0.3. It is seen that the data on the windward side indicate values somewhat larger than 0.3 while those on the leeside indicate smaller values. In both cases the values appear to decrease with increasing downstream distance and a clear correlation with the mean-flow divergence on the windward side and convergence followed by near-wall divergence on the leeside is not evident.

Figures 12 and 13 show the distributions of the eddy-viscosity, ν_t, and the mixing length, ℓ, defined by

$$-\overline{uv} = \nu_t \frac{\partial U}{\partial y} = \ell^2 \left(\frac{\partial U}{\partial y}\right)^2 \qquad (2)$$

respectively, and non-dimensionalized in the usual manner. Cebeci's (1971) two-layer eddy-viscosity model, based on a correlation of data in two-

dimensional boundary layers, indicates that the maximum value of $\nu_t/U_e\delta_1$ is constant and equal to 0.0168. From Fig. 12 it is seen that the data in the outer part of the boundary layer on the windward side are scattered around this value. The lack of data close to the surface is, however, unfortunate although there is some evidence that the maximum eddy viscosity may be larger than 0.0168. On the other hand, the data on the leeside plane of symmetry indicate markedly smaller maximum values (of the order of 0.006 - 0.008).

The mixing-length distributions show trends which are similar and consistent with those of the eddy viscosity. The generally accepted value for ℓ/δ in the outer part of a two-dimensional boundary layer is 0.09. The data on the windward side are again scattered about this value but those on the leeside indicate a substantial reduction.

Inspite of the limitations of the data on the windward side, it appears that there is a significant and consistent effect of the mean-flow convergence and divergence on the turbulence-transport properties. The decrease in ν_t and ℓ on the leeside may be attributed to the mean-flow convergence prevailing in the boundary layer over most of the development length upto Station 6. Similarly, the divergence of the flow out of the windward plane indicates an increase in these quantities.

II.5. Triple Products

With the two hot-wire configurations used, it was possible to measure only seven triple velocity products, namely $\overline{u^3}$, $\overline{v^3}$, $\overline{w^3}$, $\overline{uv^2}$, $\overline{vu^2}$, $\overline{uw^2}$, and $\overline{u^2w}$. Note that the last of these should be zero by virtue of symmetry. Of the remaining products, i.e., $\overline{vw^2}$, $\overline{wv^2}$ and $\overline{uvw}$, the last two are zero. Thus, all but one ($\overline{vw^2}$) of the nonzero triple products have been measured in these experiments.

The data for the windward side are shown in Figs. 14(a) and 15(a) while those for the leeside are shown in Figs. 14(b) and 15(b). First of all, we note that the distributions of $\overline{u^3}$ measured separately with the two configurations of the probe are in good agreement with each other. This consistency provides some confidence in the data. Secondly, from Fig. 15 we see that the correlation $\overline{u^2w}$, which should be zero, is not precisely zero everywhere and shows trends similar to those of $\overline{uw}$ discussed earlier.

However, it is small relative to the other correlations and, in the thick boundary layer at the leeside stations 5H and 6H, it is scattered around a zero mean throughout the boundary layer.

Gradients of triple velocity correlations enter the equations controlling the dynamics of the Reynolds stresses through the turbulent diffusion terms and therefore the data provide information that is of some value in the modelling of turbulence. Diffusion is known to be important in the inner part of the boundary layer. Unfortunately, the data on the windward side do not extend sufficiently close to the surface to be of more than qualitative value. The most that can be said about these data is that the three largest correlations, in the order of decreasing magnitude, are $\overline{u^3}$, $\overline{vu^2}$ and $\overline{uv^2}$. This is not particularly surprising in view of the relative magnitudes of the turbulence components u' and v'. Although $\overline{u^3}$ is large, its longitudinal derivative, which represents the diffusion of u^2, is usually neglected within thin boundary-layer approximations. The normal derivatives of $\overline{vu^2}$ and $\overline{uv^2}$ account for the diffusion of $\overline{u^2}$ and $\overline{uv}$, respectively, which are the two primary Reynolds stresses. Inspite of their obvious limitations, the data on the windward side have been presented here for completeness.

On the leeside, the relative magnitudes of the triple correlations are similar to those on the windward side. At the two upstream stations, 3H and 4H, the trends in the outer part of the boundary layer are in fact the same as those on the windward side. The large negative gradients of $\overline{vu^2}$ and $\overline{uv^2}$ observed in the wall region at these stations indicate a loss of $\overline{u^2}$ and $\overline{uv}$, respectively, due to turbulent diffusion. This is in accordance with measurements in two-dimensional boundary layers. However, by station 5H, these gradients become quite small and at station 6H their sign is reversed, indicating quite a different behavior of turbulent diffusion. The data at station 6H are particularly noteworthy since we see a large region in the outer part of the boundary layer where all triple correlations are very small and an inner region where their gradients are significant but opposite to those seen further upstream and in two-dimensional boundary layers. This is presumably due to the development of the local region of mean-flow divergence which, as shown in Fig. 4, leads to a large negative normal component of velocity. Although the evidence is rather limited, the data suggest a significant influence of the extra strain rates due to mean-flow divergence on

the diffusive mechanisms. The lack of similar data in the wall region of the windward boundary layer, which experiences continuous flow divergence, is unfortunate since they would have provided confirmation of this conjecture.

II.6. Summary

The mean-flow and turbulence measurements reported here provide a set of data which can be used to test the performance of calculation methods for plane-of-symmetry boundary layers subjected to convergence and divergence. Although the data on the windward side are not as complete as one would like for such purposes, it is clear that, taken together, the present experiments indicate a direct effect of flow convergence and divergence on the turbulence structure. The data on the leeward side are of special interest due to the joint influence of convergence and divergence beyond Station 4. The calculations presented in the next section support some of the observations made here on the basis of the experimental evidence.

III. CALCULATIONS AND COMPARISONS WITH EXPERIMENTS

As mentioned in the Introduction, the boundary layer in a plane of symmetry can be calculated independently of the flow on either side of it. If, as shown in Fig. 16, z = 0 is the plane of symmetry, the boundary-layer equations (see Nash and Patel, 1972) are

$$\frac{1}{h_1}\frac{\partial U}{\partial x} + \frac{\partial V}{\partial y} + \frac{1}{h_3}\frac{\partial W}{\partial z} + K_{31}U = 0 \tag{3}$$

$$\frac{U}{h_1}\frac{\partial U}{\partial x} + V\frac{\partial U}{\partial y} + \frac{1}{h_1}\frac{\partial}{\partial x}\left(\frac{P}{\rho}\right) + \frac{\partial}{\partial y}\left(\overline{uv}\right) - \nu\frac{\partial^2 U}{\partial y^2} = 0 \tag{4}$$

$$\frac{U}{h_1}\frac{\partial W_1}{\partial x} + V\frac{\partial W_1}{\partial y} + W_1^2 + K_{31}UW_1 - \frac{U^2}{h_3}\frac{\partial K_{13}}{\partial z}$$

$$+ \frac{1}{h_3^2}\frac{\partial^2}{\partial z^2}\left(\frac{P}{\rho}\right) + \frac{\partial W_2}{\partial y} - \nu\frac{\partial^2 W_1}{\partial y^2} = 0 \tag{5}$$

where

$$K_{31} = \frac{1}{h_1 h_3}\frac{\partial h_3}{\partial x}, \qquad K_{13} = \frac{1}{h_1 h_3}\frac{\partial h_1}{\partial z},$$
$$W_1 = \frac{1}{h_3}\frac{\partial W}{\partial z}, \qquad W_2 = \frac{1}{h_3}\frac{\partial}{\partial z}(\overline{vw}), \tag{6}$$

and h_1 and h_3 are the metrics in the x and z directions, respectively. Equations (3) and (4) are the usual continuity and momentum equations while (5) is obtained by differentiating the z-momentum equation with respect to z and evaluating it on z = 0. Thus, equation (5) gives the development of the rate of convergence or divergence, W_1.

The boundary conditions for the plane-of-symmetry flow are similar to those for two-dimensional flows. At the wall, the no-slip conditions are applied, i.e., U = W_1 = 0 at y = 0. For the flow outside the boundary layer, equations (4) and (5) simplify to

$$\frac{U_e}{h_1}\frac{\partial U_e}{\partial x} + \frac{1}{h_1}\frac{\partial}{\partial x}\left(\frac{P}{\rho}\right) = 0 \tag{7}$$

$$\frac{U_e}{h_1}\frac{\partial W_{1e}}{\partial x} + W_{1e}^2 + K_{31}U_e W_{1e} - \frac{U_e^2}{h_3}\frac{\partial K_{13}}{\partial z} + \frac{1}{h_3^2}\frac{\partial^2}{\partial z^2}\left(\frac{P}{\rho}\right) = 0 \tag{8}$$

The pressure terms in equations (4) and (5) can be eliminated by subtracting them from equations (7) and (8). Then, at the edge of boundary layer, we have

$$U \to U_e; \quad W_1 \to W_{1e} \text{ as } y \to \delta$$

where subscript e refers to the external flow. Thus, U_e and W_{1e} must be specified as functions of x. These have to be determined either from the potential-flow solution or from experiments.

For laminar flow, the Reynolds stresses $\overline{uv}$ and $\overline{vw}$ are zero, and equations (3), (4), and (5) are sufficient to determine U, V and W_1 for a given pressure distribution. For turbulent flow, the isotropic, two-layer, eddy-viscosity model of Cebeci and Smith (1968), as modified by Cebeci and Mosinskis (1971) and Cebeci (1971), is adopted. This takes into account the effects of pressure gradients, low Reynolds numbers as well as transition from laminar to

turbulent flow through an empirical intermittency function. In general three-dimensional boundary layers, the Reynolds stresses are related to the local rate of strain by

$$-\overline{uv} = \nu_t \frac{\partial U}{\partial y}, \quad -\overline{vw} = \nu_t \frac{\partial W}{\partial y} \tag{9}$$

where ν_t is the eddy viscosity. Then, the second equation yields

$$-W_2 \equiv \frac{1}{h_3}\frac{\partial}{\partial z}(-\overline{vw}) = \nu_t \frac{\partial}{\partial y}\left(\frac{1}{h_3}\frac{\partial W}{\partial z}\right) = \nu_t \frac{\partial W_1}{\partial y} \tag{10}$$

for the Reynolds-stress term in equation (5).

The calculation method chosen for this study is the Crank-Nicolson implicit method of Chang and Patel (1975) since it is easily adopted for the solution of the plane-of-symmetry equations for laminar and turbulent flows, and has been tested quite extensively (Chang and Patel, 1975; Patel and Choi, 1980; Patel and Baek, 1982; Krogstad, Baek and Patel, 1982) for a variety of two-dimensional, axisymmetric and three-dimensional flows. The numerical features of this method are described in detail in Chang and Patel (1975).

Calculations for two types of flow will be presented, namely the flow ahead of a surface-mounted symmetrical body, and the flow on a body of revolution at incidence. For the former, $h_1 = h_3 = 1$, $K_{13} = K_{31} = 0$, and $W_1 = \frac{\partial W}{\partial z}$. For the body of revolution whose surface is given by $r(X)$, the z coordinate is replaced by the azimuthal angle θ, so that the metric coefficients h_1 and h_3 are $\{1 + (dr/dX)^2\}^{1/2}$ and $r(X)$, respectively, and $W_1 = \frac{1}{r}\frac{\partial W}{\partial \theta}$. In some cases, calculations have also been performed assuming two-dimensional and axisymmetric flow, with the same pressure distribution, to illustrate the relative effects of transverse curvature and mean-flow convergence or divergence.

III.1. An Overview of the Calculations

The Crank-Nicolson method was first utilized to make a study of the laminar boundary layer on a 4:1 spheroid over a range of incidences. These calculations were performed using the exact potential-flow solutions for U_e and W_{1e} with initial conditions specified just downstream of the potential-

flow stagnation point. The results verified the major features of the earlier calculations of Wang (1972, 1974) and Patel and Choi (1980) but did not provide any new insights into either the numerical method or the physical phenomena involved. The DFVLR experiments of Meier, Kreplin and others on a 6:1 spheroid and the present experiments described in Section II provided a fresh opportunity to evaluate the various numerical aspects of the calculation method by direct comparison with data and to study the problems associated with transition, turbulence modelling and viscous-inviscid interaction on planes of symmetry.

For clarity of presentation, it is convenient to classify plane-of-symmetry boundary layers in two categories: those subjected to mean-flow divergence and those involving mean-flow convergence, or convergence and divergence simultaneously. In each case, we have selected examples of laminar as well as turbulent flow. The laminar-flow data obtained at the DFVLR are somewhat limited insofar as only the wall shear-stresses were measured. Nevertheless, they can be used to evaluate the numerical aspects of the calculation method without the added uncertainties of turbulence modelling. Secondly, the initial conditions are well defined since the solutions can be started at the stagnation point. For turbulent flow, the DFVLR data are again useful since they contain an initial region of laminar flow followed by natural transition and turbulent flow, and therefore a complete calculation can be performed by starting with the initial conditions at the stagnation point. On the other hand, the present experiments provide greater detail in the turbulent boundary layer and can be used to assess the validity of the simple eddy-viscosity model.

III.2. Boundary Layers with Flow Divergence

As noted earlier, the boundary layer in the windward plane of symmetry ($\theta = 0°$) is subjected to a continuous divergence of the external flow (i.e., $W_{1e} > 0$). This leads to a divergence of the mean flow within the boundary layer (i.e., $W_1 > 0$). A similar situation exists in the symmetry plane ahead of a symmetrical body standing on a flat surface.

(a) Laminar Flow

The DFVLR experiments on the spheroid revealed that the flow in the windward plane remains laminar over a range of combinations of incidence and Reynolds number up to the point of separation, which occurs just ahead of the sting at X/L = 0.98 used to mount the body in the wind tunnel. Two such combinations, for which tabulated data are available, are $\alpha = 10°$, $Re = Q_o L/\nu = 1.6 \times 10^6$ and $\alpha = 30°$, $Re = 7.2 \times 10^6$. Figures 17(a) and 18(a) show the distributions of the pressure coefficient for these two cases. It is interesting to note that, in both cases, the measured pressure distribution is in close agreement with that predicted by potential-flow theory except over a short distance ahead of the sting at the tail.

The calculated distributions of wall shear-stress coefficients, $C_{fo} = \tau_w/\frac{1}{2}\rho Q_o^2$, and the momentum thickness, θ_{11}, are shown in Figs. 17 and 18. From Fig. 17(b) it is seen that the calculated shear-stress distribution indicates the same trend as the data but lies some 20 percent higher than the measurements. However, at the higher incidence of 30° and the higher Reynolds number (Fig. 18b) the agreement is considerably better. The reason for the discrepancy at the lower incidence and Reynolds number is not altogether clear although the experimenters suggest that the measurements at the lower velocities are subject to considerable experimental uncertainty. Also, it is important to note that the hot-film probes used to infer C_f were "calibrated" against a calculation method in axisymmetric flow. However, Fig. 18(b) suggests that this may not be a major contributing factor since we would expect a similar discrepancy at the high Reynolds number also. Finally, the calculations indicate separation ($C_f = 0$) very close to the tail, but the comparison with the data is not meaningful due to the support sting used in the experiments and the departure of the measured pressure distribution from that in potential flow. Calculations assuming two-dimensional and axisymmetric flow with the same axial pressure gradients were also performed. These results are presented in Figs. 17 and 18 in order to show the effect of transverse curvature and that of mean-flow divergence. It is seen that the transverse-curvature effect is not very significant but the mean-flow divergence inhibits the growth of the boundary layer.

(b) Turbulent Flow

At an incidence of 10° and the higher Reynolds number of 7.2×10^6, the flow was observed to be laminar up to X/L = 0.56. The hot-film signals indicated that this was followed by a short region of natural transition and then turbulent flow. The experimental results are shown in Fig. 19. In this case, the calculations were again started at the stagnation point and transition was imposed at X/L = 0.56. The calculated wall shear-stress distribution is shown in Fig. 19(b) and the corresponding momentum thickness is plotted in Fig. 19(c). It is seen that the calculations are in excellent agreement with the data not only in the laminar part but also in the turbulent part. The eddy-viscosity correlation of Cebeci et al. also appears to mimic the changes in the transition zone quite effectively, at least with respect to the wall shear-stress variation.

In this case, the mean-velocity profiles were measured at two stations, namely X/L = 0.64 and 0.71. Figure 20 shows a comparison with calculated profiles. The observed disagreement in the shape as well as the rate of growth of the boundary layer is most probably due to the failure of the simple correlation used for the eddy-viscosity, since the measurement stations are quite close to the transition point. Also shown in Fig. 20 are the corresponding calculated profiles of W_1. For later reference, we note that the shape of these profiles is quite similar to that of the longitudinal component of velocity, U/U_e.

Figures 19 and 20 also include calculations for two-dimensional and axisymmetric flow. These comparisons reveal that transverse curvature is more important near the ends of the body where the curvature is large. However, the effect of mean-flow divergence is significant everywhere in the integral parameters as well as the axial velocity profiles.

Of the many previous experiments involving turbulent boundary layers with mean-flow divergence, we have selected that of Krogstad (1979), who made measurements in the boundary layer on a flat plate ahead of a two-dimensional half body generated by a simple two-dimensional source in a uniform stream. Figure 21 shows a comparison between the experimental and theoretical pressure distributions, the streamwise component of the external velocity U_e and the rate of flow divergence W_{1e} outside the boundary layer.

From a computational point of view, such flows are somewhat easier to deal with since the initial conditions are readily prescribed, i.e., the flow at a large distance ahead of the obstacle is two-dimensional. In the present calculation, these were prescribed at X/S = -170.7, where S is the distance between the source and the stagnation point. The initial Reynolds number based on the distance from the leading edge of the floor is about 1.24 x 10^6. Most of the experimental results are concentrated in the range of the local Reynolds number 3 to 4 x 10^6. The calculations involve some uncertainties stemming from the prescription of the distribution of W_{le}. As seen from Fig. 21, the measured distribution of U_e is not exactly the same as that obtained from two-dimensional potential-flow theory, and therefore W_{le} will also not be the same as that in potential flow. Unfortunately, as noted earlier, this can not be readily determined from the experiments. Consequently, the potential-flow distribution of W_{le} has been used, but two sets of calculations, corresponding to the theoretical and experimental distributions of U_e, were performed. The results of the calculations are shown in Figs. 22 and 23. The level of agreement seen in these figures is comparable to that obtained by Chang and Patel (1975) for the case of East and Hoxey (1969), and by many other methods for similar flows (see, for example, the calculations performed by several different methods for the test case of Dechow and Felsch (1977) at the EUROVISC Workshop in Berlin, van den Berg et al., 1984). The most significant aspect of such calculations is that they predict an earlier separation. The location of separation is, of course, of great practical importance since it indicates the position at which the horseshoe vortex along the junction of the body with the plane is located. The predictions with the experimental values of U_e in Fig. 22 show some irregularities since the boundary conditions are given by the scattered experimental values. Figure 22 shows that the region of disagreement between the calculations and experiment (i.e., $-12 < X/S < -3.3$) is of the order of 4 local boundary-layer thicknesses. Thus, the disagreement is not altogether significant since this is the region of strong viscous-inviscid interaction associated with the thickening of the boundary layer upstream of separation. Although the use of the experimental distribution of U_e yields some improvement, and a similar effect may be present due to the difference between the actual W_{le} and the potential-flow distribution used here, further improvement cannot be expected on the basis of boundary-layer theory alone.

Although the two cases of turbulent flows considered above represent a test of the calculation method, they do not yield much direct information on the problem of turbulence modelling since turbulence measurements were not made. The experiments described in the previous section were conducted to obtain such data. Unfortunately, as we have already discussed, the turbulence data on the windward side were restricted to the outer part of the rather thin boundary layer and consequently do not provide a rigorous test. Nevertheless, it is of interest to present the corresponding calcuations in order to demonstrate some general features of the method and point out certain difficulties associated with the prescription of the initial and boundary conditions for plane-of-symmetry boundary layers.

Since the present experiments utilized a trip wire, the calculations could not be started at the stagnation point. Instead, the initial conditions were provided by the data at the most upstream station (X/L = 0.169). Although this is a frequently adopted procedure in the evaluation of calculation methods for turbulent flows, it involves some uncertainty, since the measured velocity profile provides only a part of the necessary information. Another quantity that must also be prescribed is the *distribution of* W_1 *across the boundary layer*, i.e., the initial rate of divergence. Since this could not be measured accurately, it was assumed that the initial profile of W_1 is similar to that of U, as indicated by the calculations shown in Fig. 20. Calculations were performed with these initial conditions and the streamwise distribution of U_e and W_{1e} obtained from the potential-flow solution.

A comparison of the measured and potential-flow pressure distribution was presented in Fig. 2. Figure 24(a) shows that the agreement between the potential-flow and measured values of U_e/Q_o is quite satisfactory over the range of the experiments. Figure 24(b) shows the circumferential component of velocity, W_e, measured off the plane of symmetry at $\theta = \pm 4°$, at the edge of the boundary layer, using the yaw probe and the distribution calculated from potential-flow theory. This figure illustrates first the difficulty of determining W_{1e} along the plane of symmetry since the scatter in the data obscures the trend. Secondly, it is seen that the flow is not perfectly symmetric with respect to the geometric plane of symmetry of the body. Finally, the potential-flow values of U_e and W_{1e} used in the calculations can,

at best, be regarded as a good first approximation. In general, however, these problems do not appear to be very severe on the windward side.

The comparisons between the boundary-layer calculations and experimental data presented in Figs. 25 through 28 must be evaluated with the aforementioned uncertainties in mind. These figures also include the numerical results corresponding to two-dimensional and axisymmetric flow. It is seen that the transverse-curvature effect is quite small but the mean-flow divergence has a significant influence on the entire flow. From Fig. 25 it is seen that the integral parameters C_f, θ_{11} and H $(= \delta_1/\theta_{11})$ are predicted reasonably well by the plane-of-symmetry calculations. The increase in the measured C_f and a corresponding decrease in θ_{11} beyond X/L = 0.4, and the generally smaller experimental values of H, may be attributed, at least in part, to the somewhat larger flow divergence implied by Fig. 24(b). A recalculation of the flow using experimental values of U_e and W_{1e} estimated from Figs. 24(a) and (b), showed some improvement in the agreement in the areas just noted. However, the results are not included here due to the experimental uncertainties discussed above.

Figures 26 and 27 show that the mean-velocity and Reynolds-stress profiles calculated with the plane-of-symmetry equations are in reasonable agreement with the measurements while the two-dimensional and axisymmetric-flow calculations show very significant differences. Closer examination of Figs. 26 and 23 indicates that even the plane-of-symmetry calculations tend to underestimate the velocity in the inner half of the boundary layer. This may be due to the failure of the turbulence model to account for the direct influence of flow divergence. Figure 26 also shows the calculated profiles of W_1, which is related to the extra rate of strain due to flow divergence. This increases monotonically from the wall to the outer edge of the boundary layer. The major differences observed in the longitudinal velocity profiles close to the wall do not appear to correlate simply with the extra rate of strain. Since detailed turbulence measurements could not be made in the inner half of the boundary layer, definitive conclusions cannot be drawn from the Reynolds stress and eddy-viscosity comparisons which are shown in Figs. 27 and 28. These simply indicate that the measured stresses are lower and the eddy-viscosities are higher in the outer part of the boundary layer.

III.3. Boundary Layers Subjected to Flow Convergence

From a computational point of view, the plane-of-symmetry boundary layer subjected to convergence of mean flow from both sides, e.g. on the leeside of a body at incidence, poses the same problems as those encountered in the previous case. From a physical standpoint, however, the boundary-layer behavior is much more complex since prolonged convergence leads to a thickening of the boundary layer and the development of a region of flow divergence close to the surface. Thus, the boundary layer may be subjected to convergence and divergence simultaneously. Furthermore, the thickening of the boundary layer may be large enough to induce strong viscous-inviscid interaction.

As we have remarked already, experiments in boundary layers with flow convergence are quite limited. On the DFVLR spheroid, wall shear-stress data are available for the cases $\alpha = 10°$, $Re = 1.6 \times 10^6$; $\alpha = 10°$, $Re = 7.2 \times 10^6$; and $\alpha = 30°$, $Re = 7.2 \times 10^6$. The flow on the leeward plane of symmetry is laminar in the first case, but laminar and turbulent in the remaining two cases at the higher Reynolds number. Note that, at the higher incidence the flow on the windward side remained laminar (see Fig. 18). Fortunately, due to the thicker boundary layer, the data obtained from the present experiments are more complete and can be used to test the calculation method in somewhat greater detail.

(a) Laminar Flow

From the pressure distribution on the leeside of the spheroid at $\alpha = 10°$, $Re = 1.6 \times 10^6$ given in Fig. 29, it is seen that the agreement between theory and experiment is quite good since the boundary layer is thin and laminar. The results of the laminar boundary-layer calculations are shown in Figs. 29 and 30. As before, these figures also include the results of two-dimensional and axisymmetric flow calculations. It is seen that mean-flow convergence and divergence has a very pronounced effect on the wall shear-stress and the separation point. On the other hand, the effects of transverse curvature are quite small. The agreement of the plane-of-symmetry flow calculations with respect to the wall shear-stress in Fig. 29 is seen to be as good as that observed earlier on the windward plane. Since velocity-profile measurements

are not available for this case, direct comparisons cannot be made. However, the profiles of W_1 shown in Fig. 30(b) indicate a reversal in the sign of W_1 across the boundary layer as early as X/L = 0.127. The local flow divergence begins just ahead of this station. The magnitude of flow divergence and its extent, within the boundary layer, increase downstream, and associated with this is a reduced growth rate of the boundary-layer thickness.

(b) Turbulent Flow

The results of the calculations for the spheroid at the higher Reynolds number are presented in Figs. 31 through 33. The transition points were specified at the experimentally observed locations, namely X/L = 0.31 for α = 10° and X/L = 0.053 for α = 30°.

The predictions for the lower incidence (α = 10°) shown in Figs. 31 and 32 indicate excellent agreement with the measurements with regard to the wall shear-stress as well as the velocity profiles which were measured at two stations in the turbulent flow region. The fluctuations in the calculations for the wall shear-stress are due to the rapid changes in the numerical grid across the boundary layer required to accommodate the rapidly increasing boundary-layer thickness. The success of the calculations through the transition zone are particularly noteworthy.

In Fig. 32, the profiles of longitudinal velocity clearly show the laminar, transitional and turbulent flow regions. The profiles of W_1 indicate several interesting features. Initially, at X/L = 0.127, the entire laminar boundary layer experiences convergent flow (i.e., $W_1 < 0$). A small region of flow divergence near the wall is observed at X/L = 0.254. This disappears due to transition and at X/L = 0.356 and 0.508 the boundary layer is again subjected to pure convergence. However, a region of flow divergence reappears in the turbulent boundary layer at the downstream stations X/L = 0.64 and 0.71. Comparisons of the plane-of-symmetry flow calculations with two-dimensional and axisymmetric flow calculations are also shown in Figs. 31 and 32. In the laminar region, the results show the same trends as in the case of the lower Reynolds number with the same angle of attack. In the turbulent flow region, the measurements are in agreement with the plane-of-symmetry flow calculations which include the important effects of the mean-flow convergence and divergence.

At the higher incidence of $\alpha = 30°$, Fig. 33(a) shows that the measured pressure distribution is quite different from that predicted by potential-flow theory beyond X/L = 0.2. This indicates strong viscous-inviscid interaction and it is not surprising to see that the calculated wall shear-stresses disagree with the data and indicate separation around X/L = 0.77. The use of the measured pressure distribution would have improved the prediction somewhat but this was not undertaken due to the difficulty of determining the necessary external-flow conditions.

The calculations corresponding to the present experiments presented the same difficulties as discussed earlier in detail for the windward side. The initial conditions were again specified at X/L = 0.169 using the measured velocity profile and assuming that the initial distribution of W_1 across the boundary layer is similar to that of (U/U_e). In this case, the subsequent solution was found to be highly sensitive to the initial distribution of W_1. The similarity assumption used here appeared to be the most reasonable one that could be made. The second uncertainty concerning the prescription of the axial variation of W_{1e} was also found to be somewhat greater on the leeside. Figure 34(a), which shows the distribution of the velocity outside the boundary layer, confirms the pressure distribution comparison shown in Fig. 2. However, from Fig. 34(b) it is seen that the circumferential component of velocity measured on either side of the symmetry plane (at $\theta = 180° \pm 4°$) is significantly different from that predicted by potential-flow theory. As in the previous case, the calculations presented below utilize the potential-flow boundary conditions.

The predicted integral parameters are compared with the measurements in Fig. 35. This figure also includes the calculations for two-dimensional and axisymmetric flows. The comparisons again demonstrate the large effect of the mean-flow convergence and divergence. It is also seen that the agreement between the complete plane-of-symmetry calculations and experimental data is not as good as that in the windward side (Fig. 25) and, in particular, the discrepancy is consistently in the opposite direction in all respects, e.g., θ_{11} and H are underestimated while C_f is overpredicted. The application of corrections for the increased rate of convergence of the external flow suggested by Fig. 34(b), however, provided only a marginal improvement in the predictions. Thus, it can be concluded that the observed disagreement between

the measurements and calculations is largely due to the inadequacy of the turbulence model used. This is further confirmed by the profiles of velocity, Reynolds stress and eddy-viscosity shown in Figs. 36, 37 and 38.

A comparison of Fig. 36 with Fig. 26 on the windward side shows that the disagreement between the measured and calculated velocity profiles is largest near the wall and in opposite directions. It is interesting to note that the agreement improves somewhat in the downstream direction, as was also observed in the spheroid experiments at the lower incidence and higher Reynolds number (Fig. 31). This improvement is perhaps due to the increasing region of flow divergence ($W_1 > 0$) developing in the wall region which, according to Fig. 36, starts between stations 2 and 3. The overestimation of the velocity by the calculation method is consistent with the overestimation of the Reynolds stress and the eddy-viscosity shown in Fig. 37 and 38. The results of the two-dimensional and axisymmetric flow calculations confirm the importance of mean-flow convergence and divergence in the mean-flow equations. However, it is also clear that the net effect of flow convergence on the turbulence is to decrease the Reynolds stress and the eddy-viscosity. The predictions with the complete plane-of-symmetry equations could therefore be improved by incorporating an extra rate-of-strain effect in the turbulence model. Although empirical correlations for extra strain effects due to factors such as curvature, rotation and buoyancy have been suggested in the literature, the authors are not aware of such corrections for the effect of lateral convergence or divergence.

The calculations for the spheroid at the higher incidence clearly demonstrate the possible effects of viscous-inviscid interaction on the leeside. We may expect such an effect in the present experiments also. However, as shown in Fig. 34 the interaction appears to be quite weak, at least over the region in which the above comparisons were made. Comparison of the convergence rates shown in Figs. 32 and 36 suggests that the boundary layer on the combination body is subjected to extra strain rates similar to those on the spheroid at the smaller incidence and higher Reynolds number. The small changes in the results of the calculations using the corrected distributions of U_e and W_{1e} also suggest that the influence of the interaction is quite weak up to station 6 (X/L = 0.641) in the present experiments.

IV. CONCLUSIONS

The comparisons between the calculations and the present and previous experimental data for plane-of-symmetry boundary layers lead to the following observations. (a) In laminar flow, the calculations yield quite accurate predictions for both convergent and divergent flows, provided regions of strong viscous-inviscid interactions which are observed on the leeside of bodies of revolution at large incidences are excluded. (b) Extensive comparisons made between the plane-of-symmetry flow calculations and those using two-dimensional and axisymmetric-flow assumptions clearly indicate the gross effects of mean-flow convergence and divergence. (c) For turbulent flow, the present experiments and calculations indicate a consistent and direct influence of the rate of convergence and divergence on the mean-velocity and Reynolds-stress profiles. The influence of convergence is opposite to that of divergence. Thus, further improvements in the calculation method can be made by incorporating such an effect in the turbulence model. It would also be of interest to repeat these calculations using other turbulence models. (d) Since the flow in the plane of symmetry serves as a boundary condition for the complete three-dimensional boundary layer on the body, the above observations should be taken into account in the evaluation of calculation methods for the general three-dimensional case.

ACKNOWLEDGEMENTS

This research was supported by the U.S. Army Research Office and U.S. Air Force Office of Scientific Research under Grant No. AFOSR-80-0148B. The authors also acknowledge the assistance of Dr. A.W. Fiore of AFFDL and Dr. H.U. Meier of the DFVLR, Project Officers of the U.S.A.-Federal Republic of Germany Data Exchange Agreement, in making available tabulated data from the DFVLR experiments.

REFERENCES

J.H. Baek, (1984) "Three-Dimensional Turbulent Boundary Layers on Bodies of Revolution at Incidence", Ph.D. Thesis, The University of Iowa.

B. van den Berg, D.A. Humphreys, E. Krause and J.P.F. Lindhout, (1984) "Computation of Three-Dimensional Boundary Layers", Proc. EUROVISC Workshop, Berlin, April 1982 (to be published).

P. Bradshaw, (1973) "Effects of Streamline Curvature on Turbulent Flow", AGARDograph No. 169.

T. Cebeci, (1971) "Calculation of Compressible Turbulent Boundary Layers with Heat and Mass Transfer", AIAA J., Vol. 9, p. 1091.

T. Cebeci and G.J. Mosinskis, (1971) "Calculation of Incompressible Turbulent Boundary Layers at Low Reynolds Number", AIAA J., Vol. 9, p. 1632.

T. Cebeci and A.M.O. Smith, (1968) "A Finite-Difference Solution of the Incompressible Turbulent Boundary-Layer Equations by an Eddy-Viscosity Concept", Proc. AFOSR-IFP-Stanford Conf. :Computation of Turbulent Boundary Layers, Vol. 1, ed. by Kline, et al.

K.C. Chang and V.C. Patel, (1975) "Calculation of Three-Dimensional Boundary Layers on Ship Forms", Iowa Inst. Hydraulic Research, The University of Iowa, IIHR Report 205.

D.H. Choi, (1978) "Three-Dimensional Boundary Layers on Bodies of Revolution at Incidence", Ph.D. Thesis, The University of Iowa.

R. Dechow and K.O. Felsch, (1977) "Measurements of the Mean Velocity and of the Reynolds Stress Tensor in a Three-Dimensional Turbulent Boundary Layer Induced by a Cylinder Standing on a Flat Wall", Proc. 1st Symp. Turbulent Shear Flows, Penn State University, PA., p. 9.11-9.20.

L.F. East and R.P. Hoxey, (1969) "Low-speed Three-Dimensional Turbulent Boundary Layer Data. Part 1", ARC R & M No. 3653.

H.P. Hoffmann, (1976) "Utersuchung der 3-Dimensionalen, Turbulenten Grenzschicht an einem Schiffdoppelmodell im Windkanal", Inst. Schiffbau, Uni. Hamburg, Rept. 343.

H.G. Hornung and P.N. Joubert, (1963) "The Mean Velocity Profile in Three-Dimensional Turbulent Boundary Layers", J. Fluid Mech., Vol. 15, p. 368-385.

H.P. Kreplin, H. Vollmers and H.U. Meier, (1980) "Experimental Determination of Wall Shear Stress Vectors on an Inclined Prolate Spheroid", Proc. 5th USAF-FRG Data Exchange Agreement Meeting, Technical Report AFFDL-TR-80-3088, p. 315-332.

H.P. Kreplin, H. Vollmers and H.U. Meier, (1982) "Measurements of the Wall Shear Stress on an Inclined Plolate Spheroid", Z. Flugwiss. Weltraumforschung, Vol. 6, p. 248-252.

P.A. Krogstad, (1979) "Investigation of a Three-dimensional Turbulent Boundary Layer Driven by Simple Two-Dimensional Potential Flow", Dr.-Ing. Thesis, The Norwegian Institute of Tech., Trondheim.

P.A. Krogstad, J.H. Baek and V.C. Patel, (1982) "Three-Dimensional Turbulent Boundary Layer Calculations by an Implicit Crank-Nicolson Method", Eurovisc Workshop on 3 D Boundary Layers, Berlin, Apr. 1982; Also, IIHR Report 254.

L. Landweber and M. Macagno, (1969) "Irrotational Flow about Ship Forms", Iowa Inst. Hydraulic Research, The University of Iowa, IIHR Report 123.

L. Larsson, (1974) "Boundary Layers of Ships. Part III: An Experimental Investigation of the Turbulent Boundary Layer on a Ship Model", SSPA, Goteborg, Report No. 46.

H.U. Meier and H.P. Kreplin, (1980) "Experimental Study of Boundary Layer Velocity Profiles on a Prolate Spheroid at Low Incidence in the Cross-Section X/L=0.64", Proc. 5th USAF-FRG Data Exchange Agreement Meeing, Technical Report AFFDL-TR-80-3088, p. 169-189.

H.U. Meier and H.P. Kreplin, (1980) "Experimental Investigation of Boundary Layer Transition and Separation on a Body of Revolution", Z. Flugwiss Weltraumforschung, Vol. 4, p. 65-71.

H.U. Meier, H.P. Kreplin and H. Vollmer, (1981) "Velocity Distributions in 3-D Boundary Layers and Vortex Flows on an Inclined Prolate Spheroid", Proc. 6th USAF-FRG Data Exchange Agreement Meeting, DFVLR-AVA Report IB 22281 CP1, p. 202-217.

J.F. Nash and V.C. Patel, (1972) "Three Dimensional Turbulent Boundary Layers", SBC Tech Books, Atlanta.

V.C. Patel and J.H. Baek, (1982) "Calculation of Three-Dimensional Boundary Layers on Bodies at Incidence", Iowa Inst. of Hydraulic Research, The University of Iowa, IIHR Report 256.

V.C. Patel and D.H. Choi, (1980) "Calculation of Three-Dimensional Laminar and Turbulent Boundary Layers on Bodies of Revolution at Incidence", Turbulent Shear Flows II, Springer, New York, p. 199-217.

F.J. Pierce and J.E. McAllister, (1980) "Near-Wall Similarity in a Pressure-Driven Three-Dimensional Turbulent Boundary Layer", Virginia Polytech. Inst. and State Univ., Report VPI-E-80.32.

B.R. Ramaprian, V.C. Patel and D.H. Choi, (1981) "Mean Flow Measurements in the Three-dimensional Boundary Layer over a Body of Revolution at Incidence", J. Fluid Mech., Vol. 103, p. 479-504.

G.R. Schneider, (1983) "Calculation of Three-Dimensional Boundary Layers in the Plane of Symmetry of a Prolate Spheroid at Incidence Including the Laminar-Turbulent Transition", 8th USAF-FRG Data Exchange Agreement Meeting, Gottingen, May 1983.

K.C. Wang, (1969) "Three-Dimensional Boundary Layer near the Plane of Symmetry of a Spheroid at Incidence", J. Fluid Mech., Vol. 43, p. 187-209.

K.C. Wang, (1972) "Separation Patterns of Boundary Layer over an Inclined Body of Revolution", AIAA J., Vol. 10, p. 1044-1050.

K.C. Wang, (1974) "Laminar Boundary Layer near the Symmetry Plane of a Prolate Spheroid", AIAA J., Vol. 12, p. 949-958.

K.C. Wang, (1974) "Boundary Layer over a Blunt Body at High Incidence with an Open-Type of Separation", Proc. Royal Society, Vol. A340, p. 33-55.

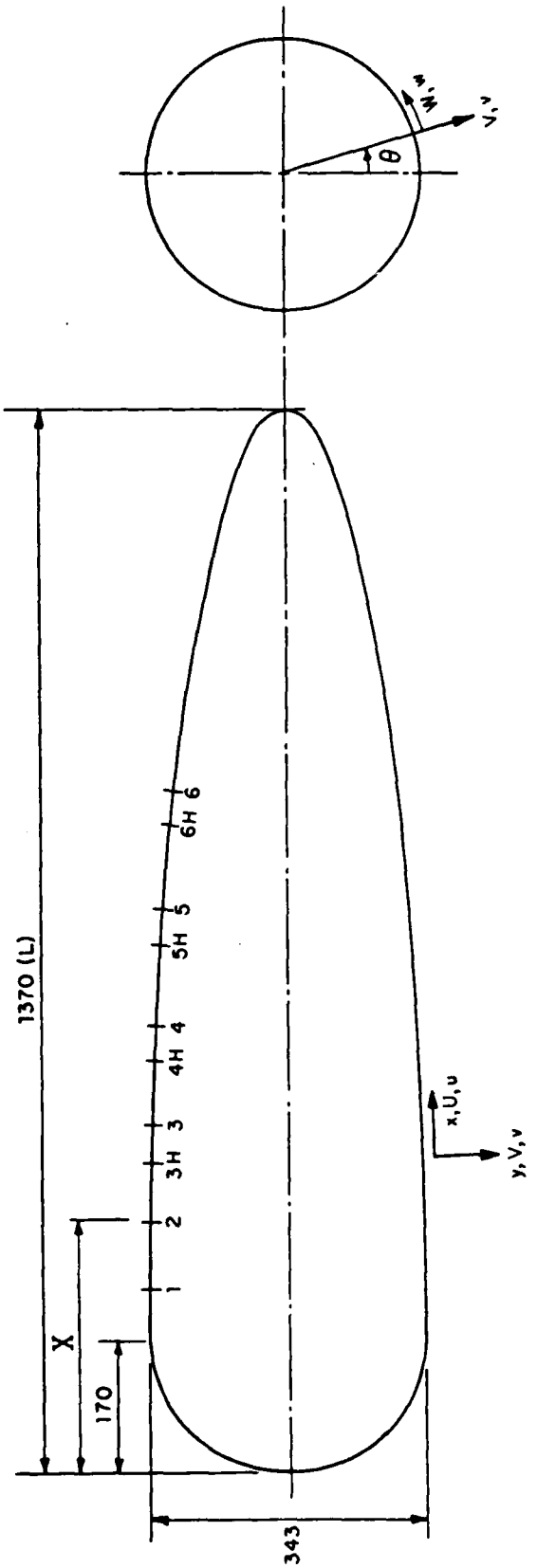

Figure 1. Coordinates and notation of the combination body (all dimensions in MM)

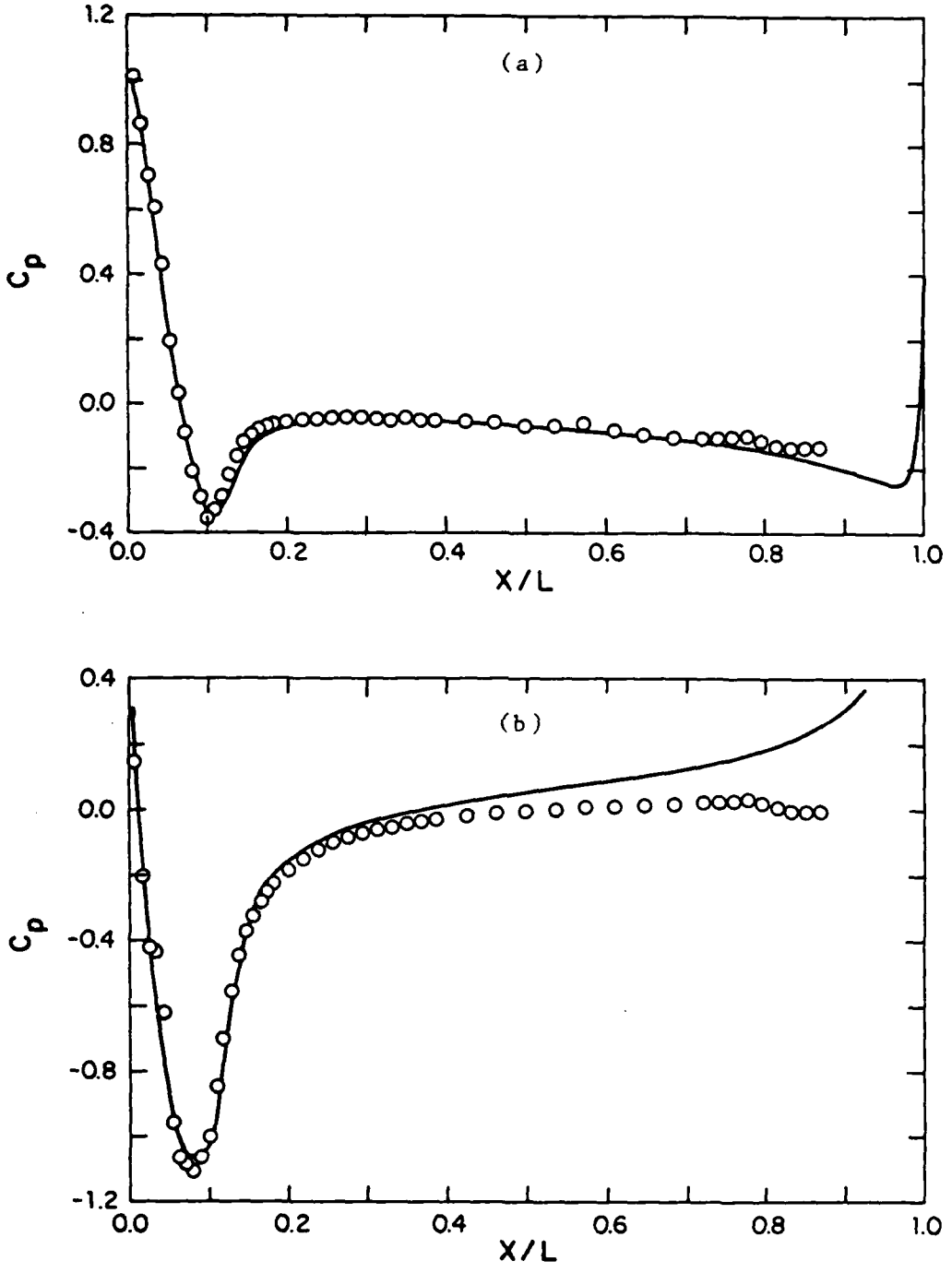

Figure 2. Wall static pressure distribution on the combination body. o: experimental data; —— inviscid theory(15°)
(a) windward plane, (b) leeward plane

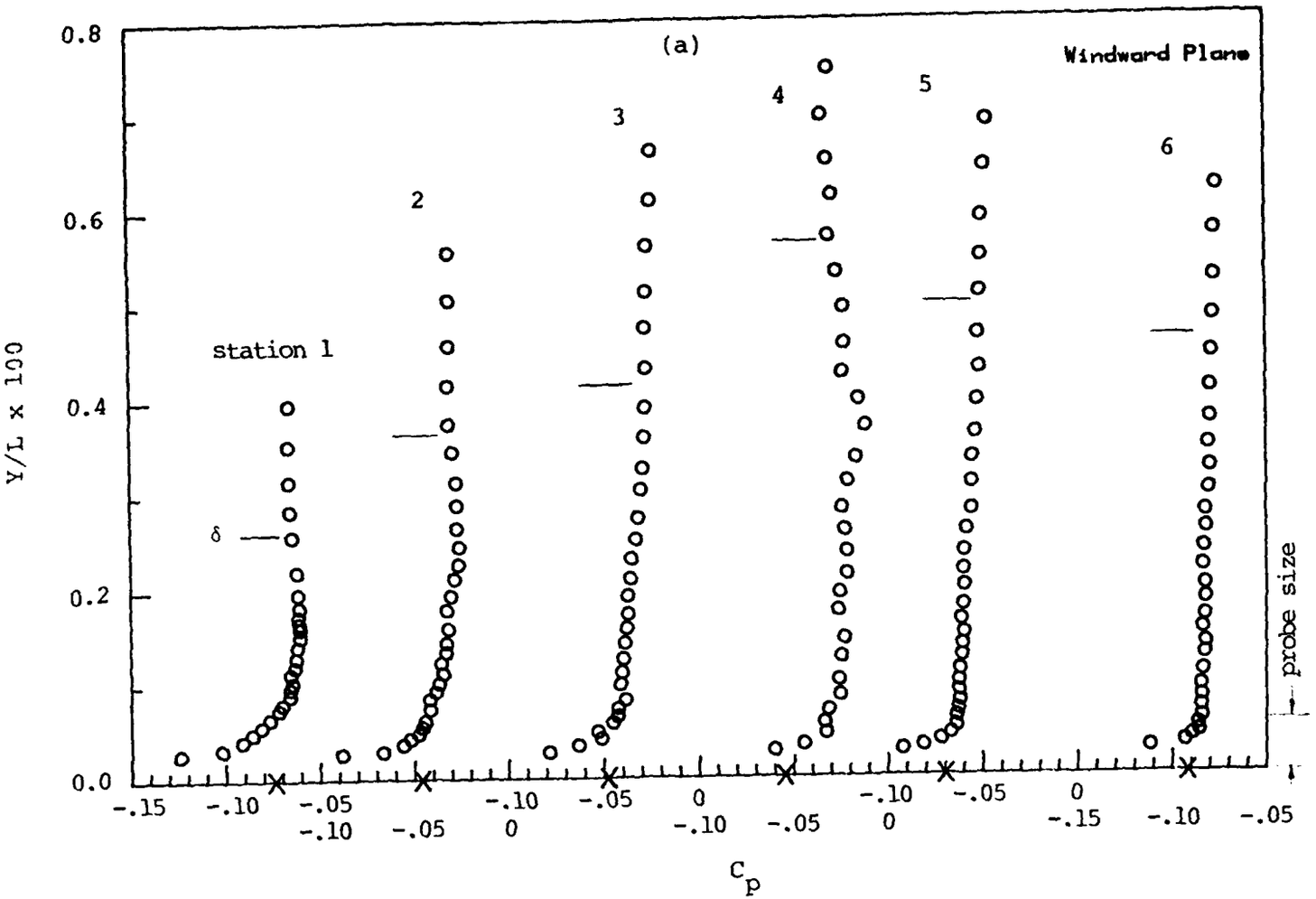

Figure 3. Static pressure profiles. X;wall static pressure
(a) windward plane

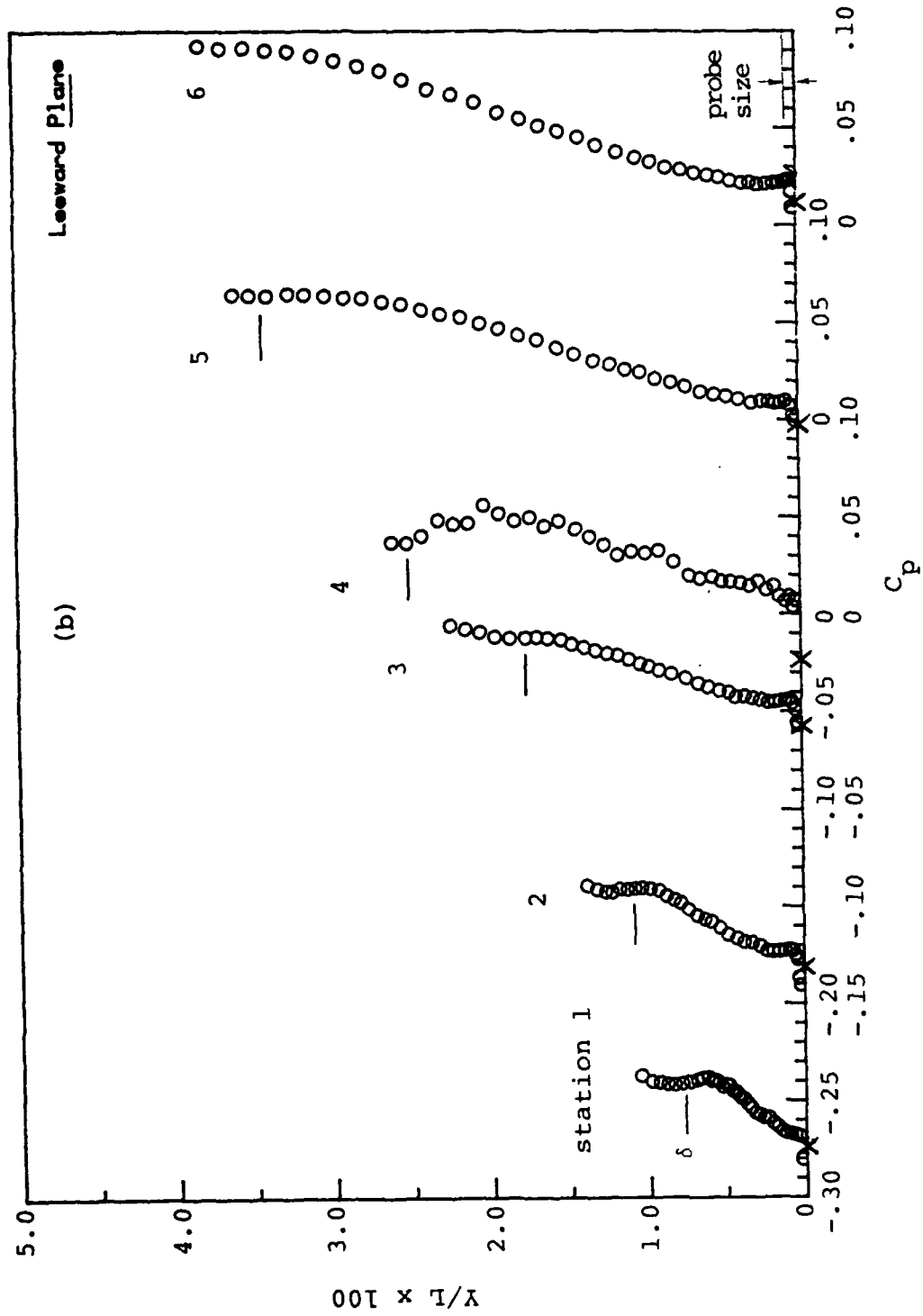

Figure 3. Continued
(b) leeward plane

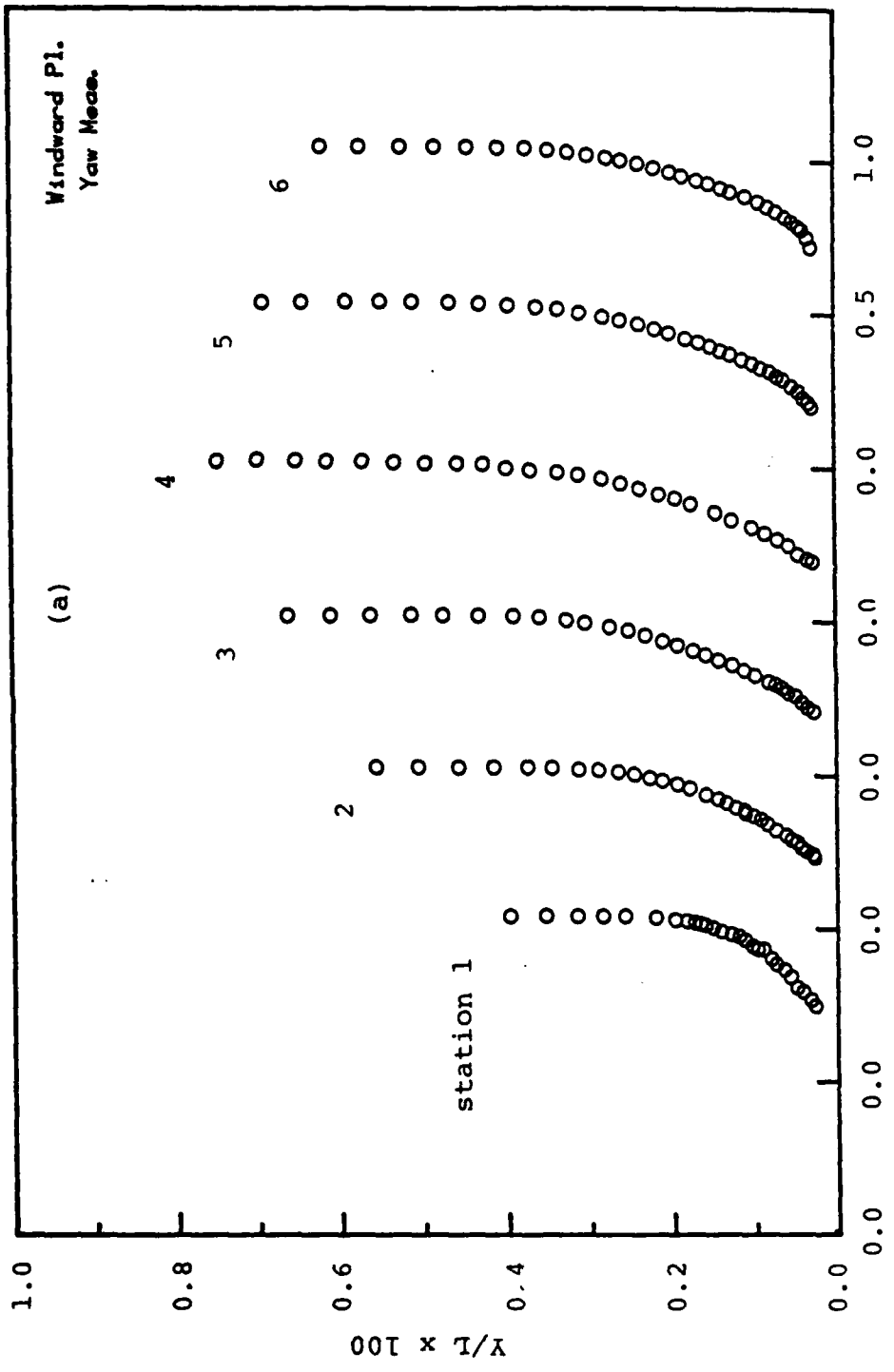

Figure 4. Mean velocity profiles measured by yaw probe.
o; experimental data,
(a) windward plane

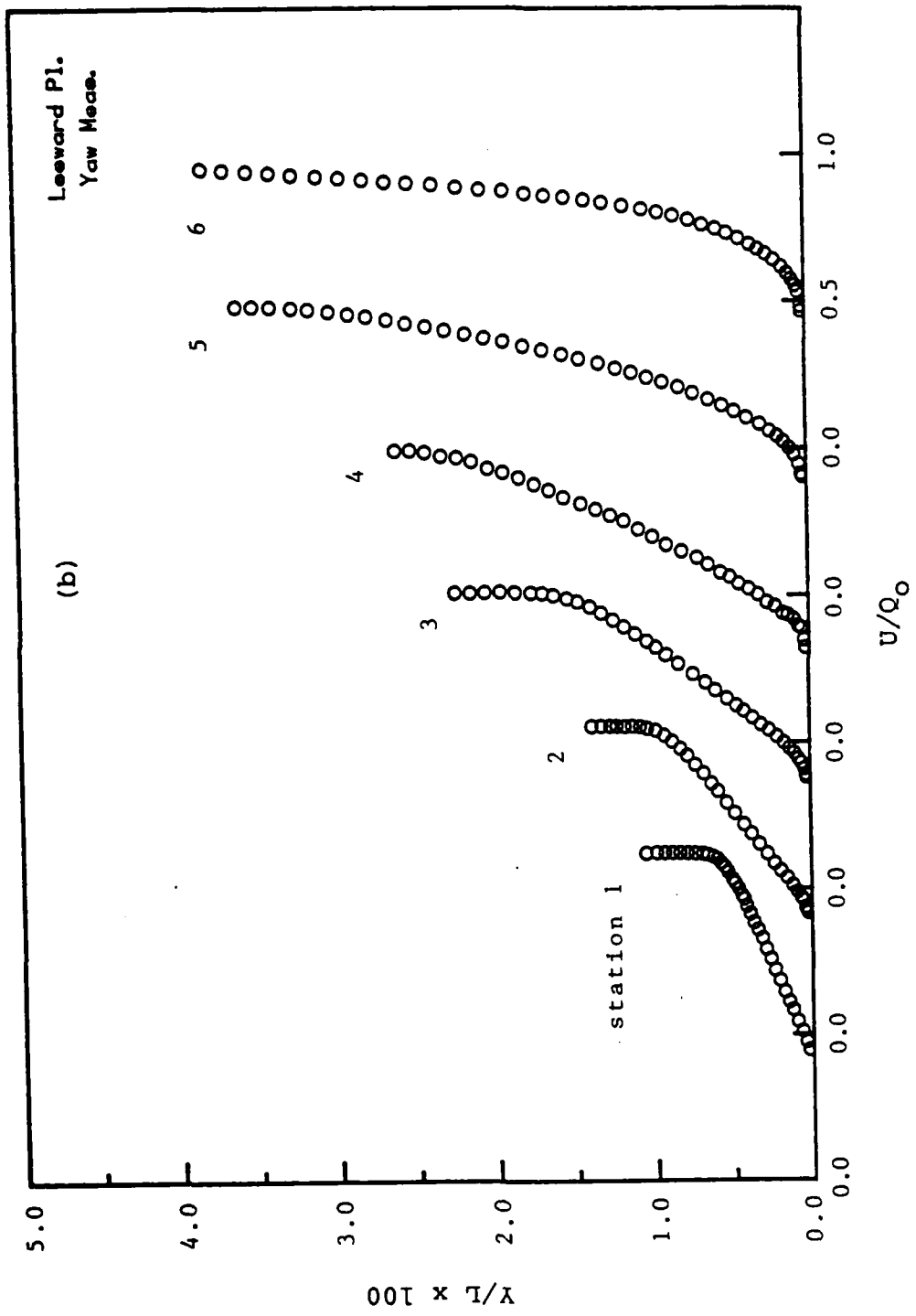

Figure 4. Continued
(b) leeward plane

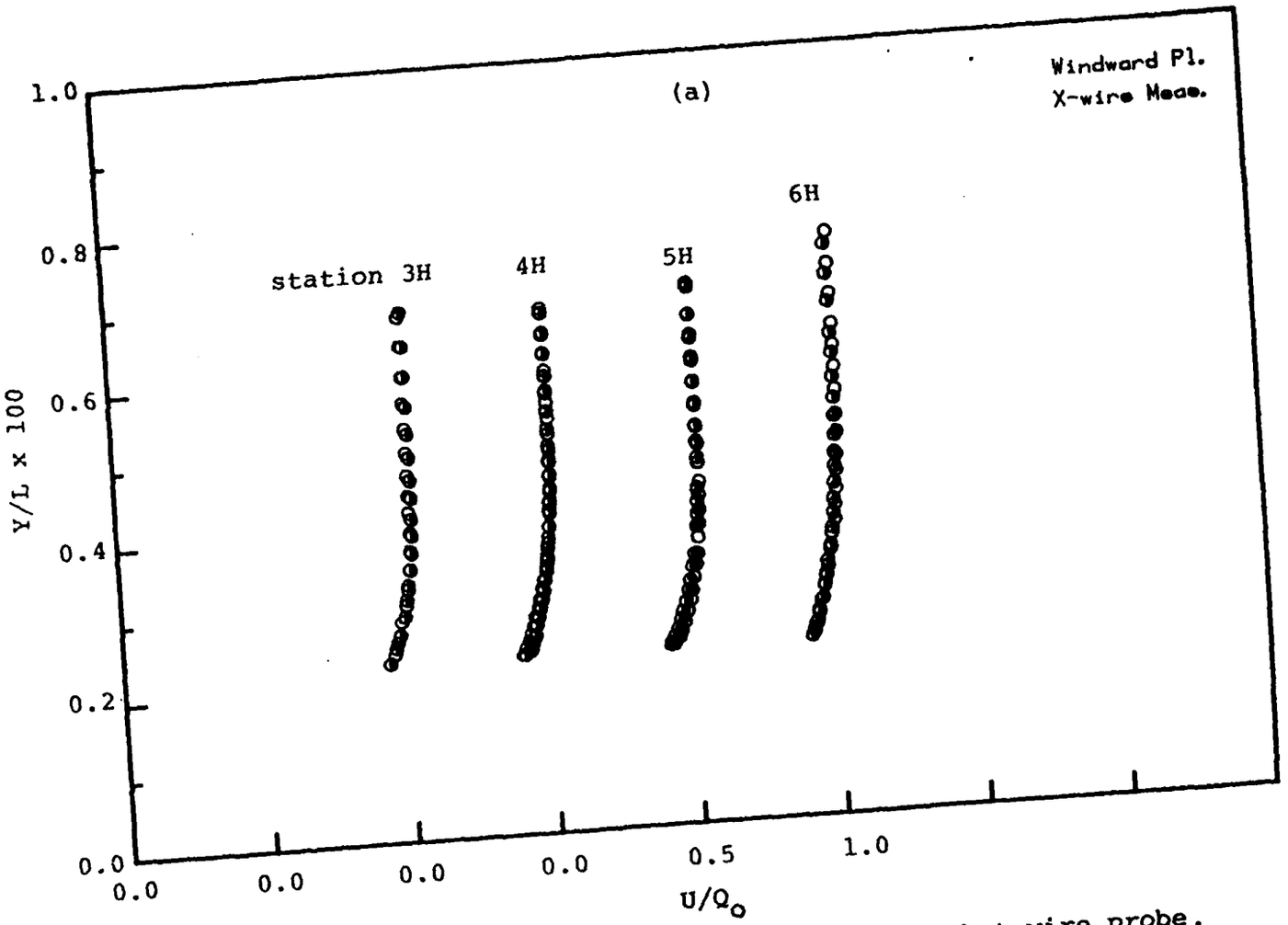

Figure 5. Mean velocity profiles measured by hot-wire probe. o: u-v configuration; ●: u-w configuration; (a) windward plane

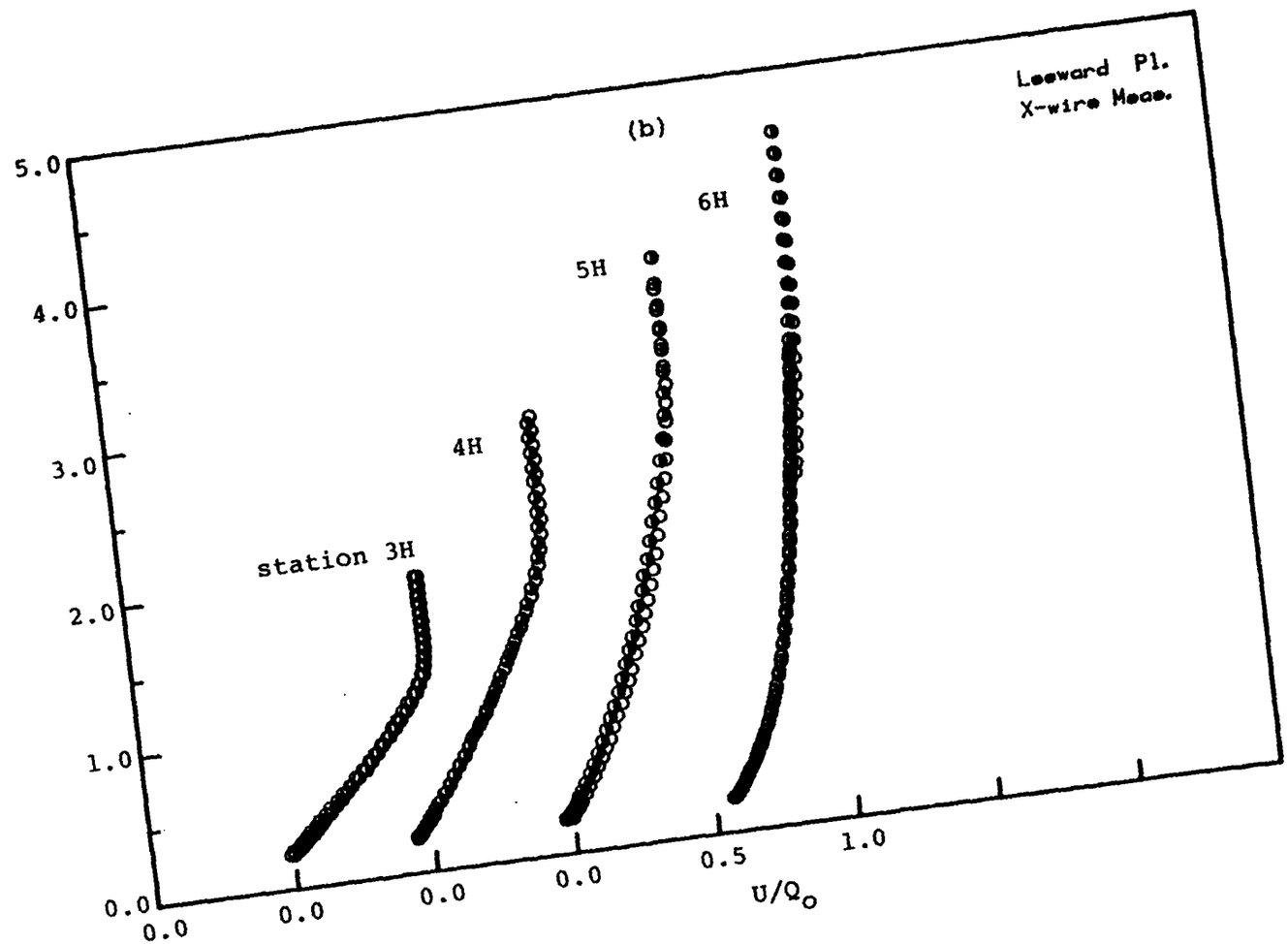

Figure 5. Continued
(b) leeward plane

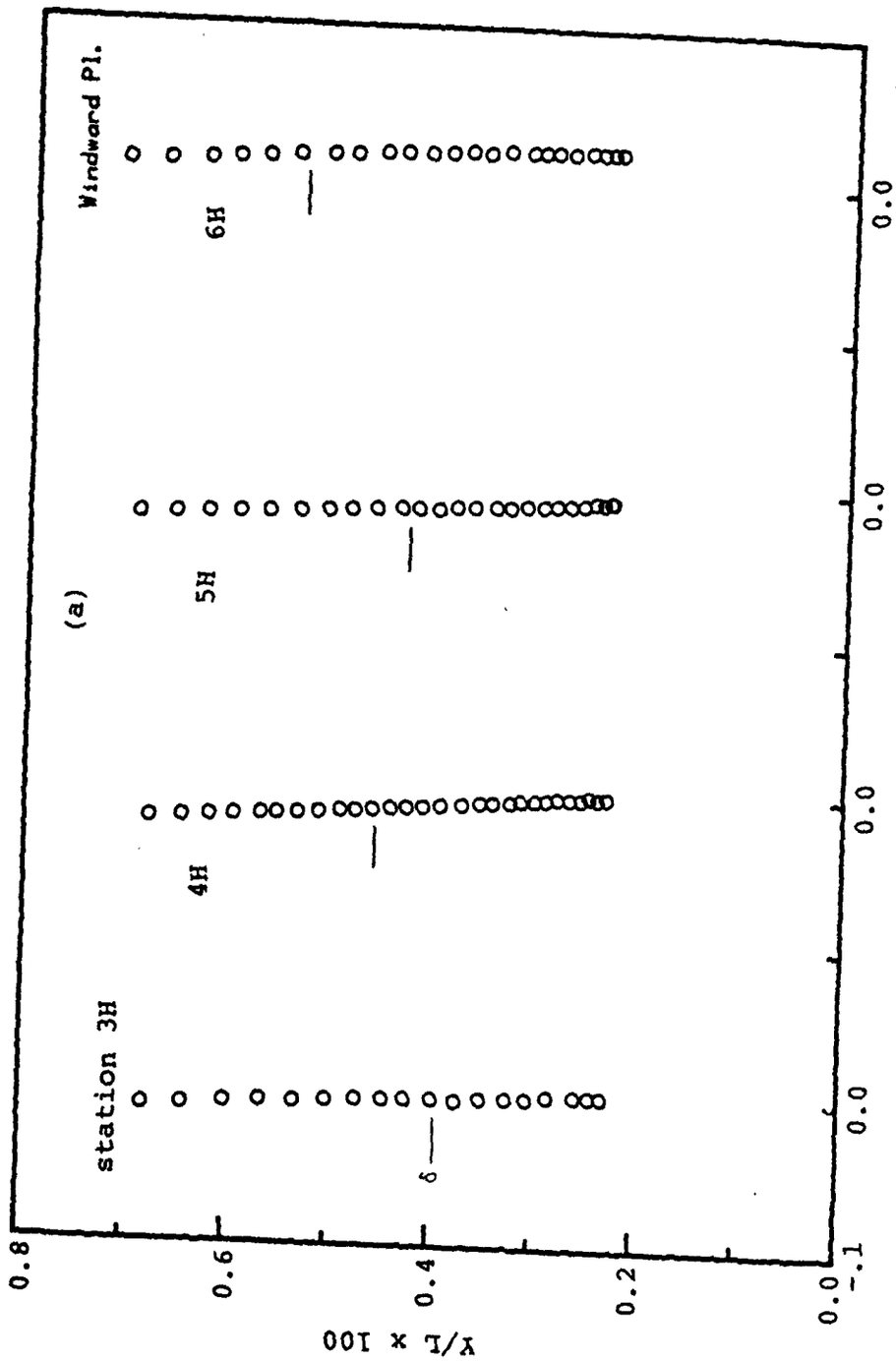

Figure 6. Normal component of mean velocity.
(a) windward plane

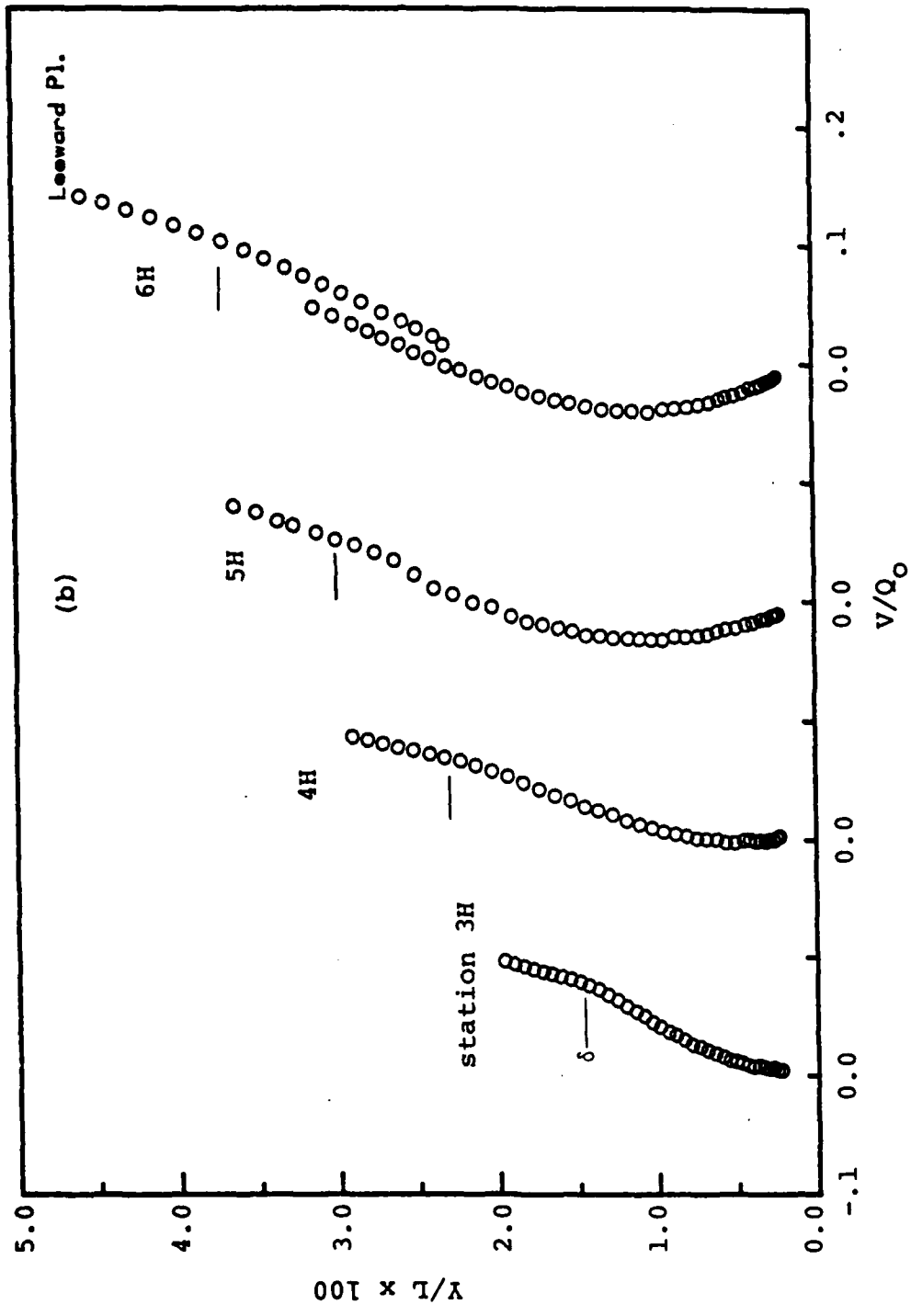

Figure 6. Continued
(b) leeward plane

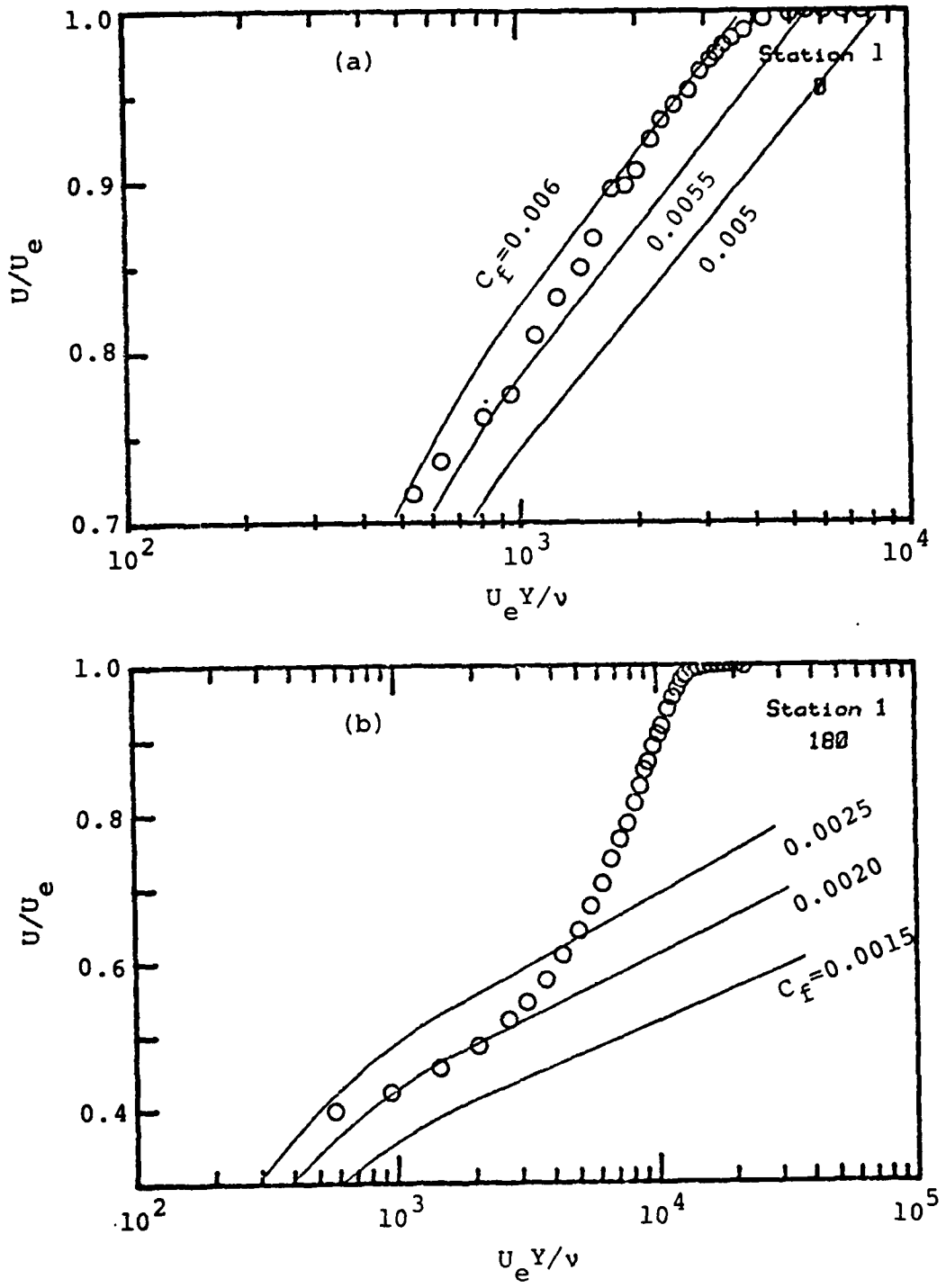

Figure 7. Clauser plots at station 1,
(a) windward plane, (b) leeward plane.

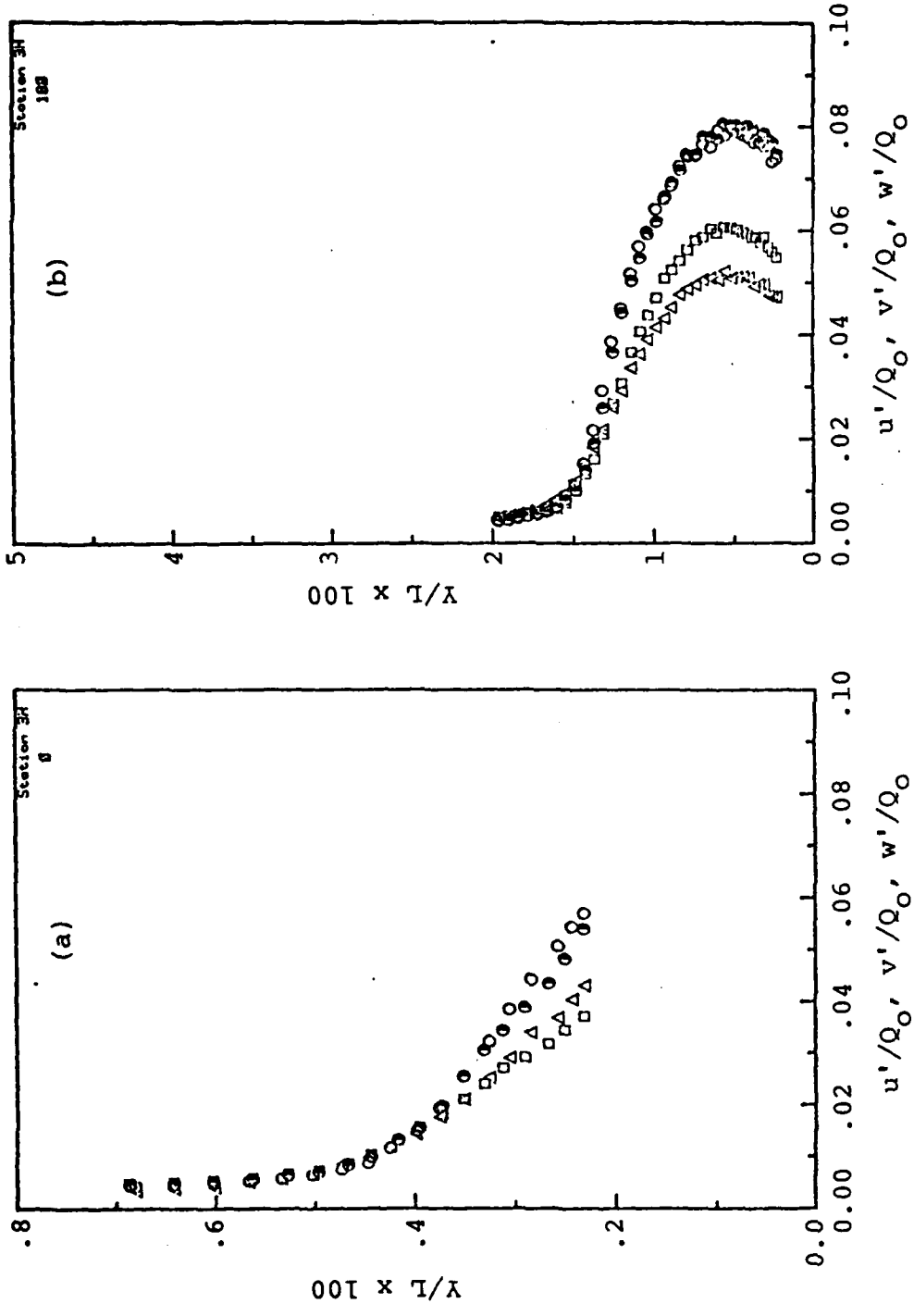

Figure 8. Turbulence intensities, (a) windward plane, (b) leeward plane. o: u'(u-v); ●: u'(u-w); Δ: v'; □: w', (station 3H)

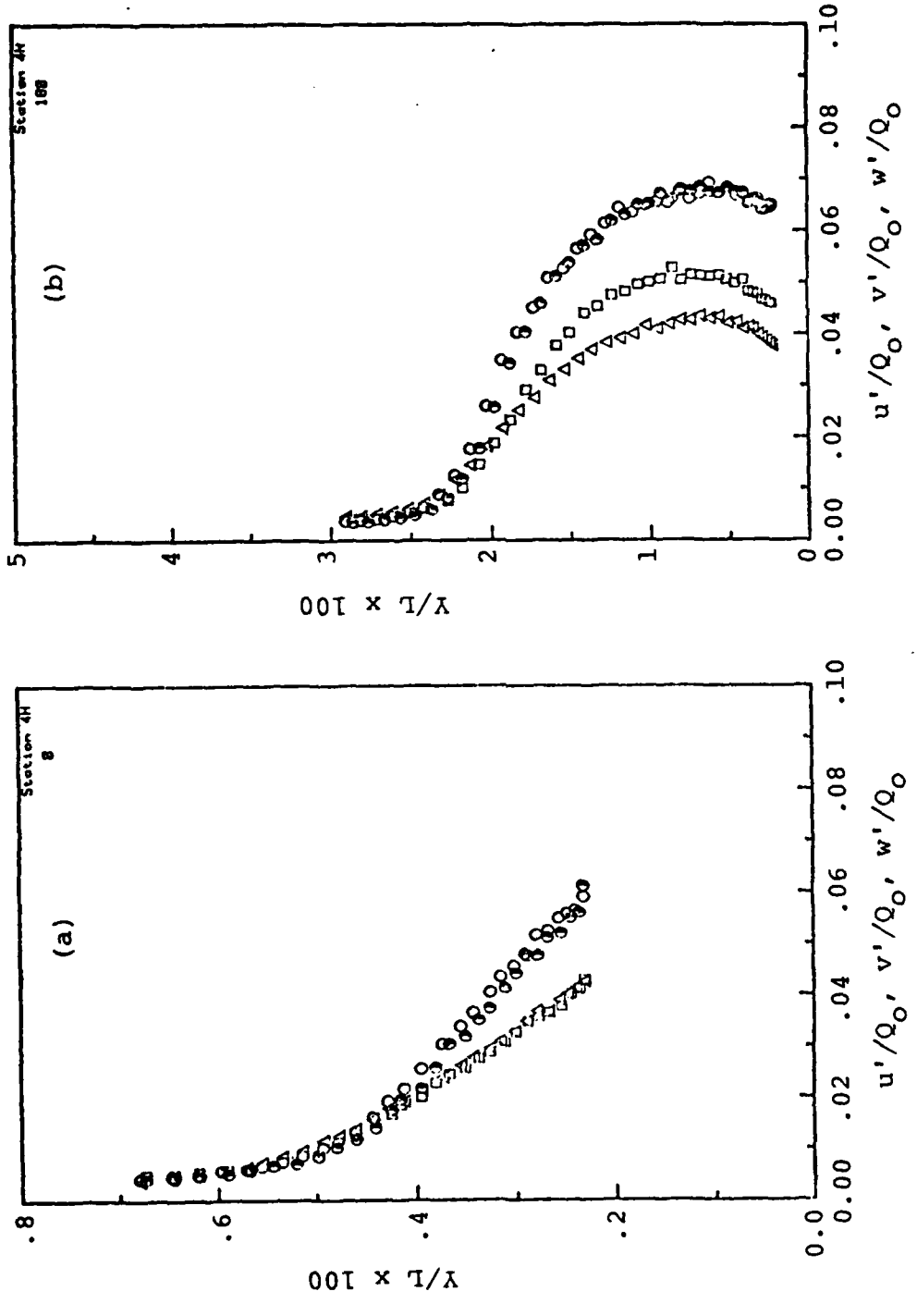

Figure 8. Continued (station 4H)

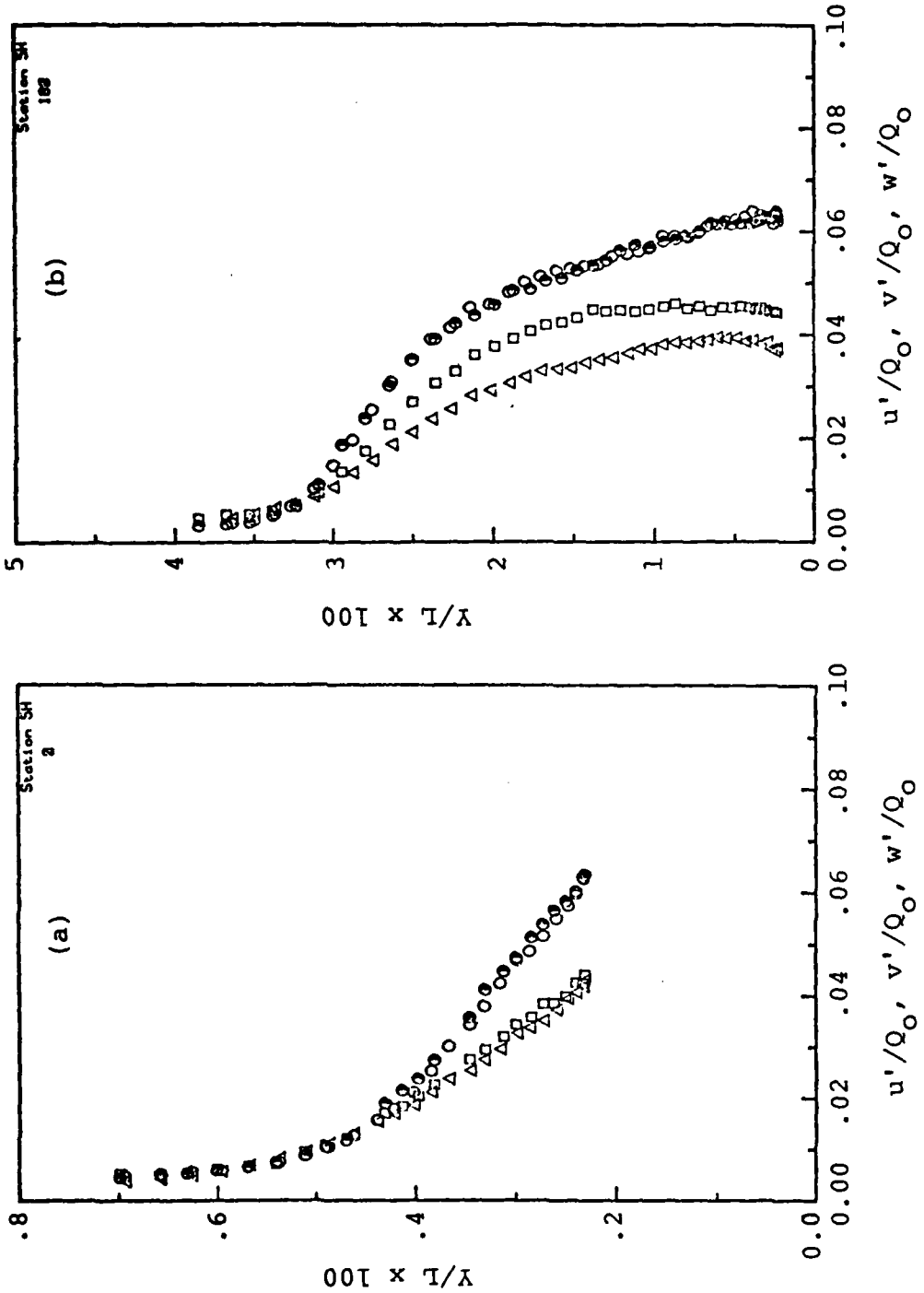

Figure 8. Continued (station 5H)

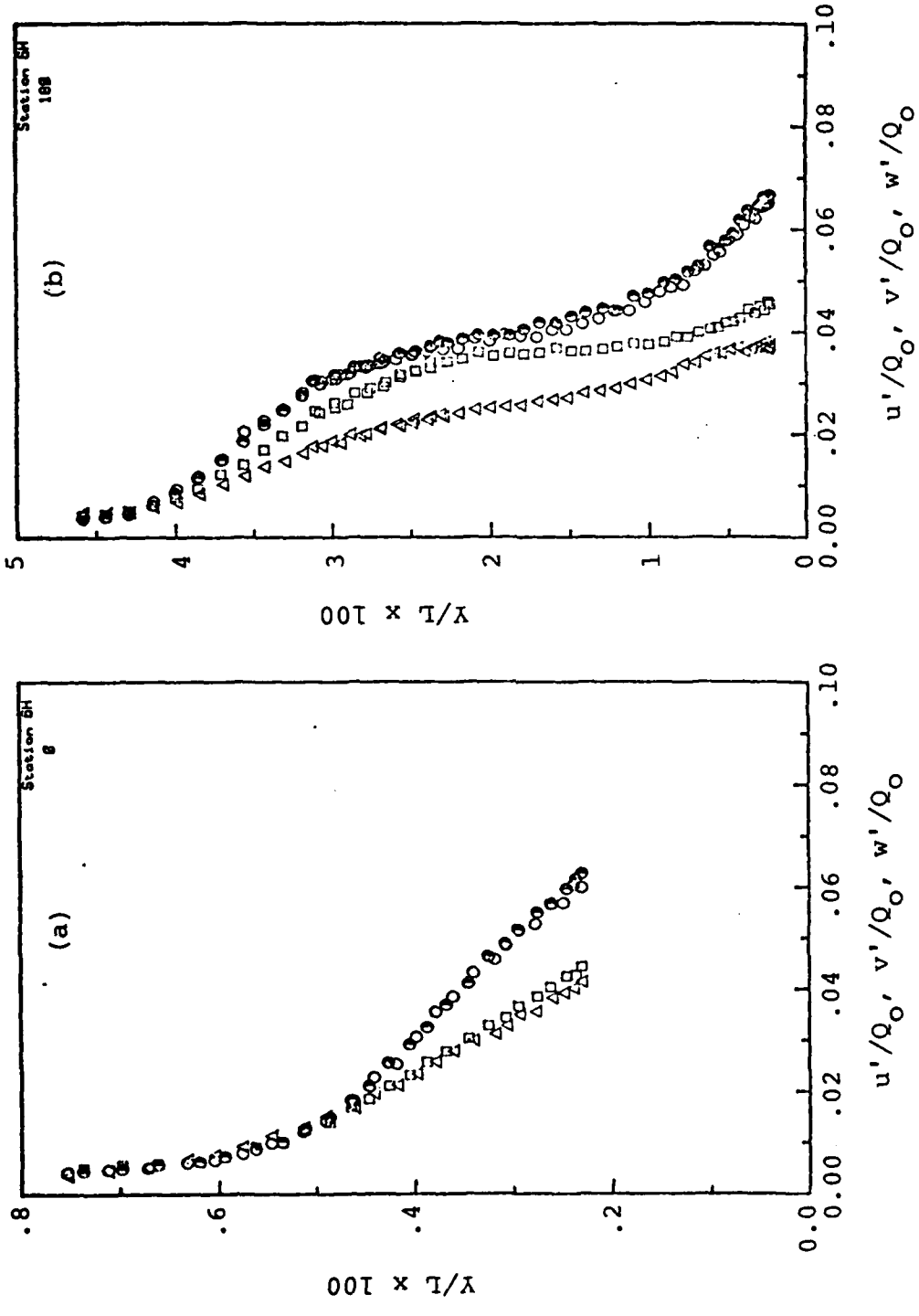

Figure 8. Continued (station 6H)

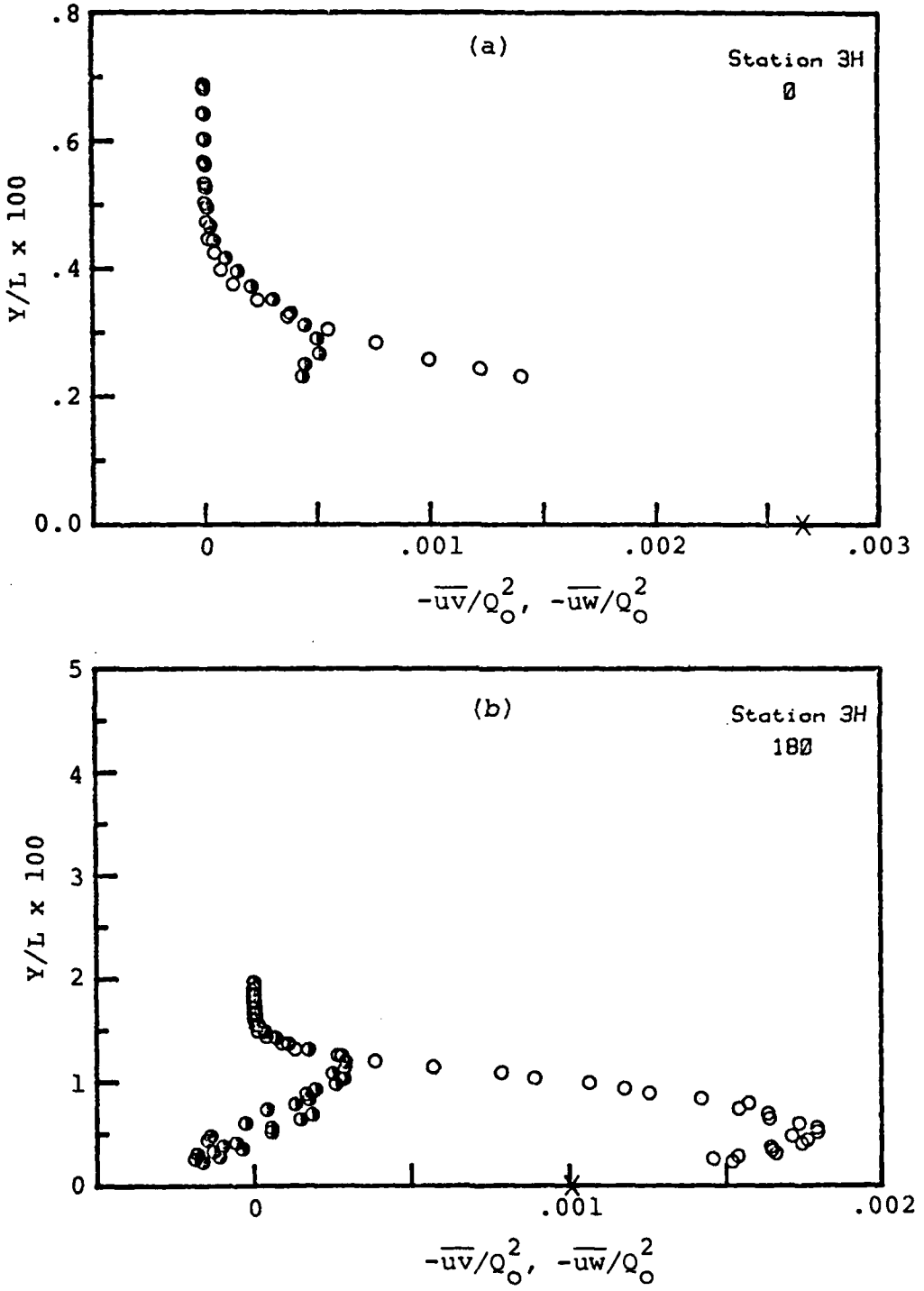

Figure 9. Reynolds shear-stress profiles, (a) windward plane, (b) leeward plane. o; $\overline{uv}$, ●; $\overline{uw}$, x; $C_f/2$ on the wall, (station 3H)

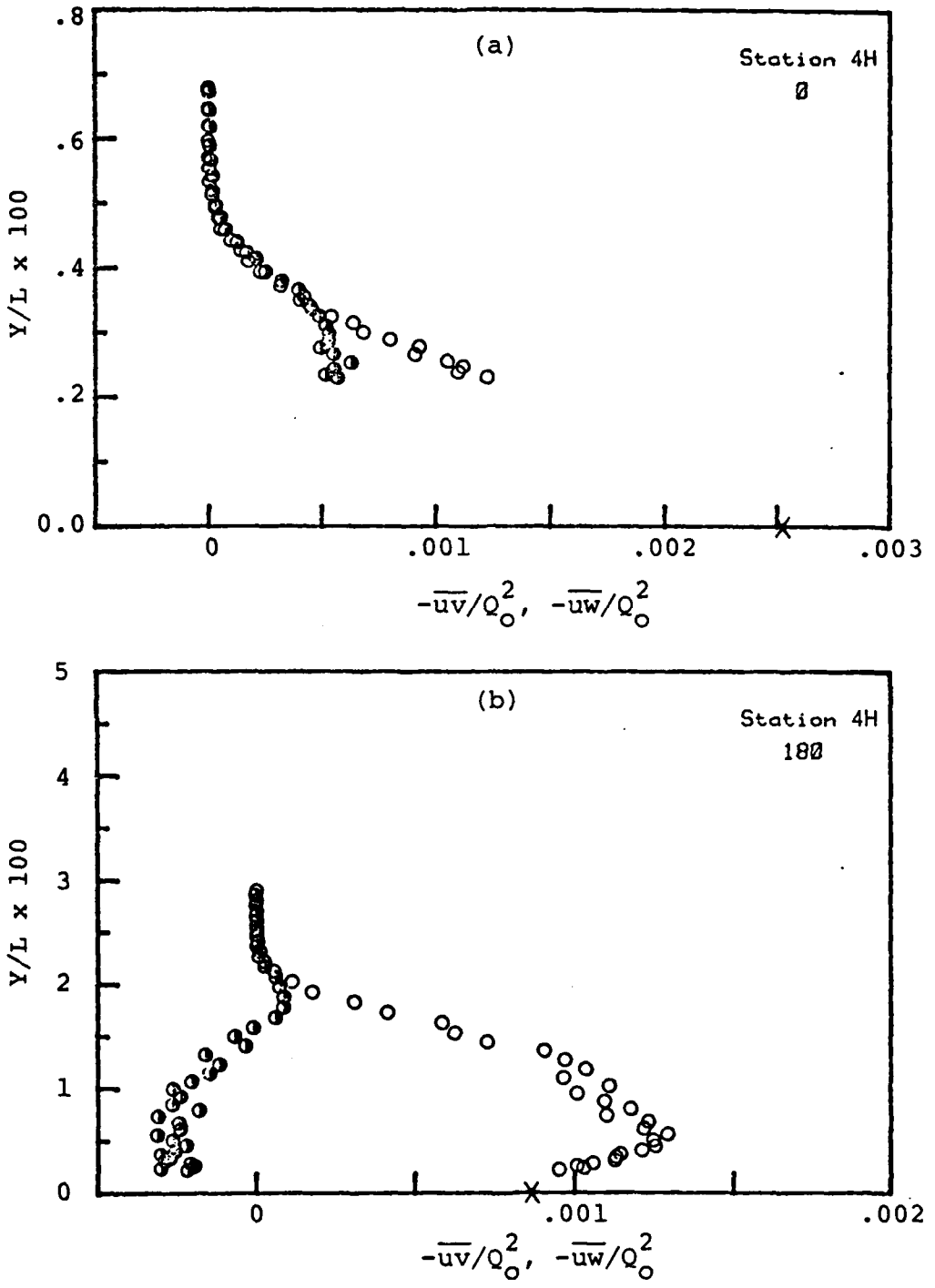

Figure 9. Continued (station 4H)

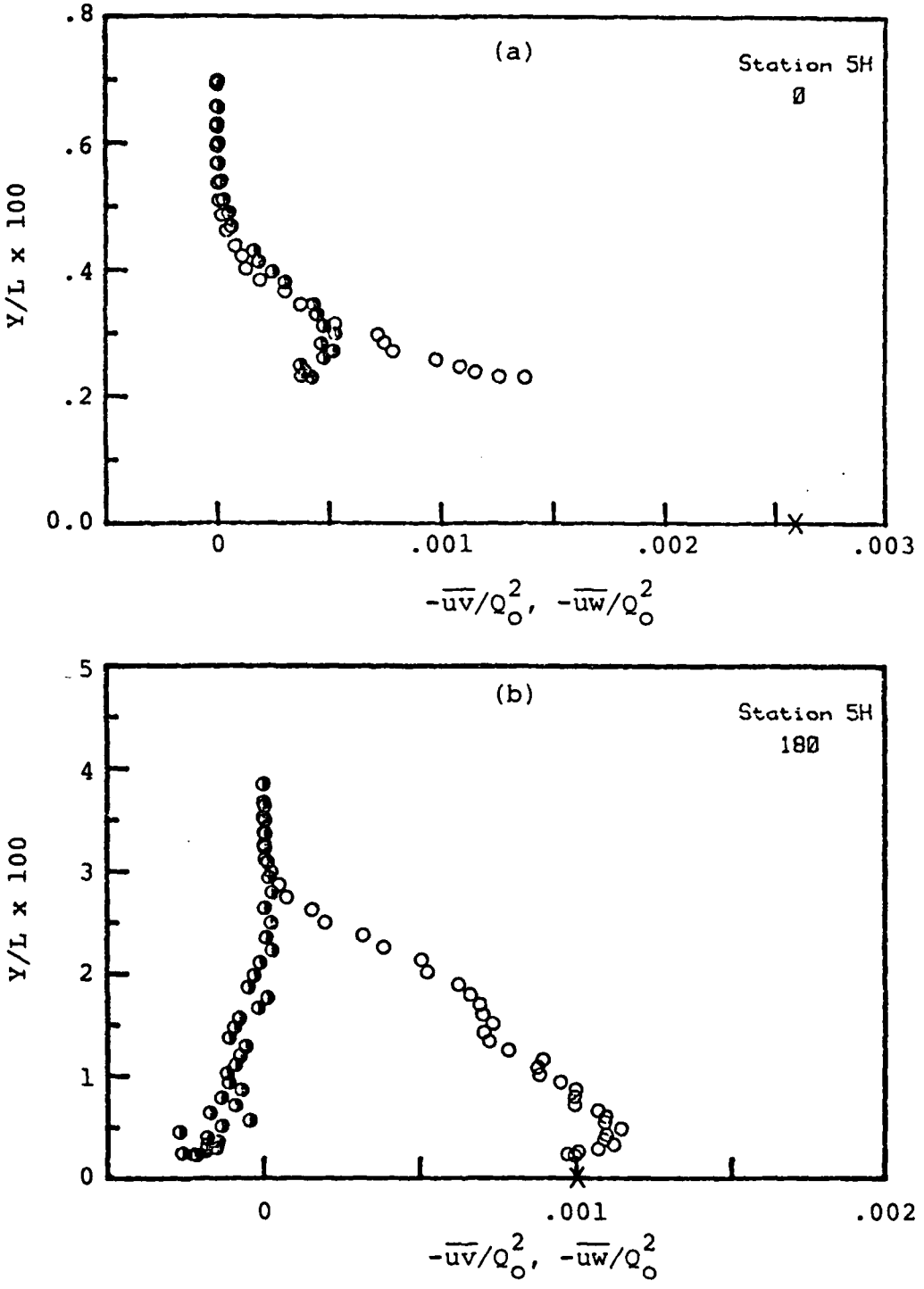

Figure 9. Continued (station 5H)

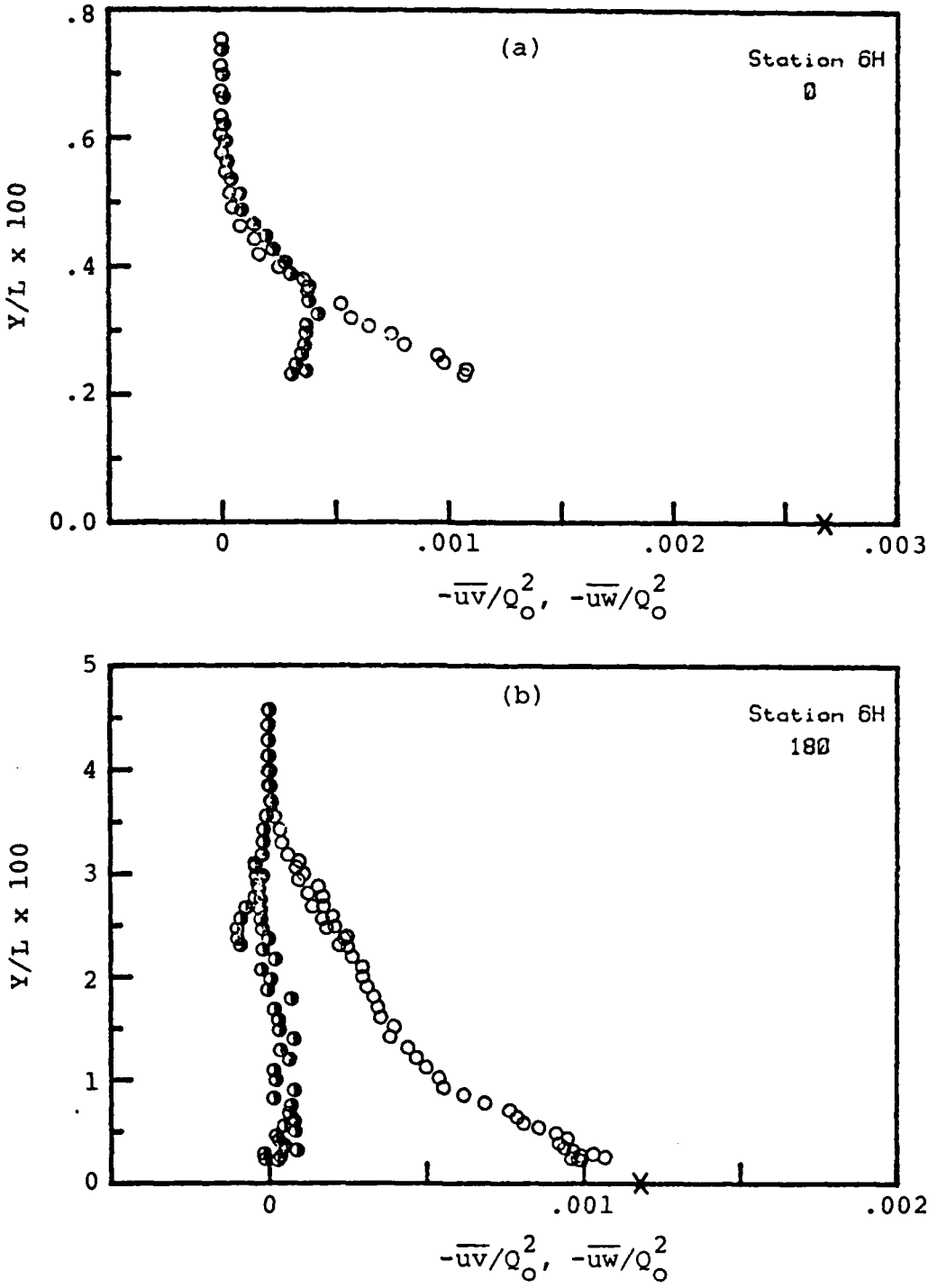

Figure 9. Continued (station 6H)

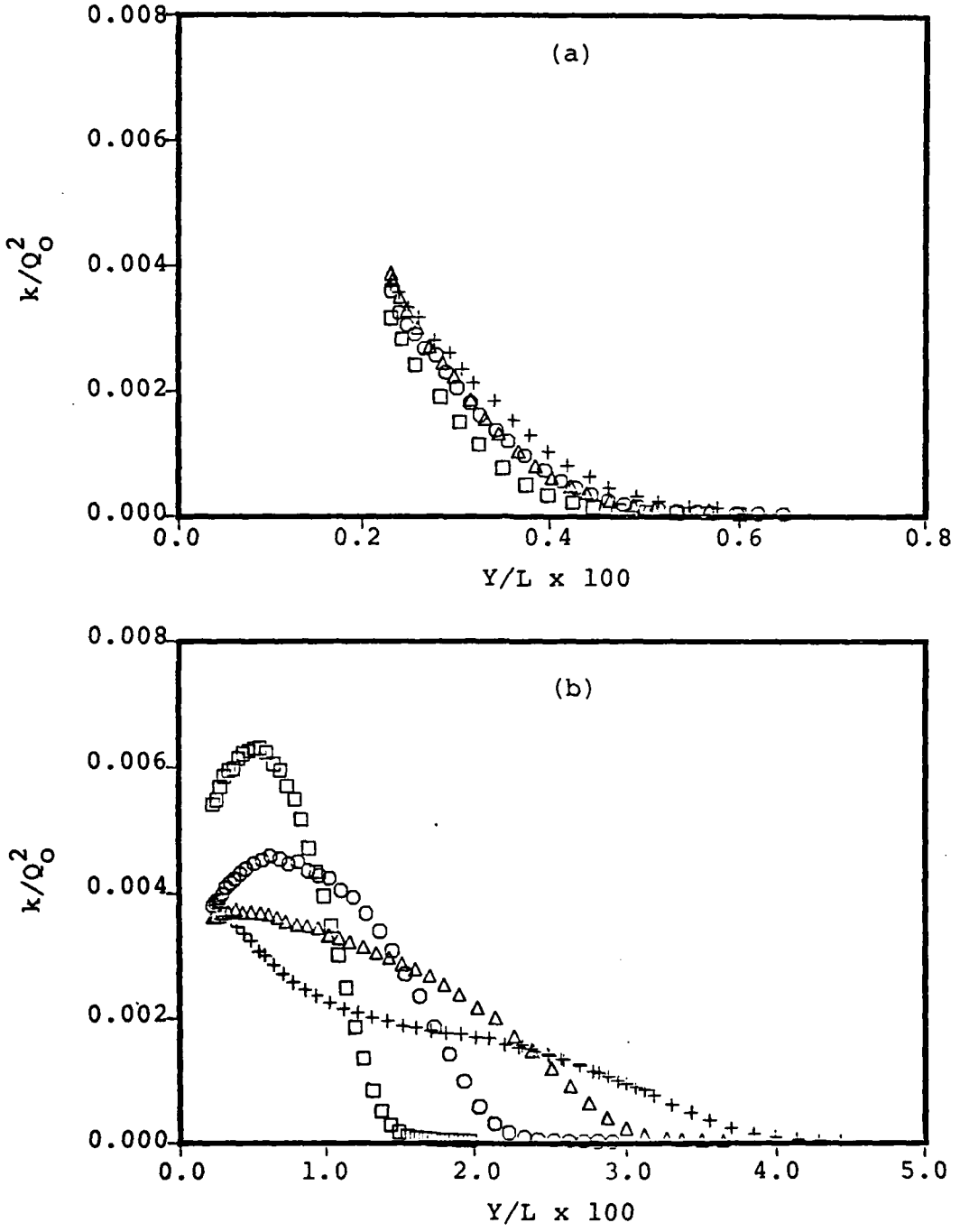

Figure 10. Turbulent kinetic energy distribution, (a) windward plane, (b) leeward plane. □;station 3H, o;station 4H, Δ;station 5H +;station 6H

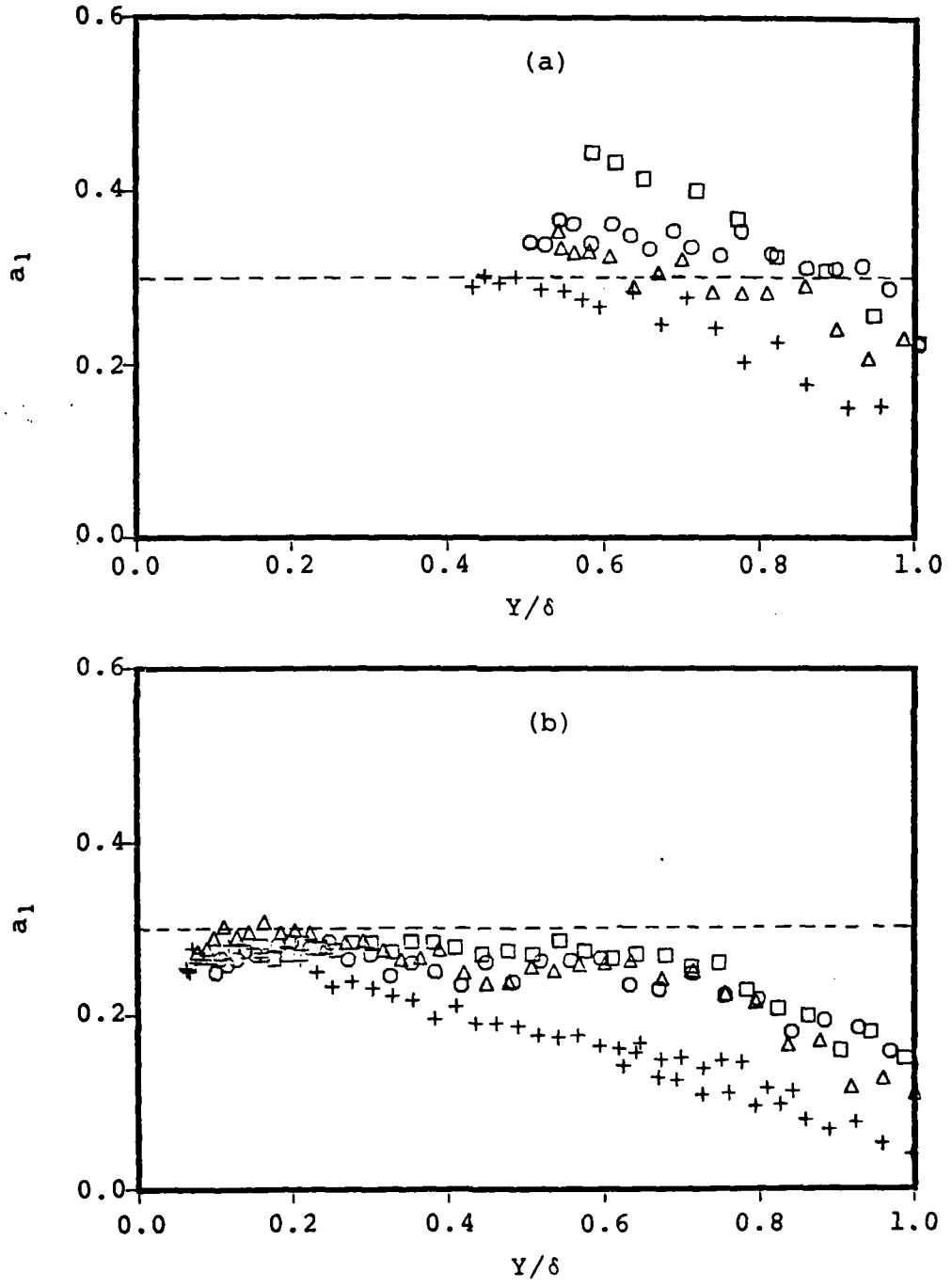

Figure 11. Structural similarity parameter, (a) windward plane, (b) leeward plane. □;station 3H, o;station 4H, Δ;station 5H, +;station 6H

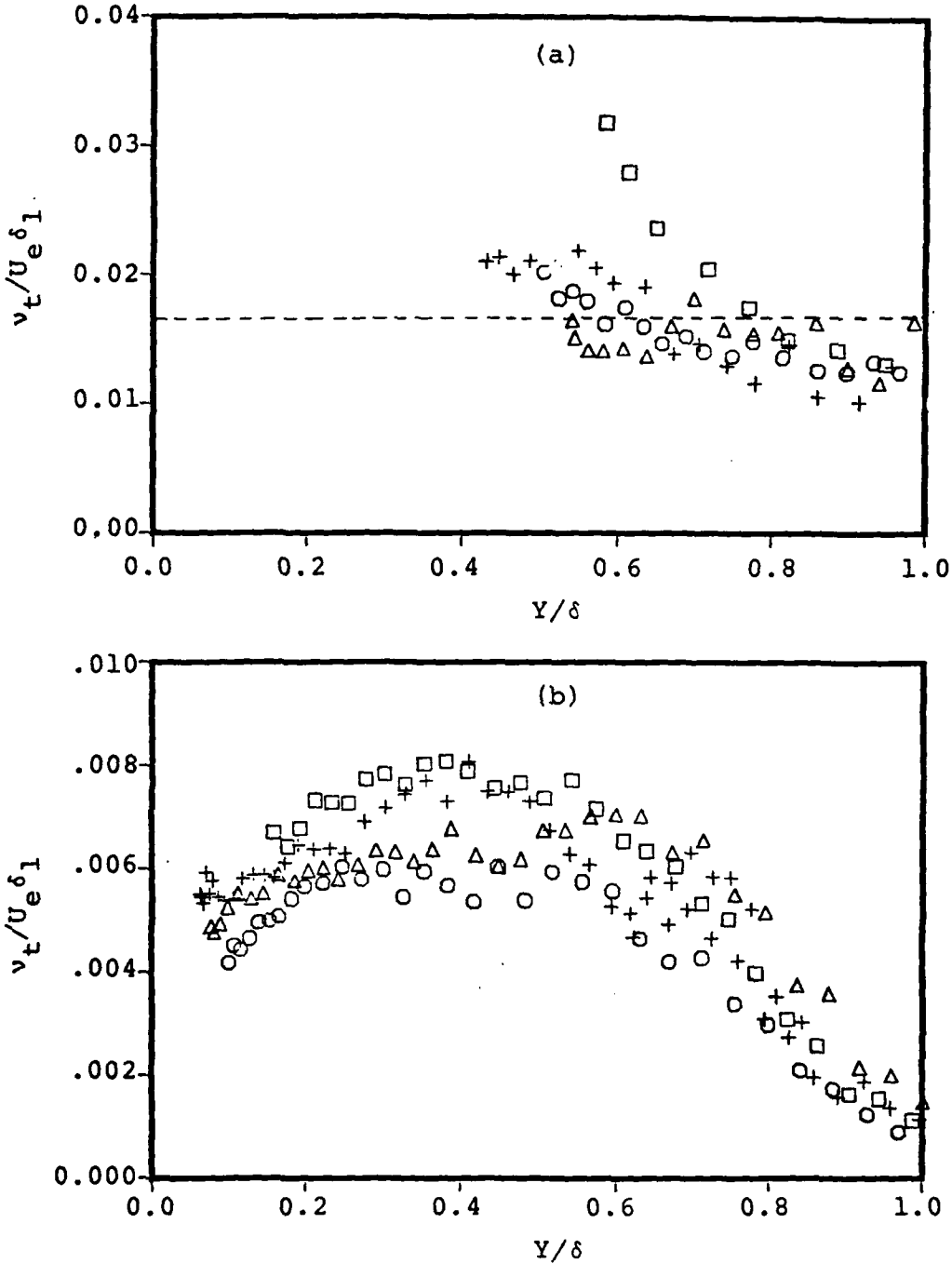

Figure 12. Eddy-viscosity distributions, (a) windward plane, (b) leeward plane. □;station 3H, o;station 4H, △;station5H, +;station 6H

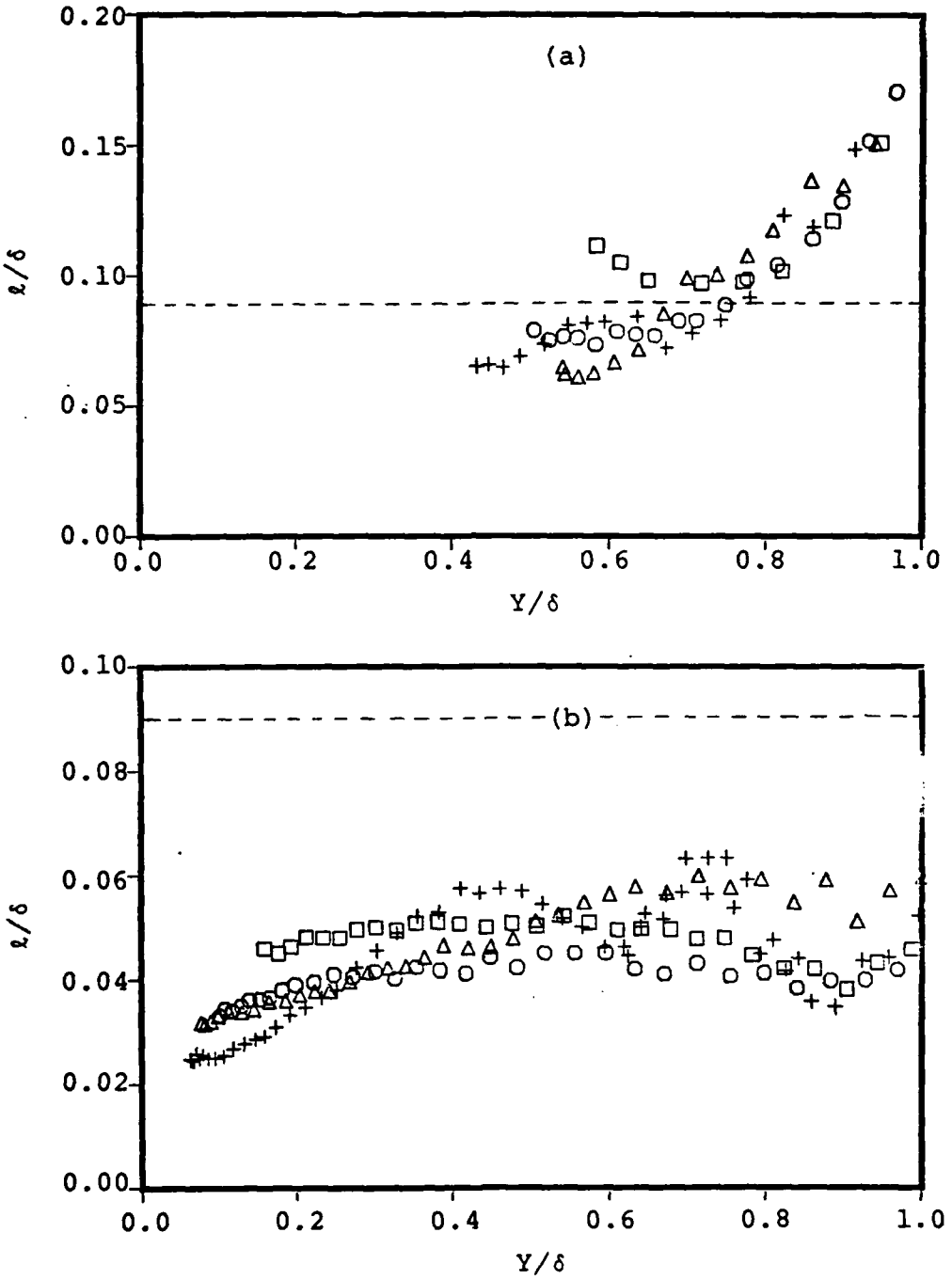

Figure 13. Mixing-length distributions, (a) windward plane, (b) leeward plane. □;station 3H, o;station 4H, Δ;station 5H, +;station 6H

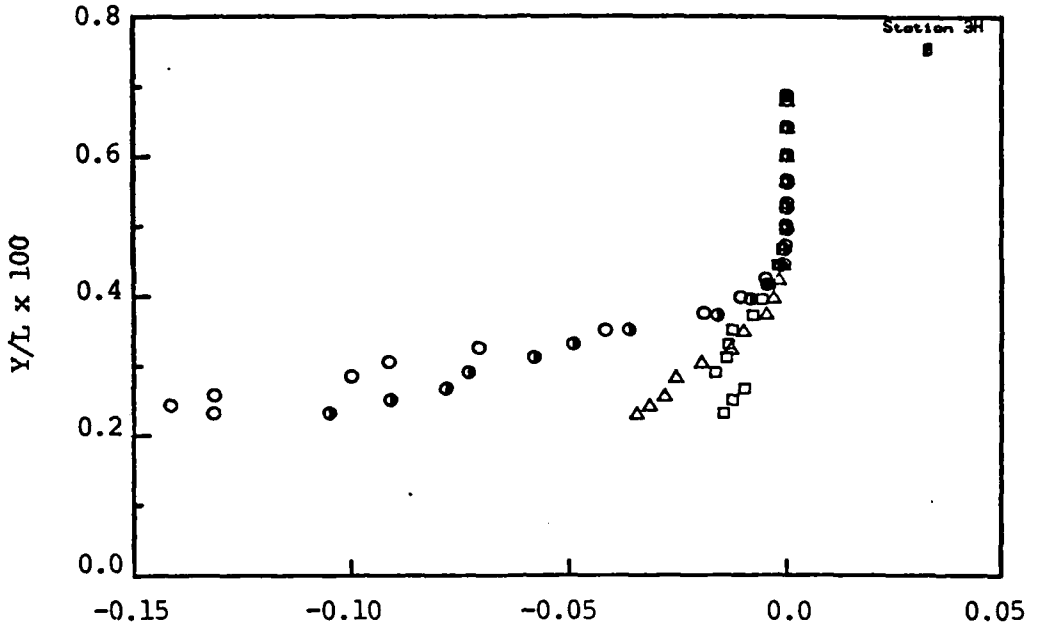

(a)

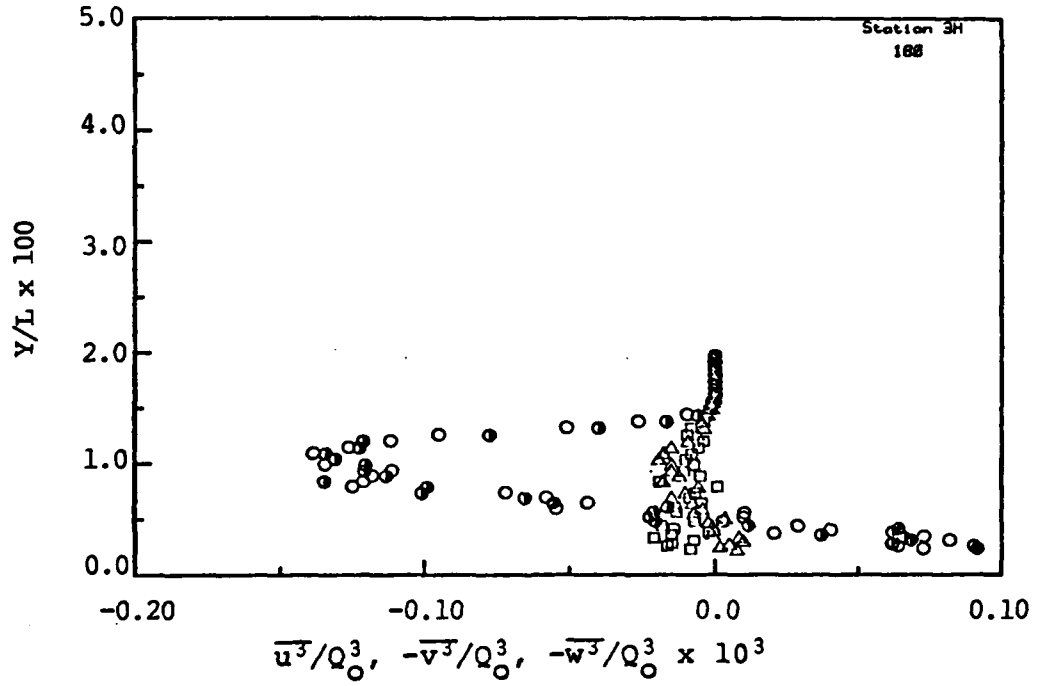

(b)

Figure 14. Triple correlations, (a) windward plane, (b) leeward plane. o:$\overline{u^3}$(u-v); o:$\overline{u^3}$(u-w) Δ:$\overline{v^3}$; □ :$\overline{w^3}$, (station 3H)

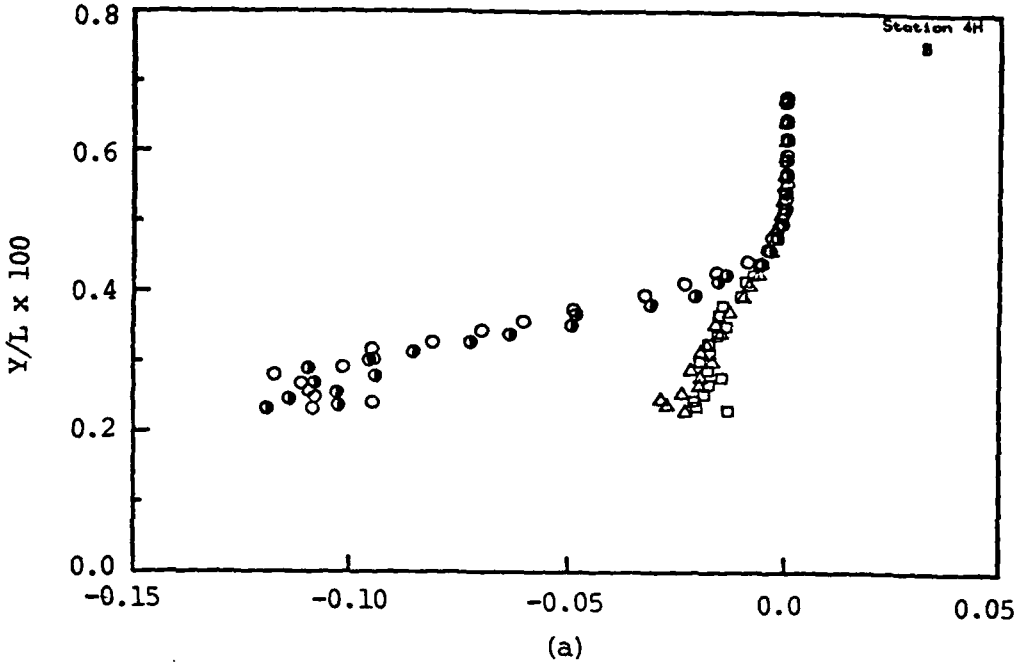

(a)

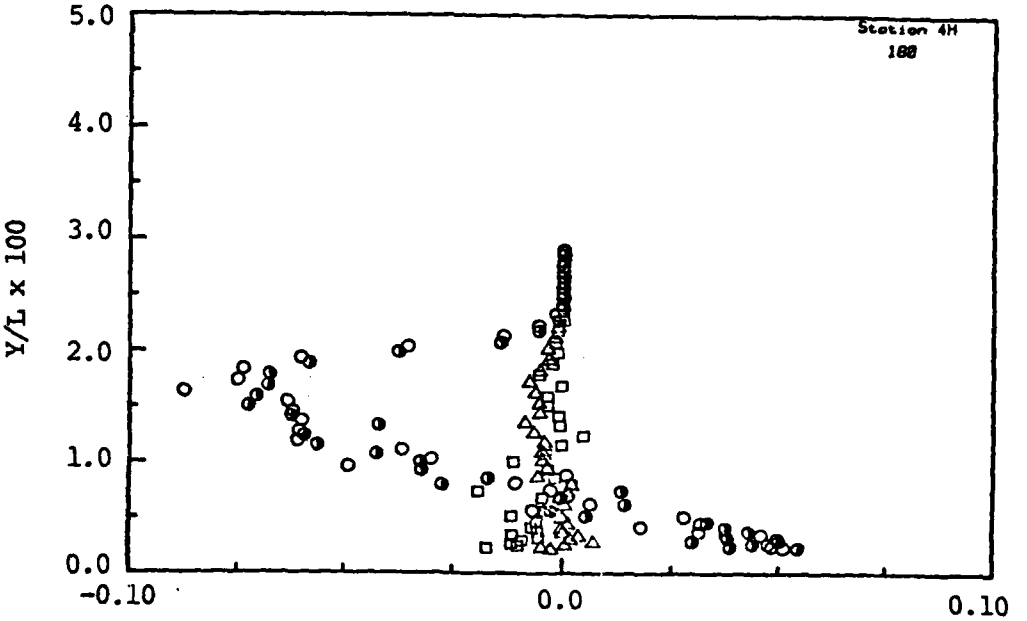

$\overline{u^3}/Q_o^3$, $-\overline{v^3}/Q_o^3$, $-\overline{w^3}/Q_o^3$ x 10^3

(b)

Figure 14. Continued (station 4H)

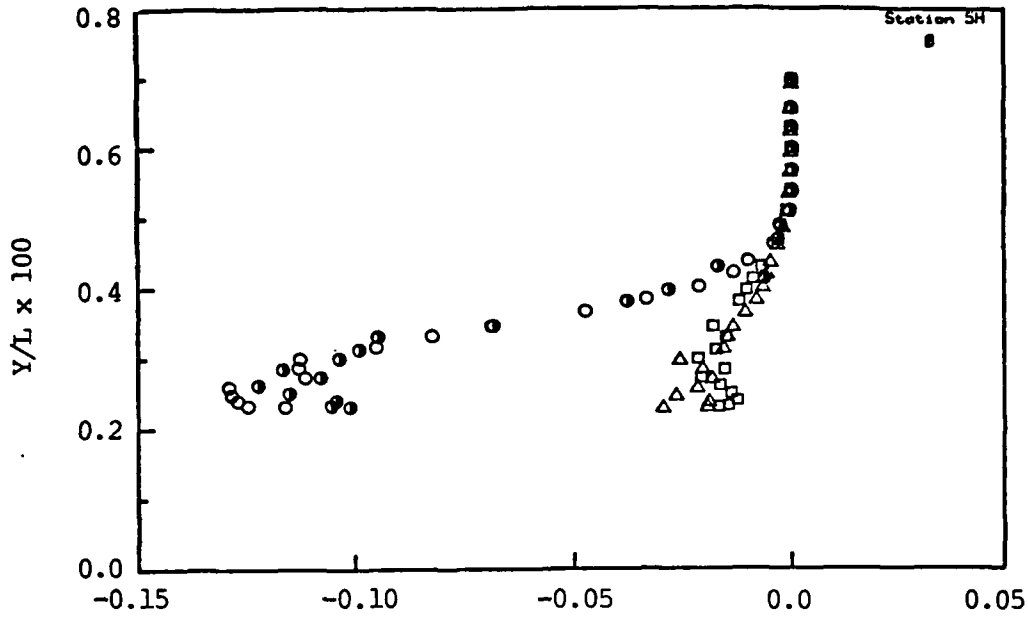

(a)

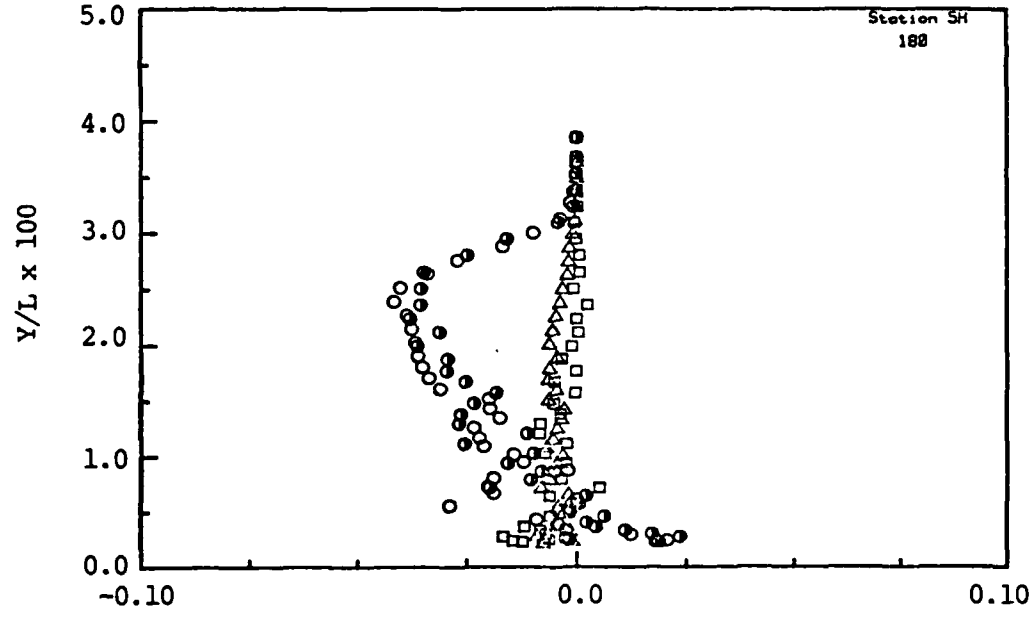

(b)

Figure 14. Continued (station 5H)

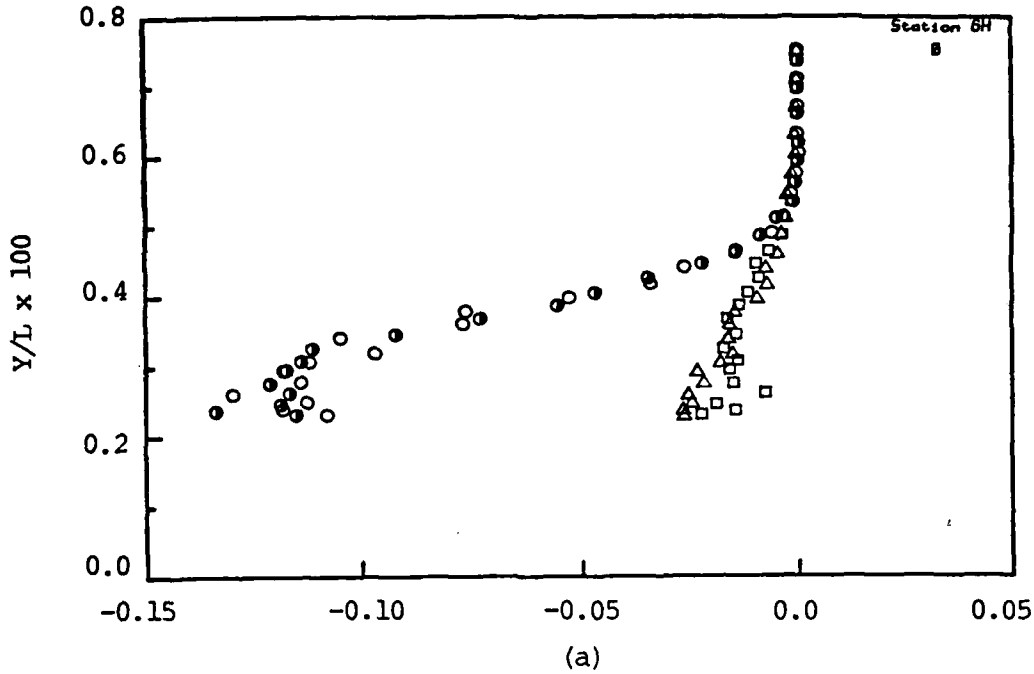

(a)

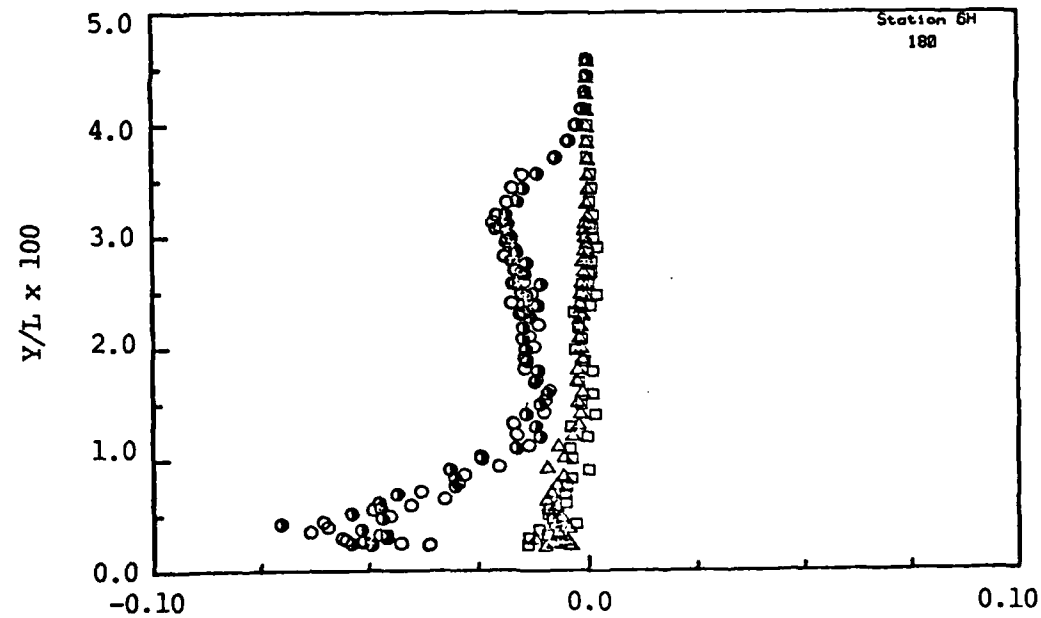

$\overline{u^3}/Q_o^3$, $-\overline{v^3}/Q_o^3$, $-\overline{w^3}/Q_o^3 \times 10^3$

(b)

Figure 14. Continued (station 6H)

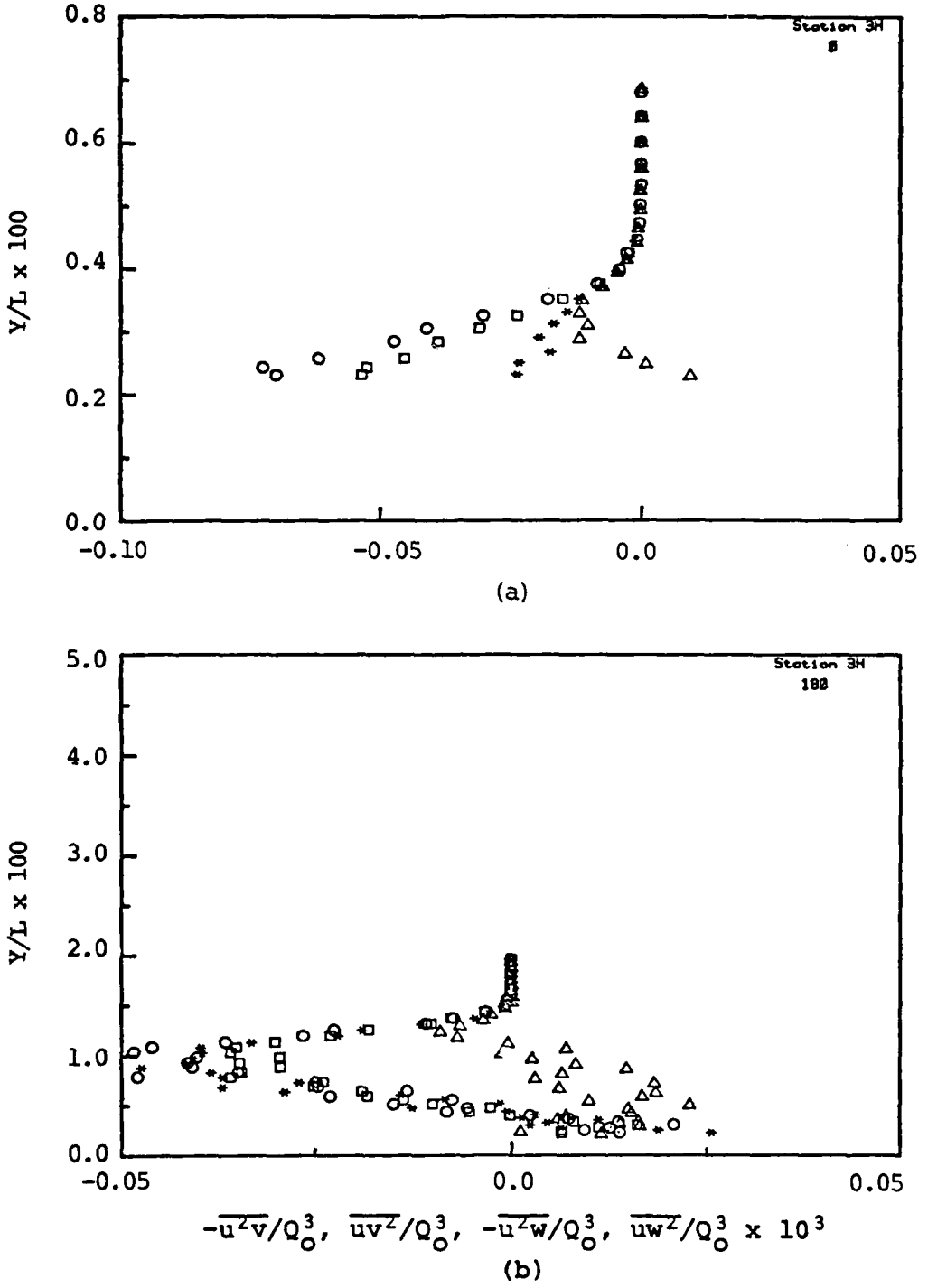

Figure 15. Triple correlations, (a) windward plane, (b) leeward plane. o:$\overline{u^2v}$; □ :$\overline{uv^2}$; Δ:$\overline{u^2w}$; ✕:$\overline{uw^2}$; (station 3H)

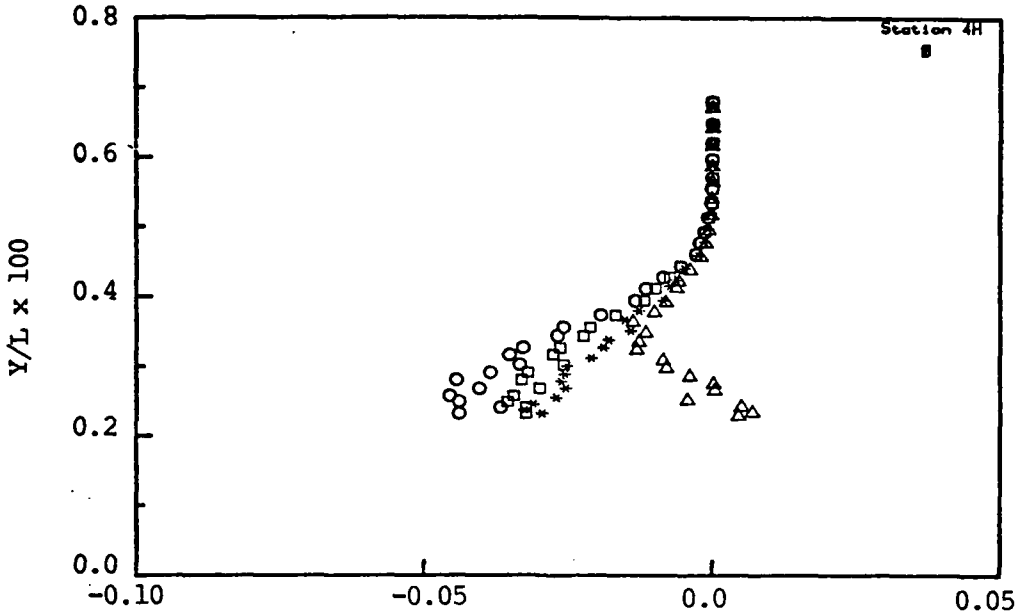

(a)

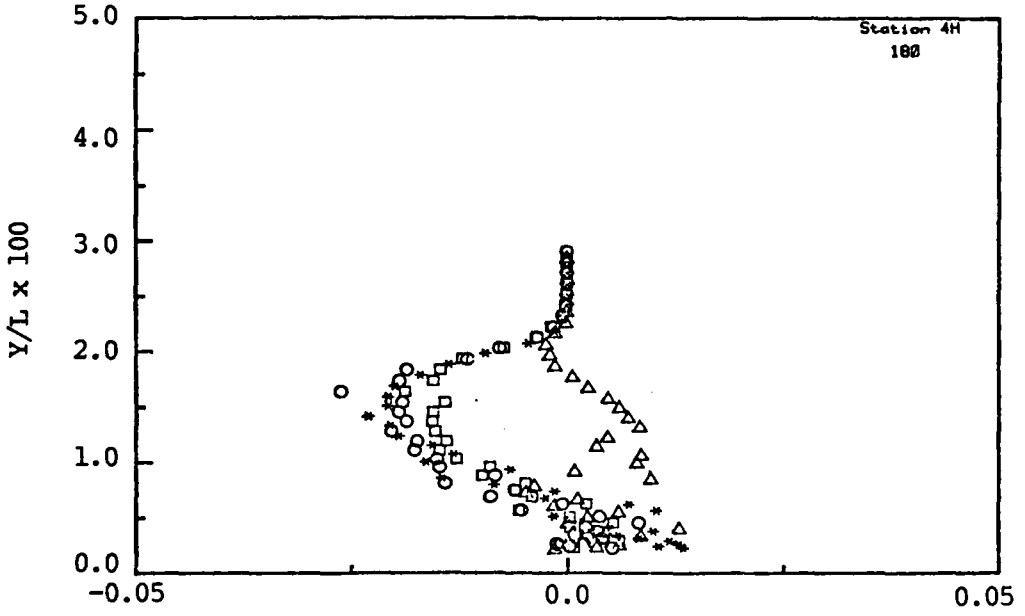

$-\overline{u^2v}/Q_o^3$, $\overline{uv^2}/Q_o^3$, $-\overline{u^2w}/Q_o^3$, $\overline{uw^2}/Q_o^3$ x 10^3

(b)

Figure 15. Continued (station 4H)

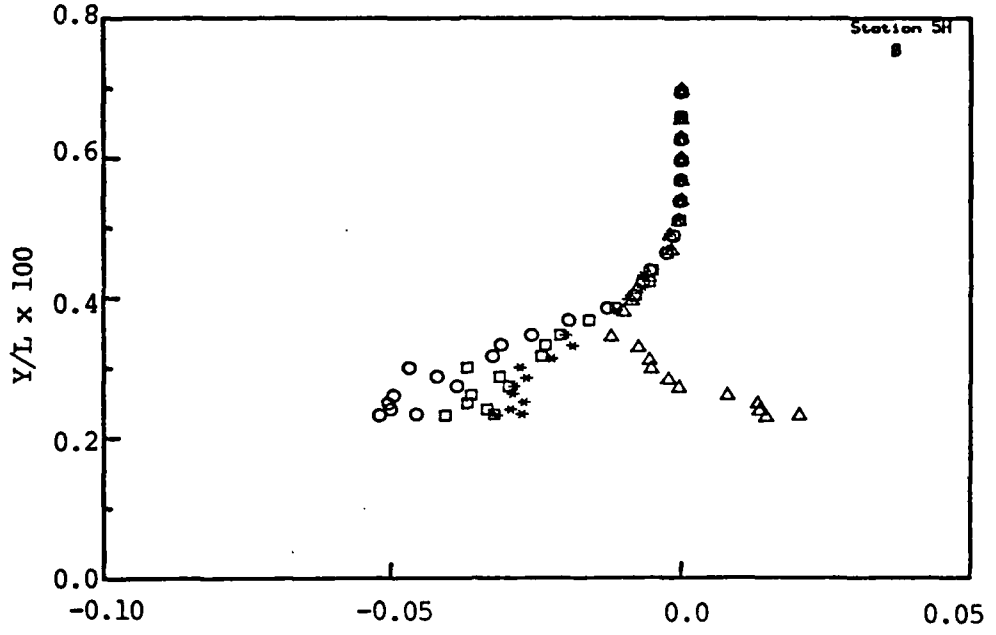

(a)

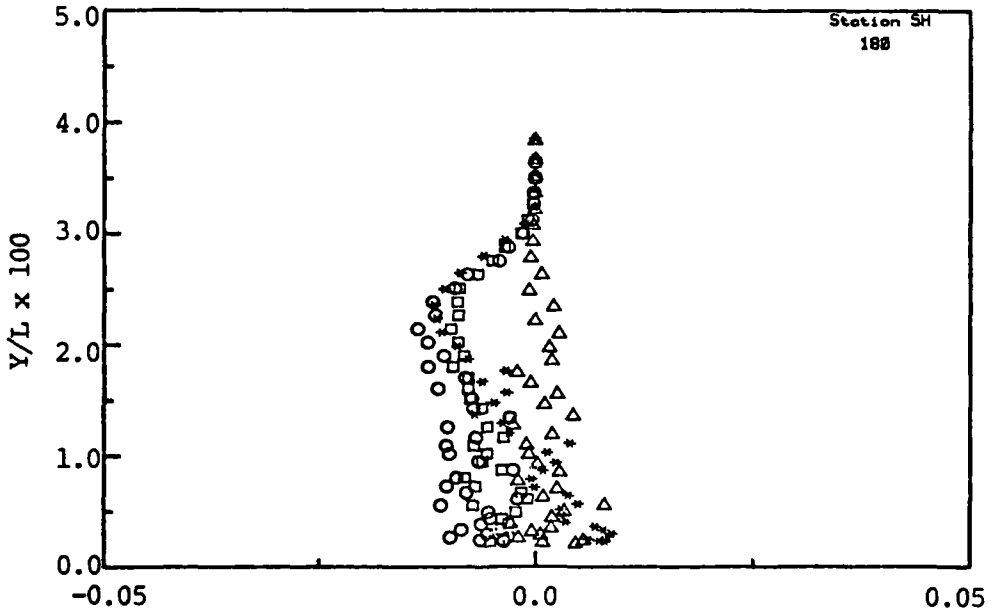

$-\overline{u^2v}/Q_o^3$, $\overline{uv^2}/Q_o^3$, $-\overline{u^2w}/Q_o^3$, $\overline{uw^2}/Q_o^3$ x 10^3

(b)

Figure 15. Continued (station 5H)

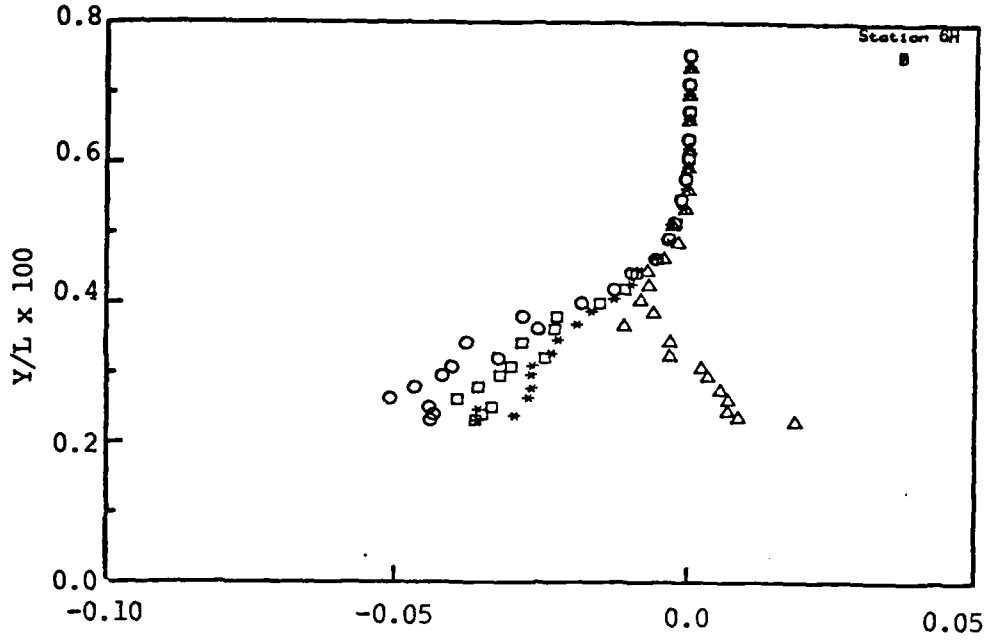

(a)

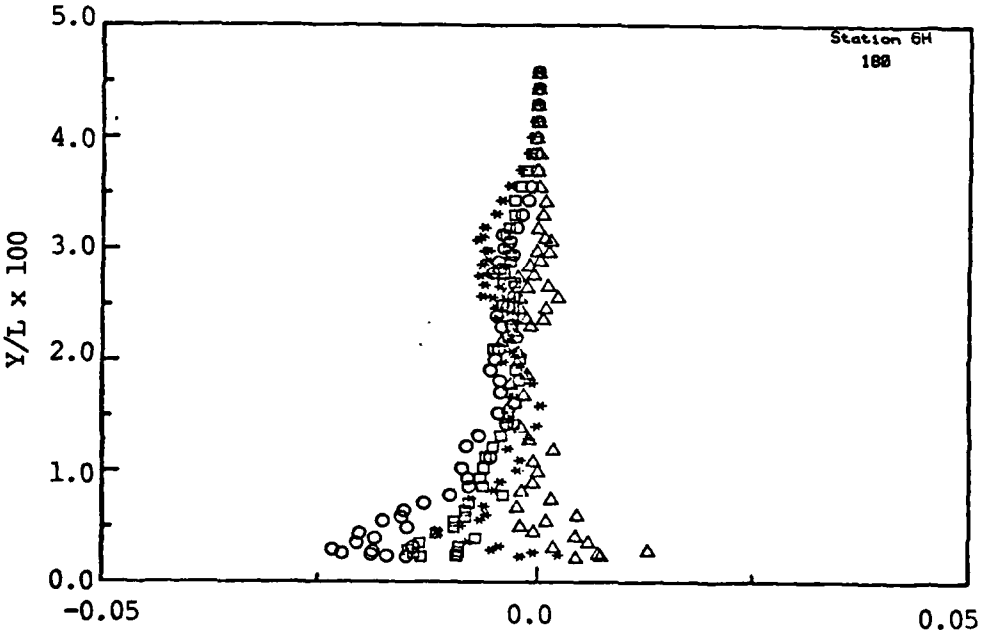

$-\overline{u^2v}/Q_o^3$, $\overline{uv^2}/Q_o^3$, $-\overline{u^2w}/Q_o^3$, $\overline{uw^2}/Q_o^3$ x 10^3

(b)

Figure 15. Continued (station 6H)

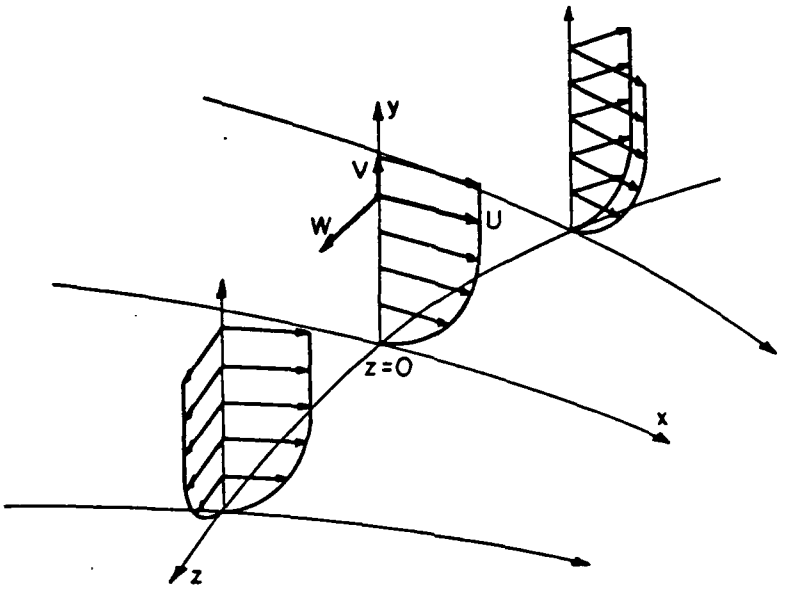

DIVERGENT FLOW

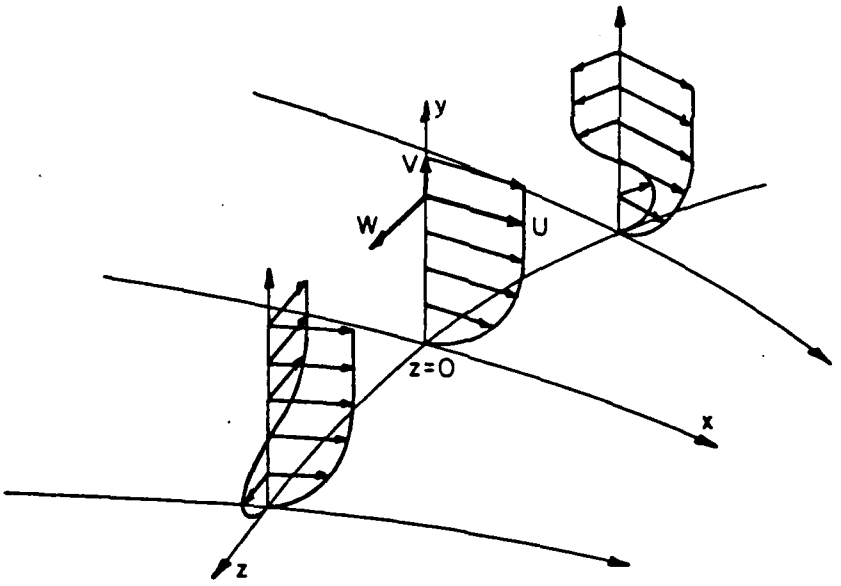

CONVERGENT AND DIVERGENT FLOW

Figure 16. Coordinate system for plane-of-symmetry flows

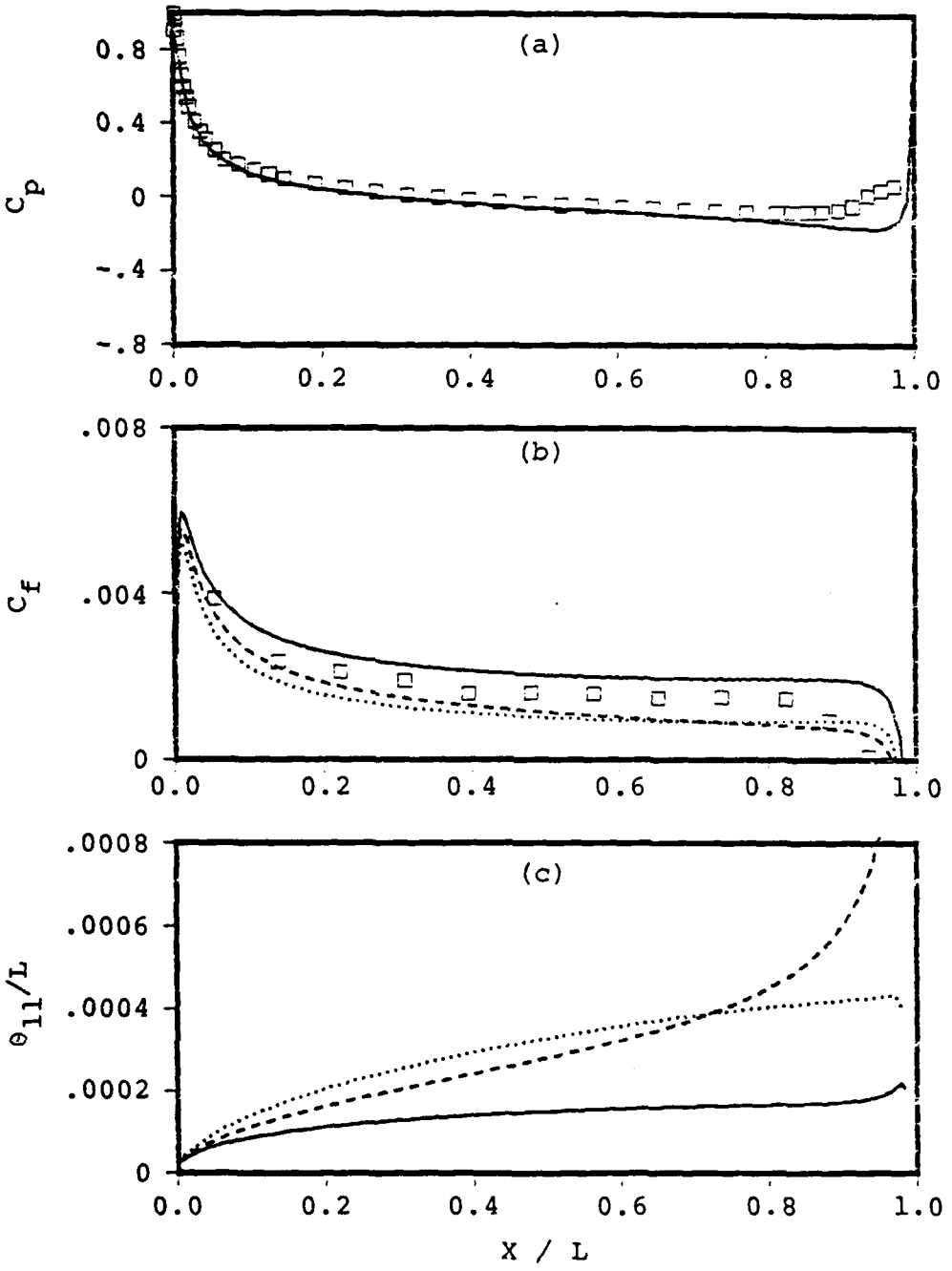

Figure 17. Comparison of predictions with the experimental results on the 6:1 spheroid, windward plane, $\alpha = 10^{0}$, Re = 1.6 x 10^{6}. —— plane of symmetry flow, ... 2-D flow, --- axisymmetric flow

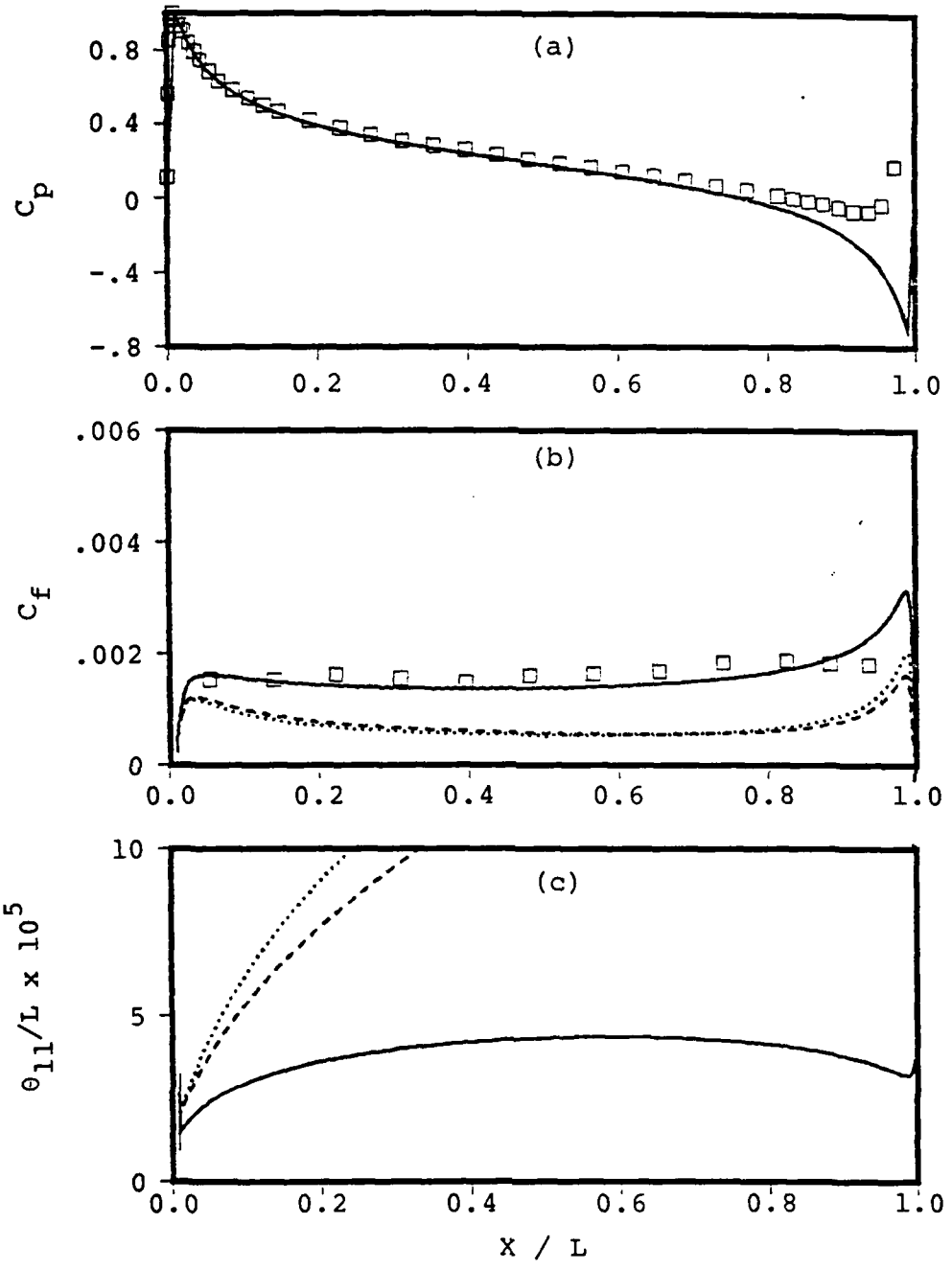

Figure 18. Comparison of predictions with the experimental results on the 6:1 spheroid, windward plane, $\alpha = 30^\circ$, $Re = 7.2 \times 10^6$. —— plane of symmetry flow, ... 2-D flow, --- axisymmetric flow

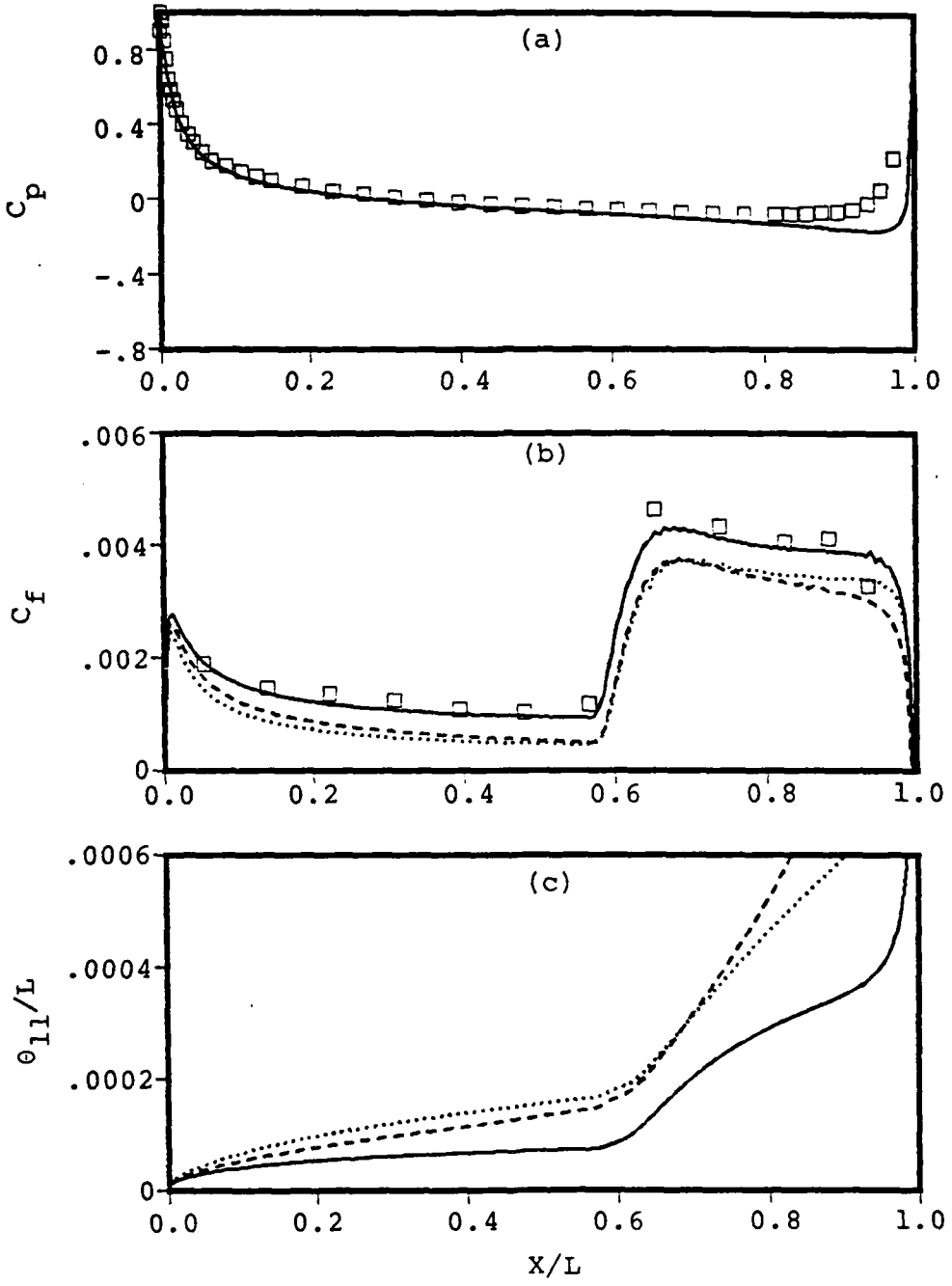

Figure 19. Comparison of predictions with the experimental results on the 6:1 spheroid, windward plane, $\alpha = 10^{\circ}$, Re = 7.2 x 10^6. —— plane of symmetry flow, ... 2-D flow, --- axisymmetric flow.

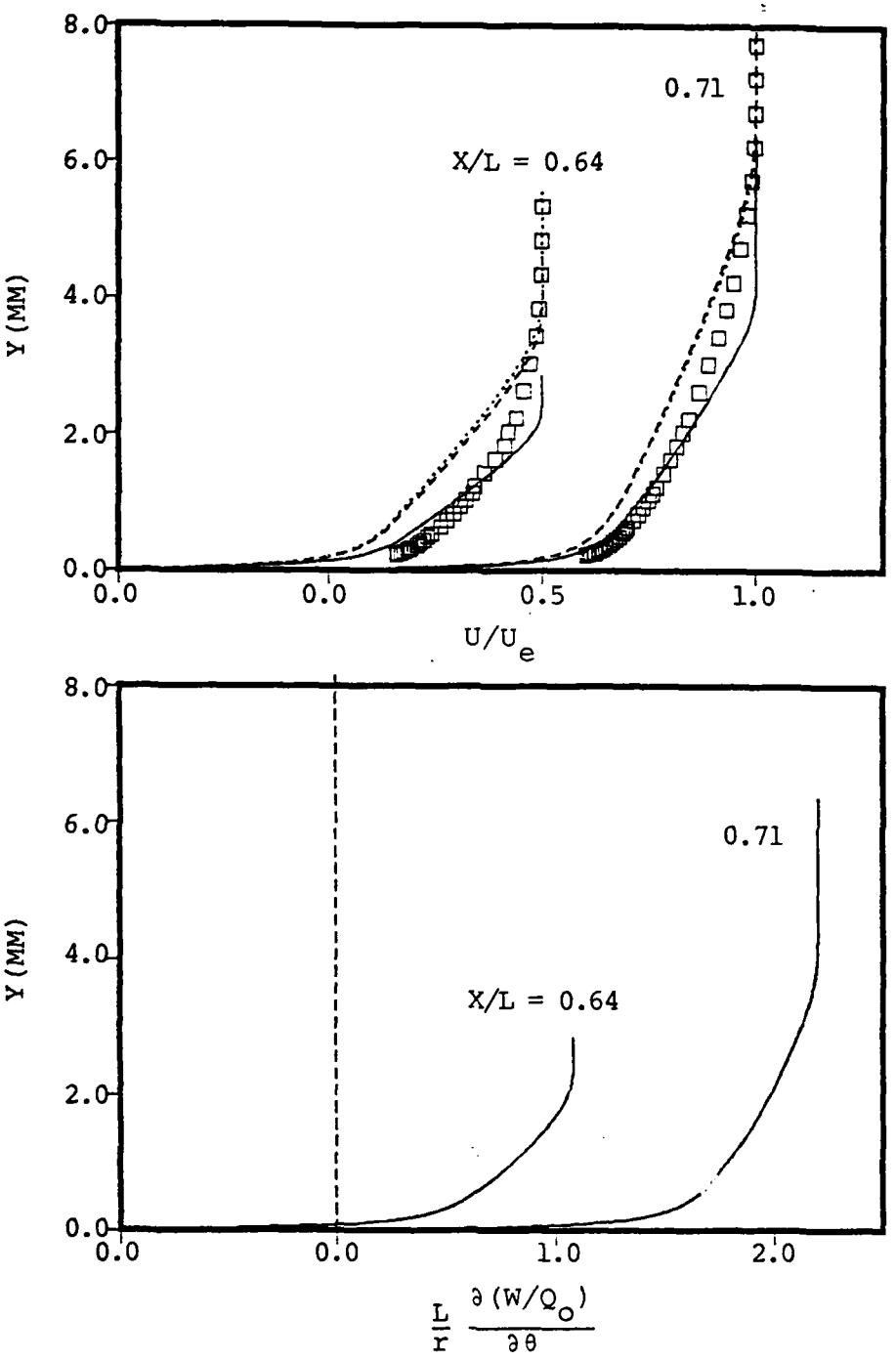

Figure 20. Velocity profiles predicted and measured on the 6:1 spheroid, windward plane, $\alpha = 10^{0}$, Re = 7.2×10^{6}. —— plane of symmetry flow, ... 2-D flow, --- axisymmetric flow.

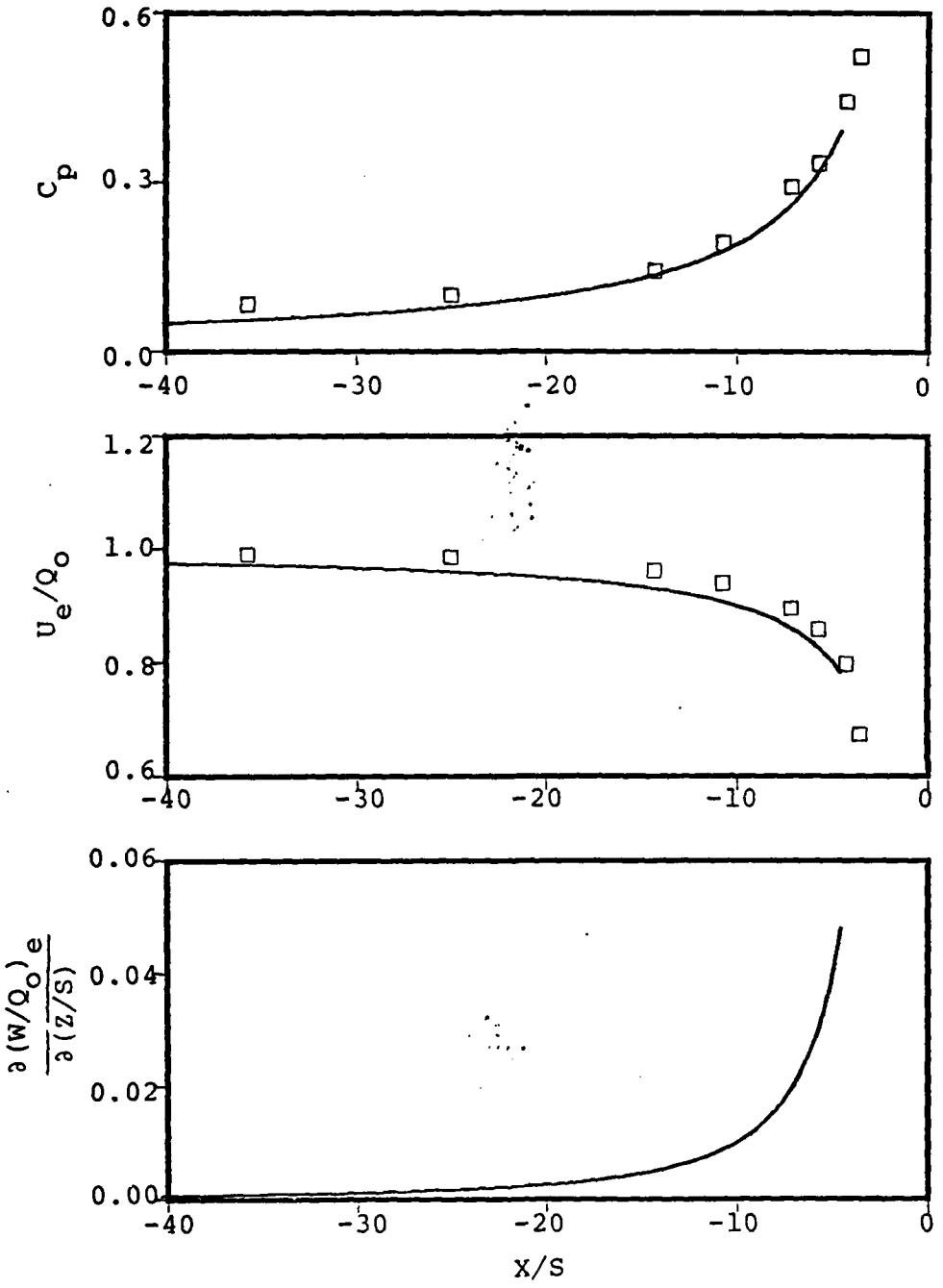

Figure 21. Measured and theoretical boundary conditions in Krogstad's experiment

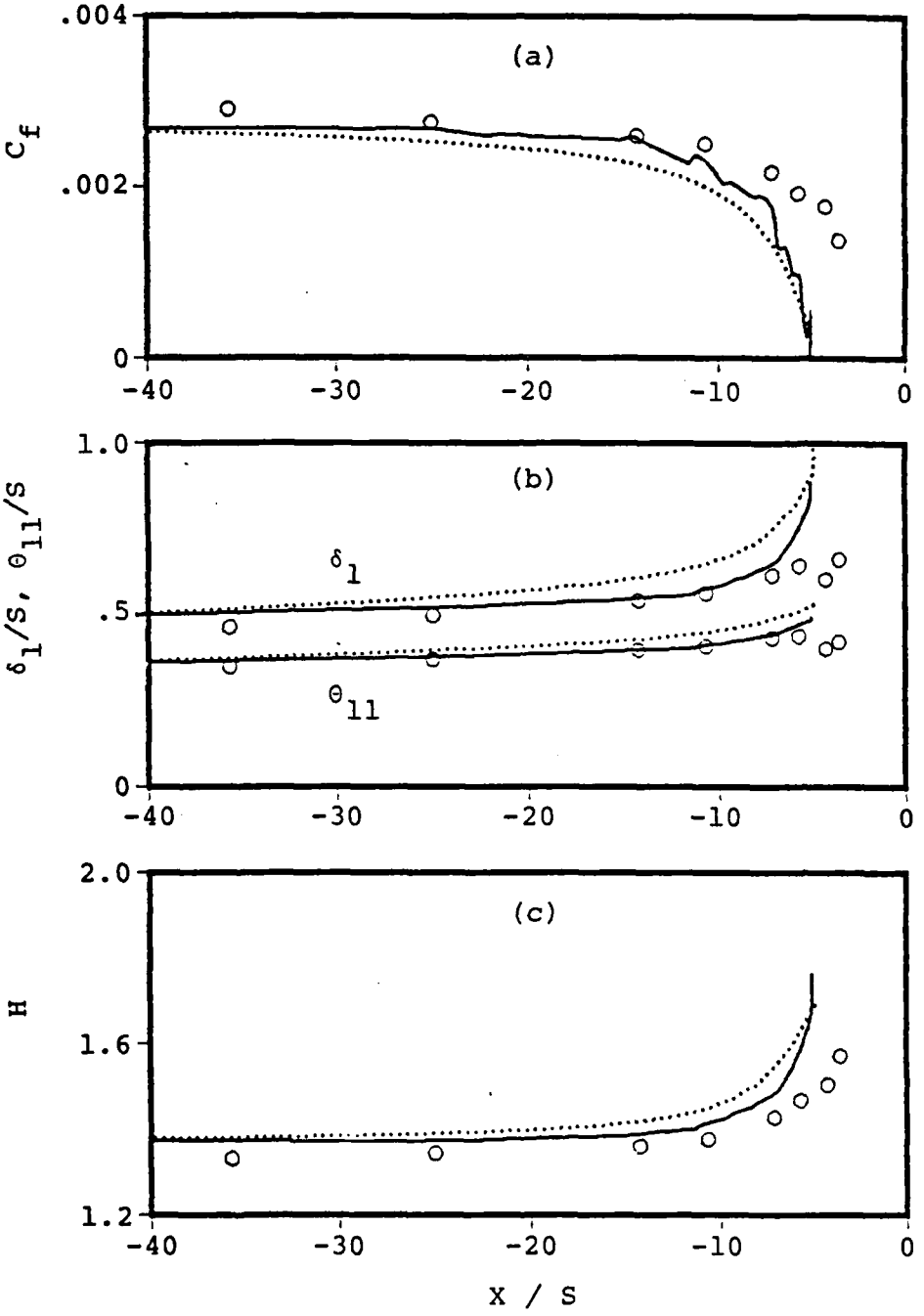

Figure 22. Comparison between measured and predicted integral parameters in Krogstad's experiment. o measurement, —— plane of symmetry flow(with experimental U_e), ... plane of symmetry flow(with potential U_e)

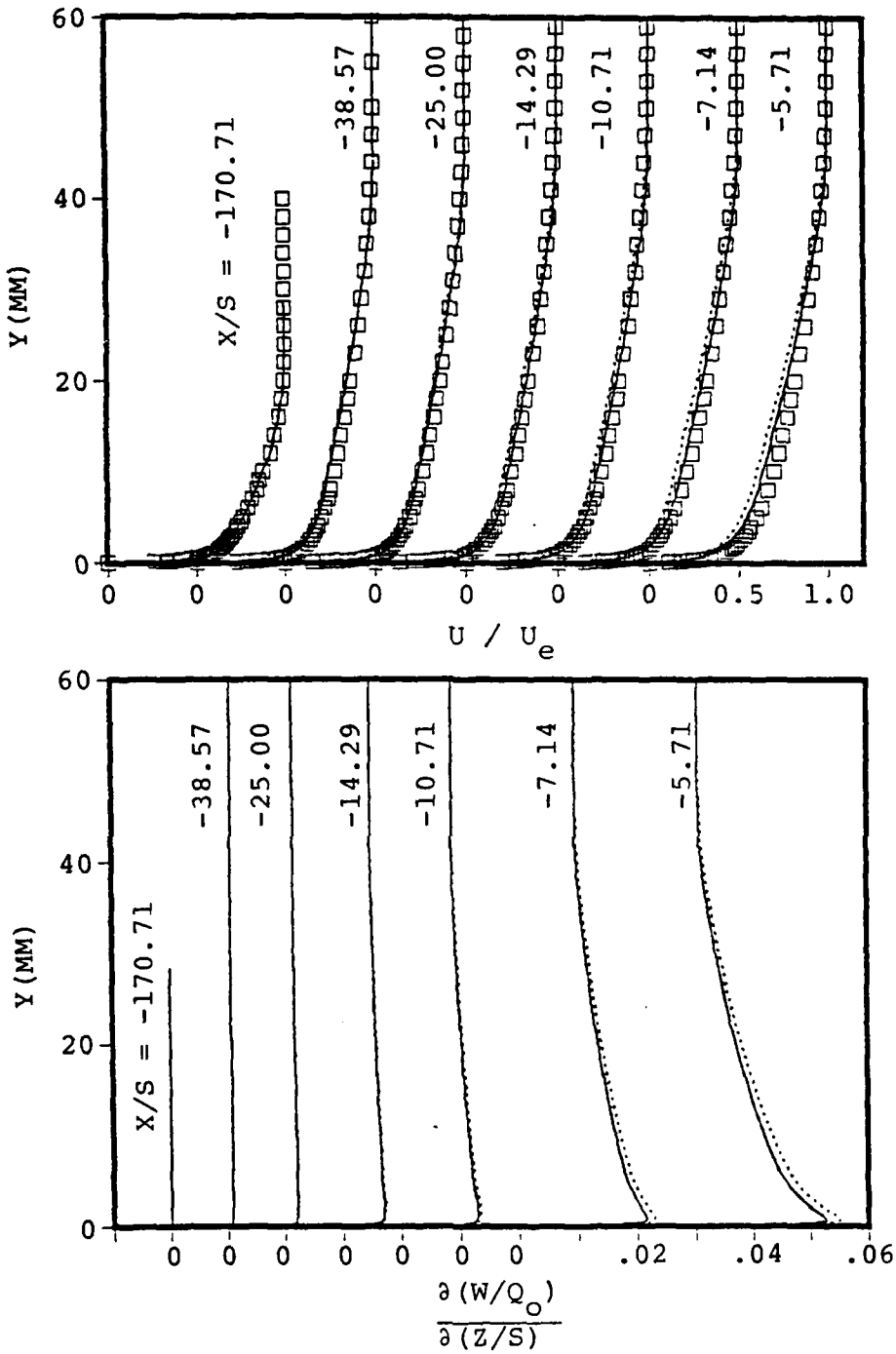

Figure 23. Predicted and measured velocity profiles of Krogstad's experiment. □ measurement, —— plane of symmetry flow(with experimental U_e), ... plane of symmetry flow(with potential U_e)

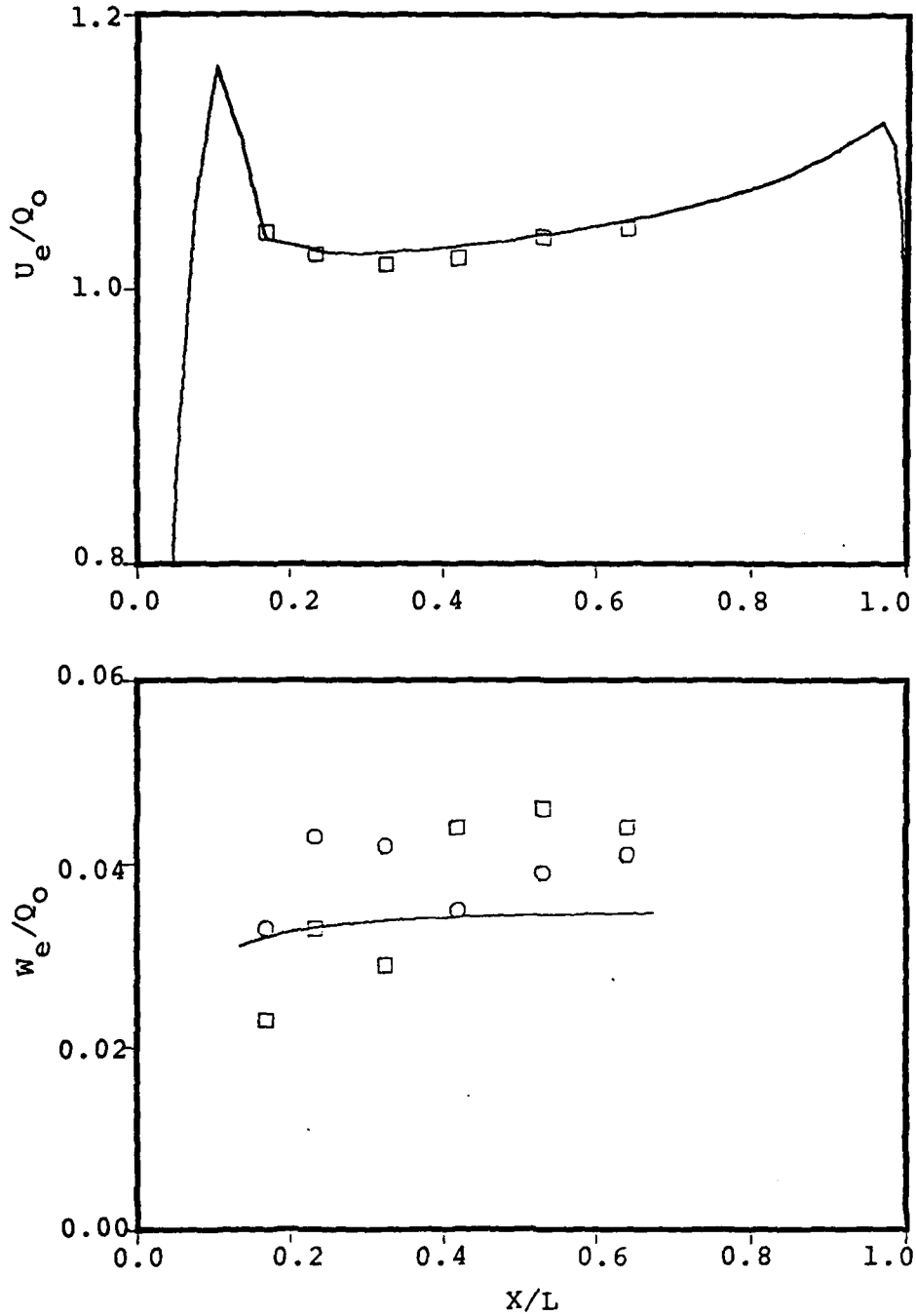

Figure 24. Boundary conditions on the windward plane on the combination body. Ue(——;potential flow, □;experiment), We(——;potential flow, □; $\theta=-4^{\circ}$, o; $\theta=4^{\circ}$)

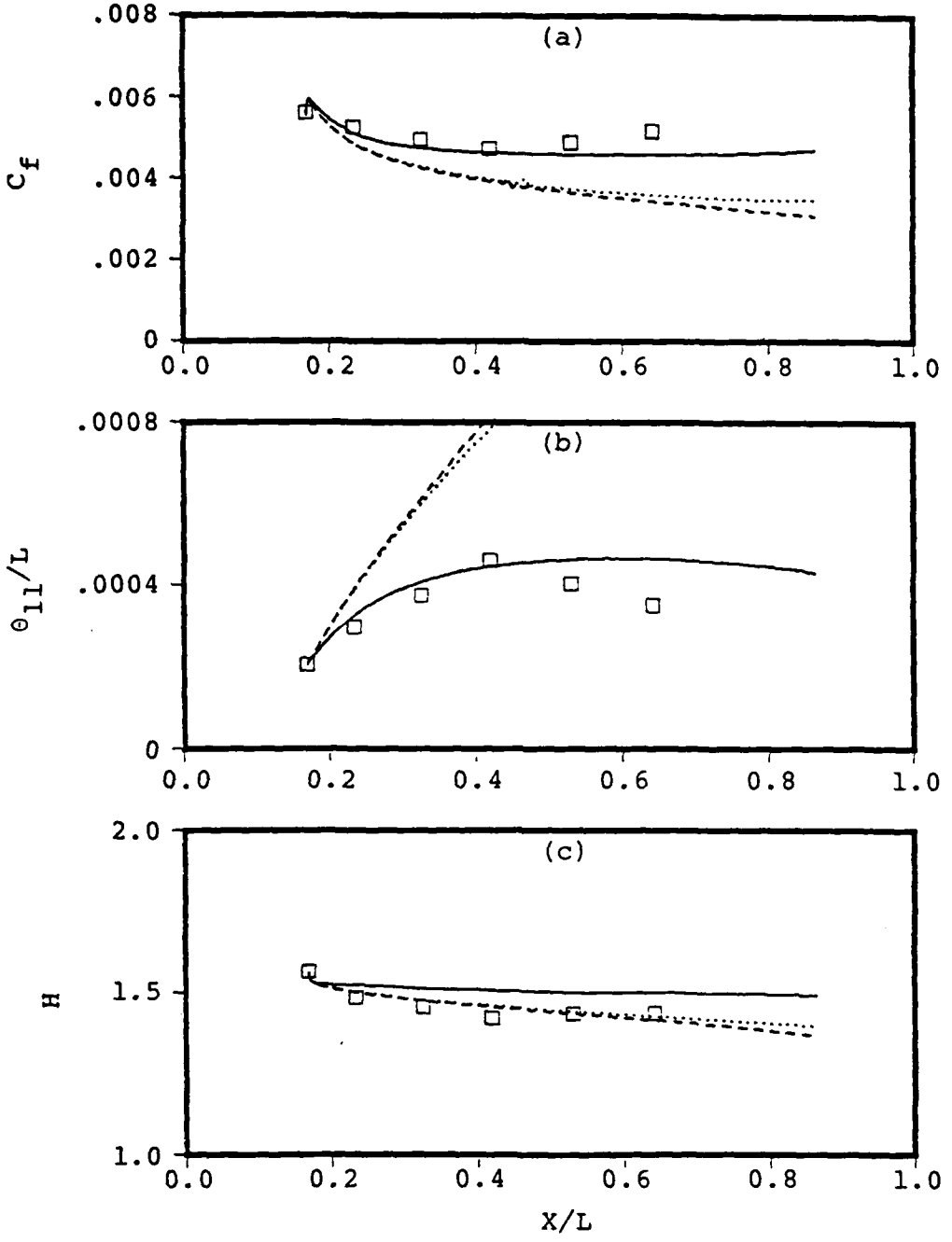

Figure 25. Predicted and measured integral parameters on the windward plane of the combination body. □ measurement, —— plane of symmetry flow, ... 2-D flow, --- axisymmetric flow.

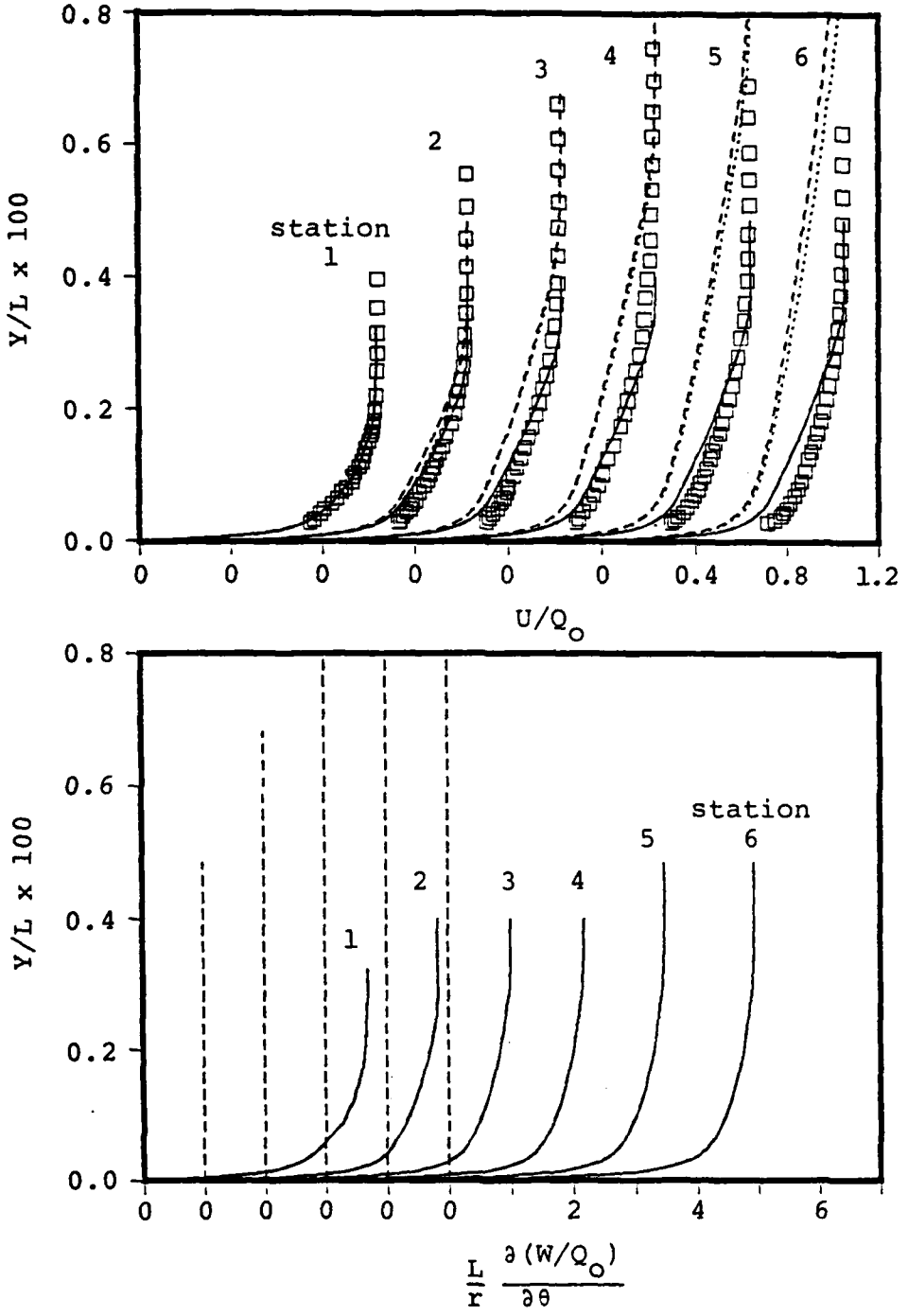

Figure 26. Velocity profiles on the windward plane of the combination body. Yaw-probe measurement; □ measurement, —— plane of symmetry flow, ... 2-D flow, --- axisymmetric flow.

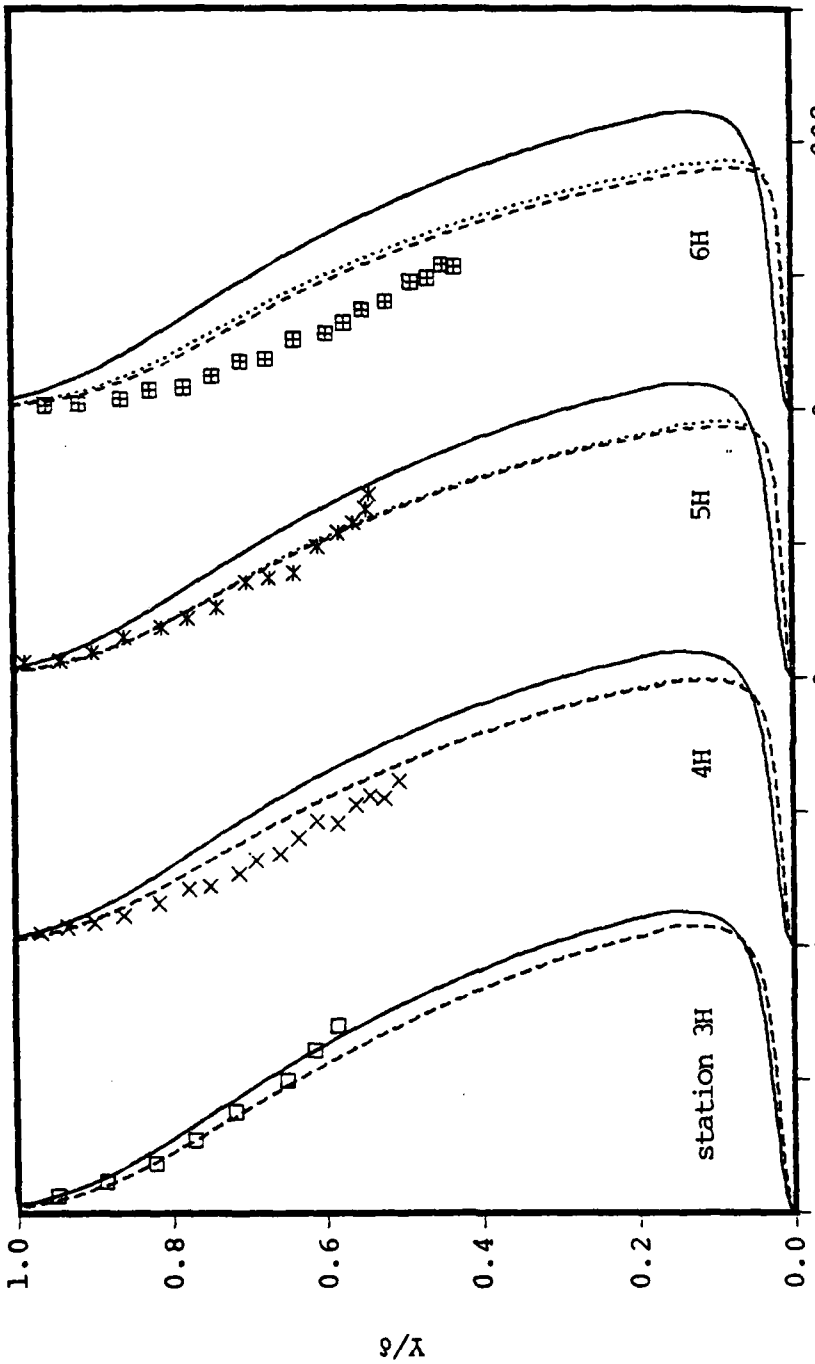

Figure 27. Reynolds-stress profiles on the windward plane of the combination body. symbols;experiment, ——;plane of symmetry flow, ...;2-D flow, ---;axisymmetric flow

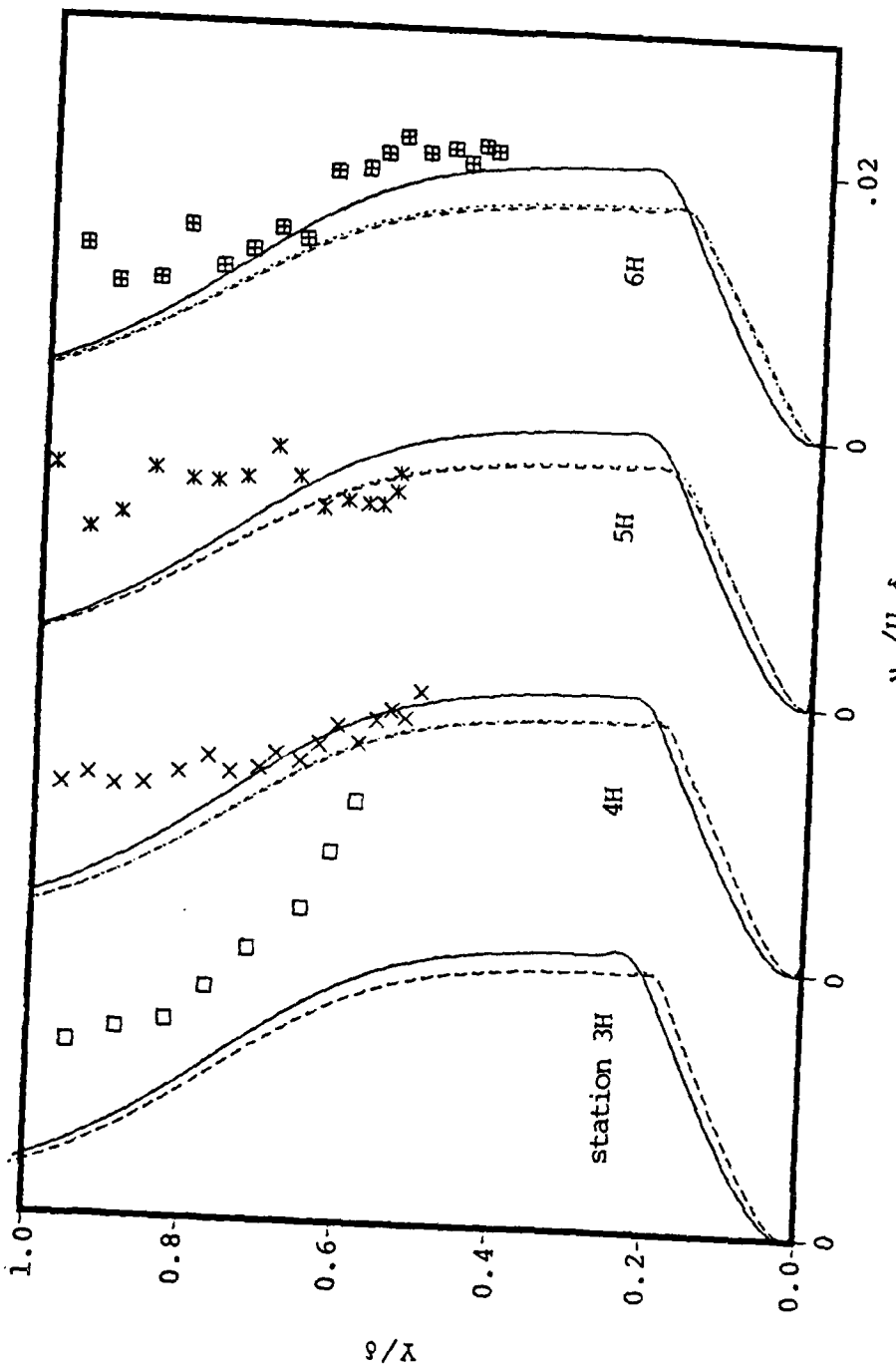

Figure 28. Eddy-viscosity profiles on the windward plane of the combination body. symbols;measurement, ——;plane of symmetry flow, ····;2-D flow, – – –;axisymmetric flow. (using Cebeci's model)

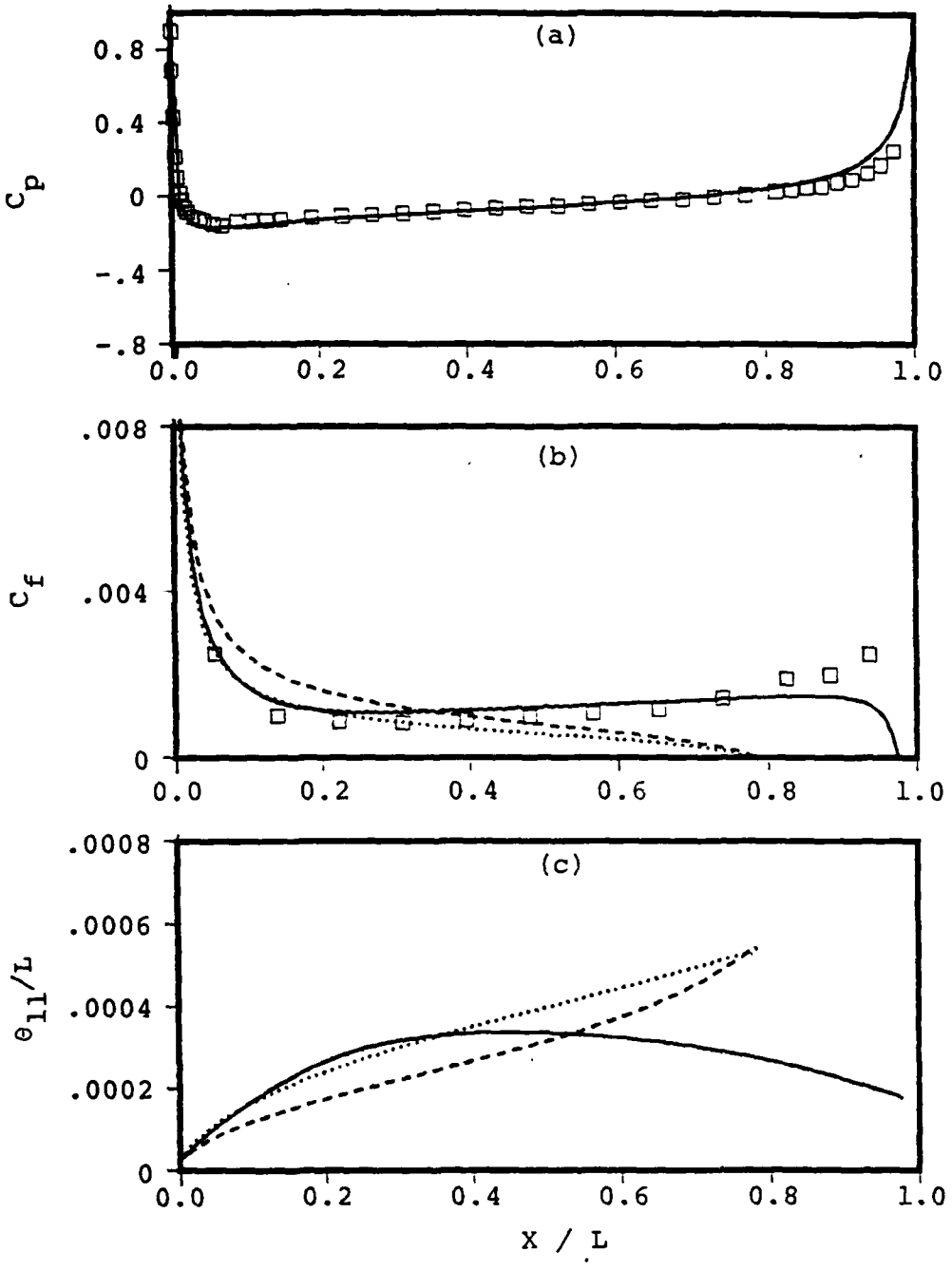

Figure 29. Comparison of predictions with the experimental results on the 6:1 spheroid, leeward plane, $\alpha = 10^{0}$, Re = 1.6 x 10^{6}. —— plane of symmetry flow, ... 2-D flow, --- axisymmetric flow

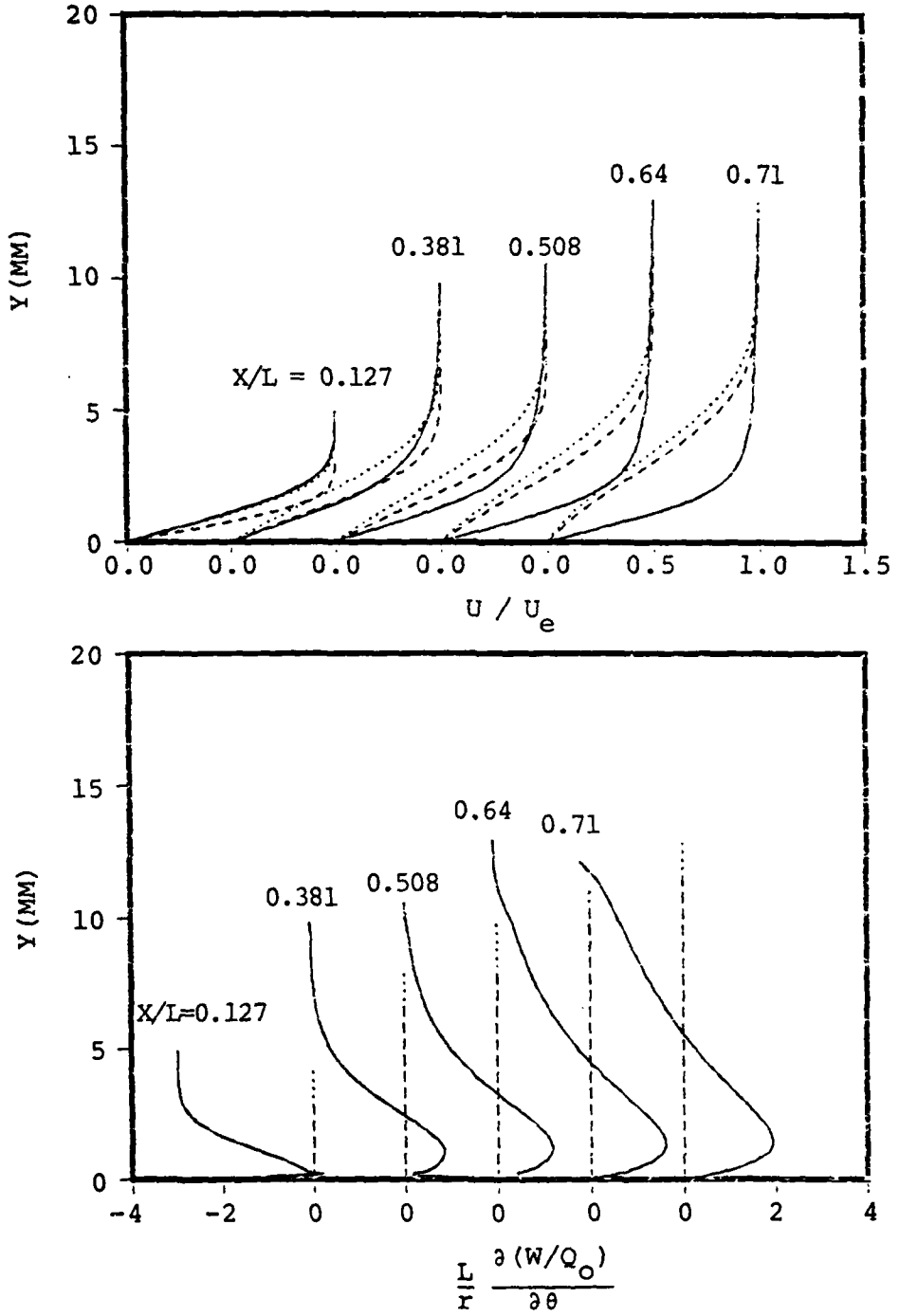

Figure 30. Predicted velocity profiles on the leeward plane of the 6:1 spheroid, $\alpha = 10^{\circ}$, Re = 1.6×10^{6}. —— plane of symmetry flow, ... 2-D flow, --- axisymmetric flow.

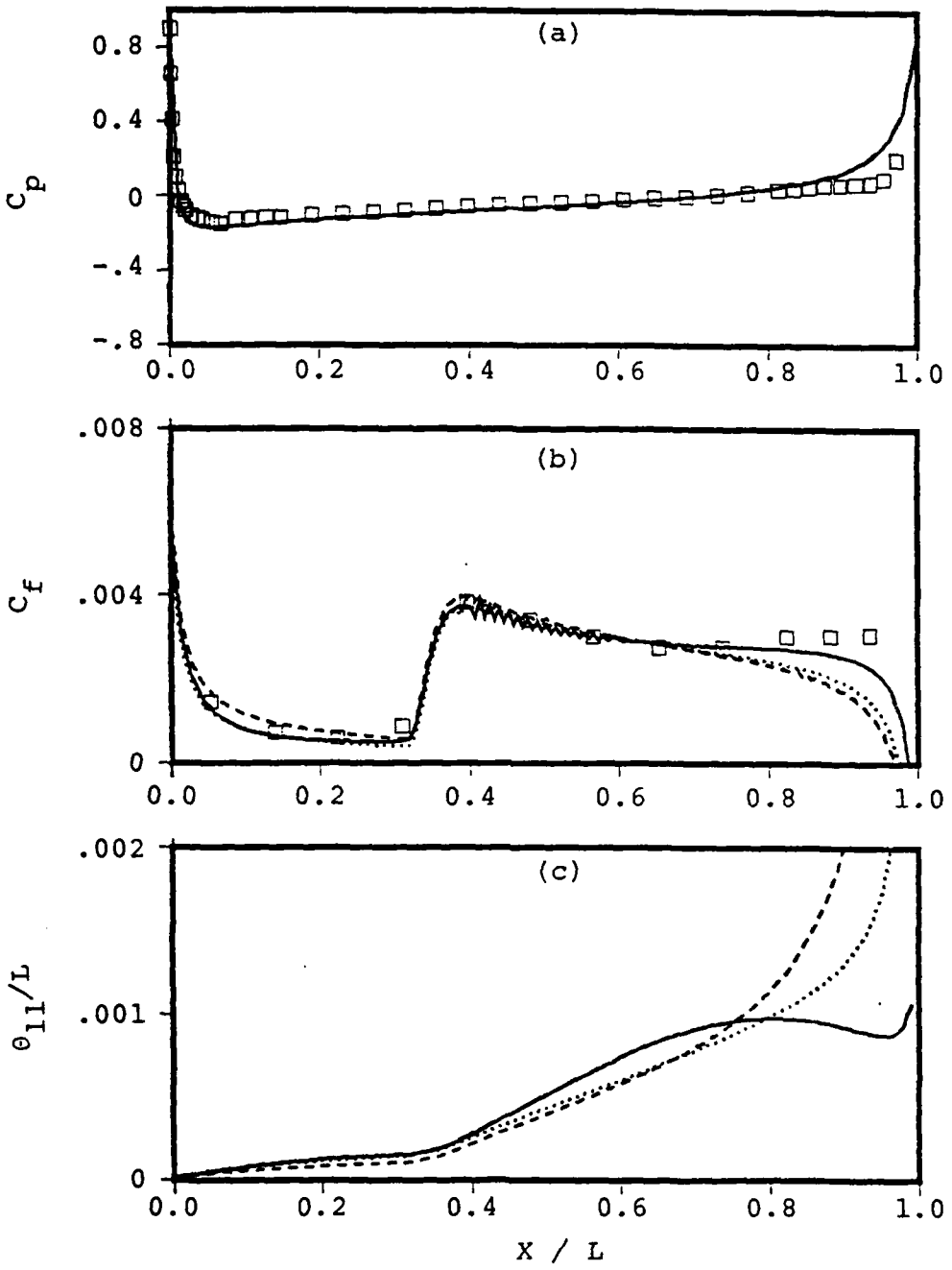

Figure 31. Comparison of predictions with the experimental results on the 6:1 spheroid, leeward plane, $\alpha = 10^{\circ}$, Re = 7.2 x 10^6. —— plane of symmetry flow, ... 2-D flow, --- axisymmetric flow.

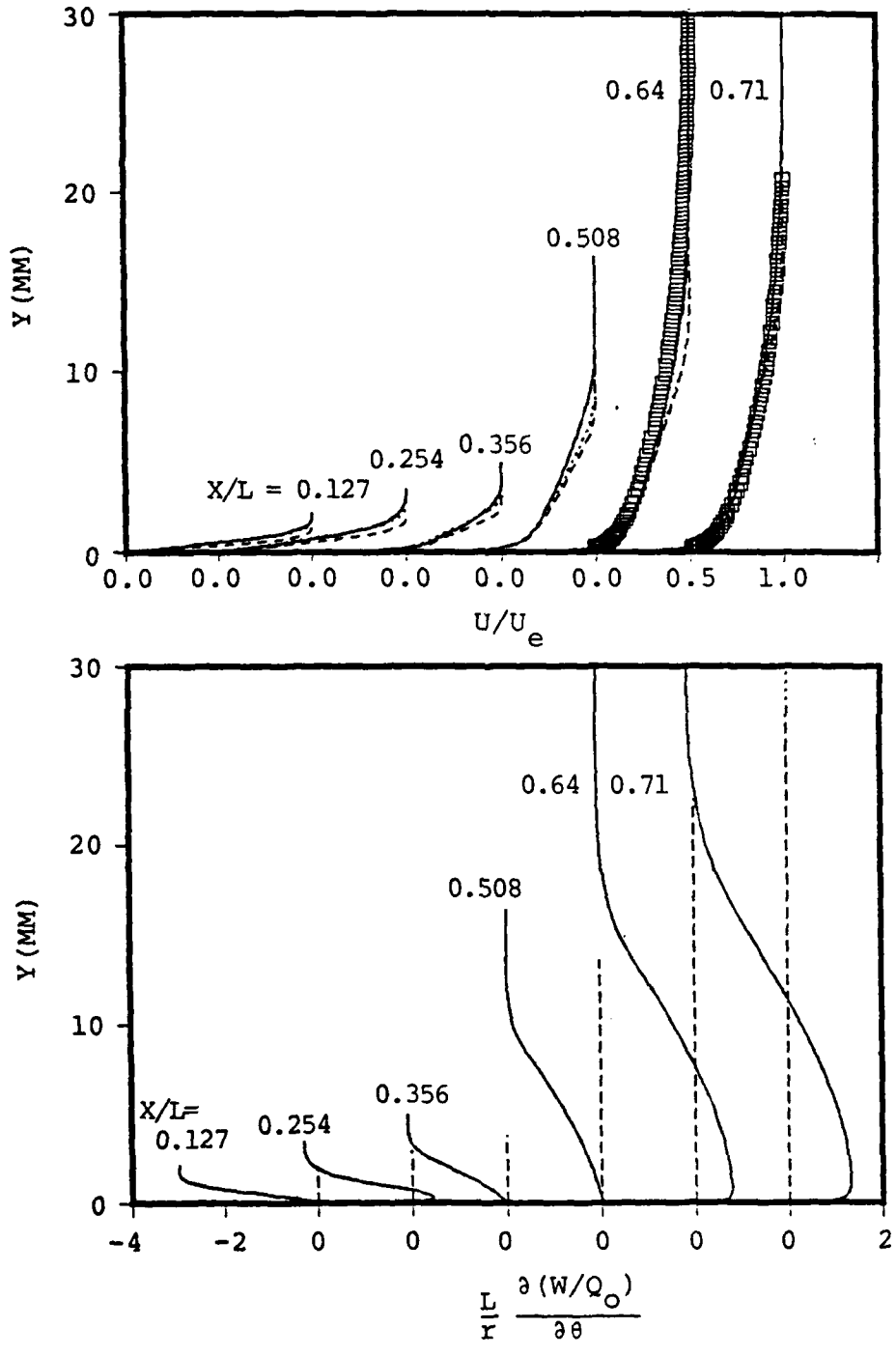

Figure 32. Velocity profiles predicted and measured on the 6:1 spheroid, windward plane, $\alpha = 10^{\circ}$, Re = 7.2×10^{6}. —— plane of symmetry flow, ... 2-D flow, --- axisymmetric flow, □ measurement.

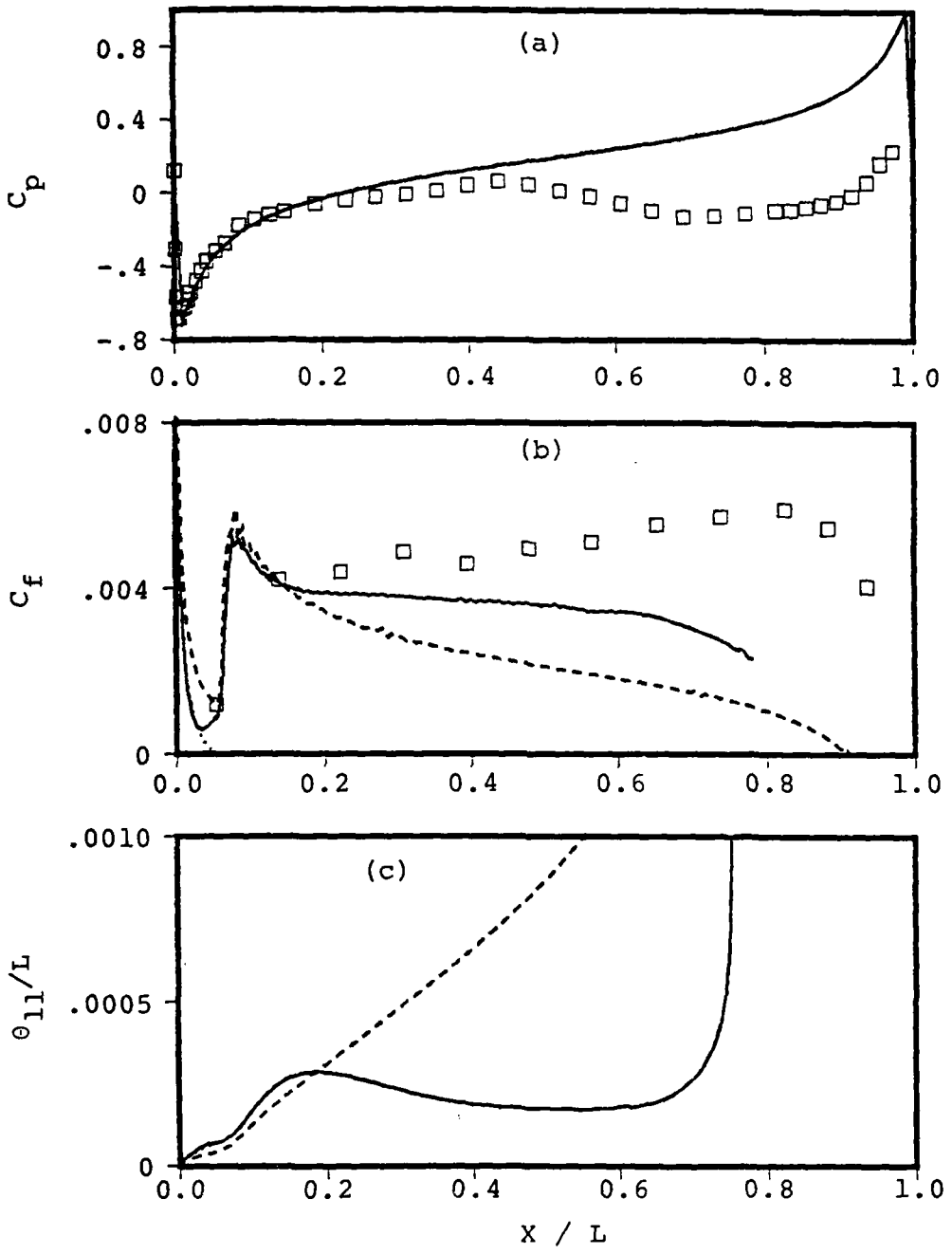

Figure 33. Comparison of predictions with the experimental results on the 6:1 spheroid, leeward plane, $\alpha = 30^{\circ}$, $Re = 7.2 \times 10^{6}$. —— plane of symmetry flow, ... 2-D flow, --- axisymmetric flow.

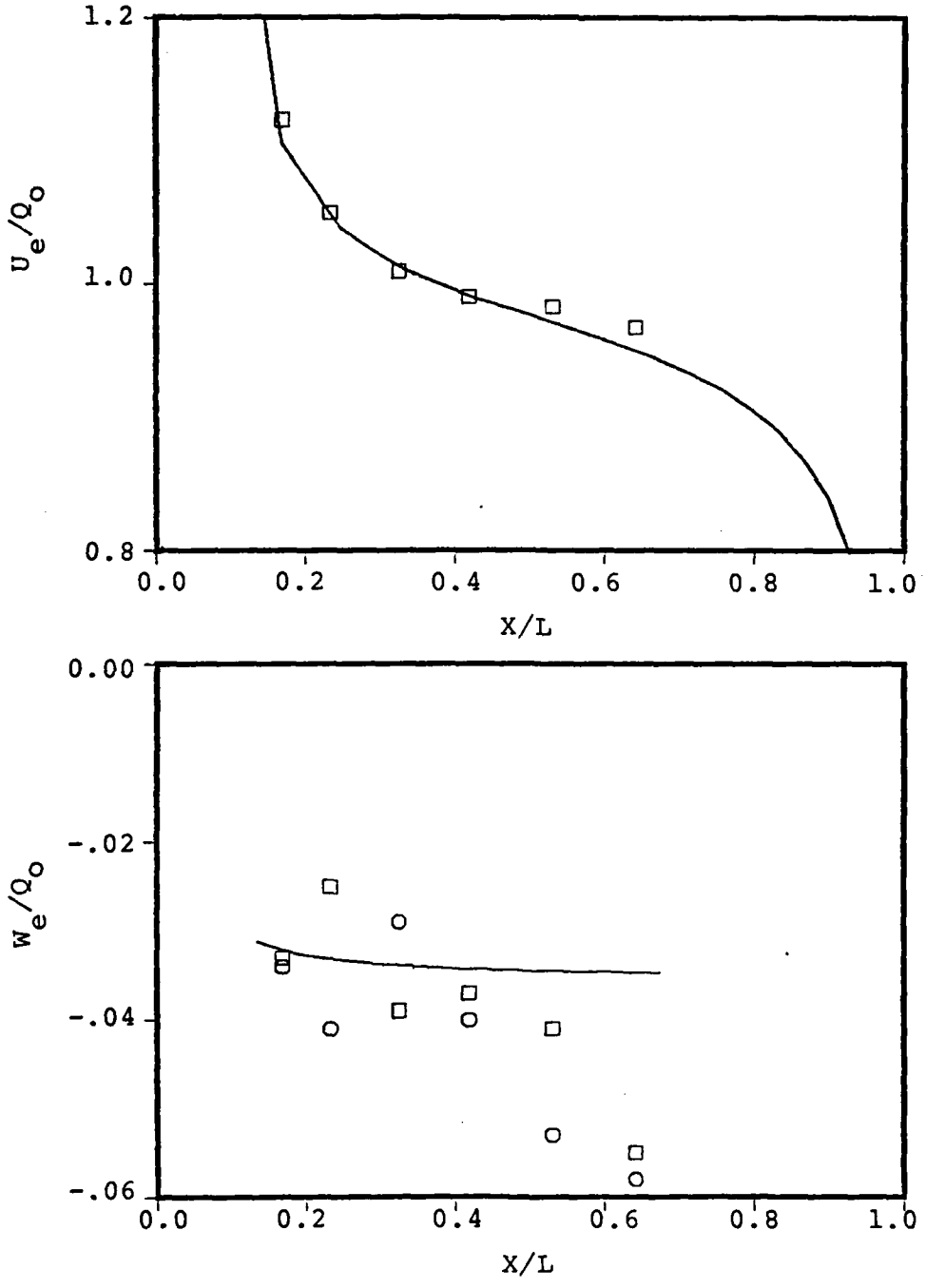

Figure 34. External flow conditions on the leeward side of the combination body. Ue(——;potential flow, □;experiment), We(——;potential flow, □; θ=176° o; θ=184°)

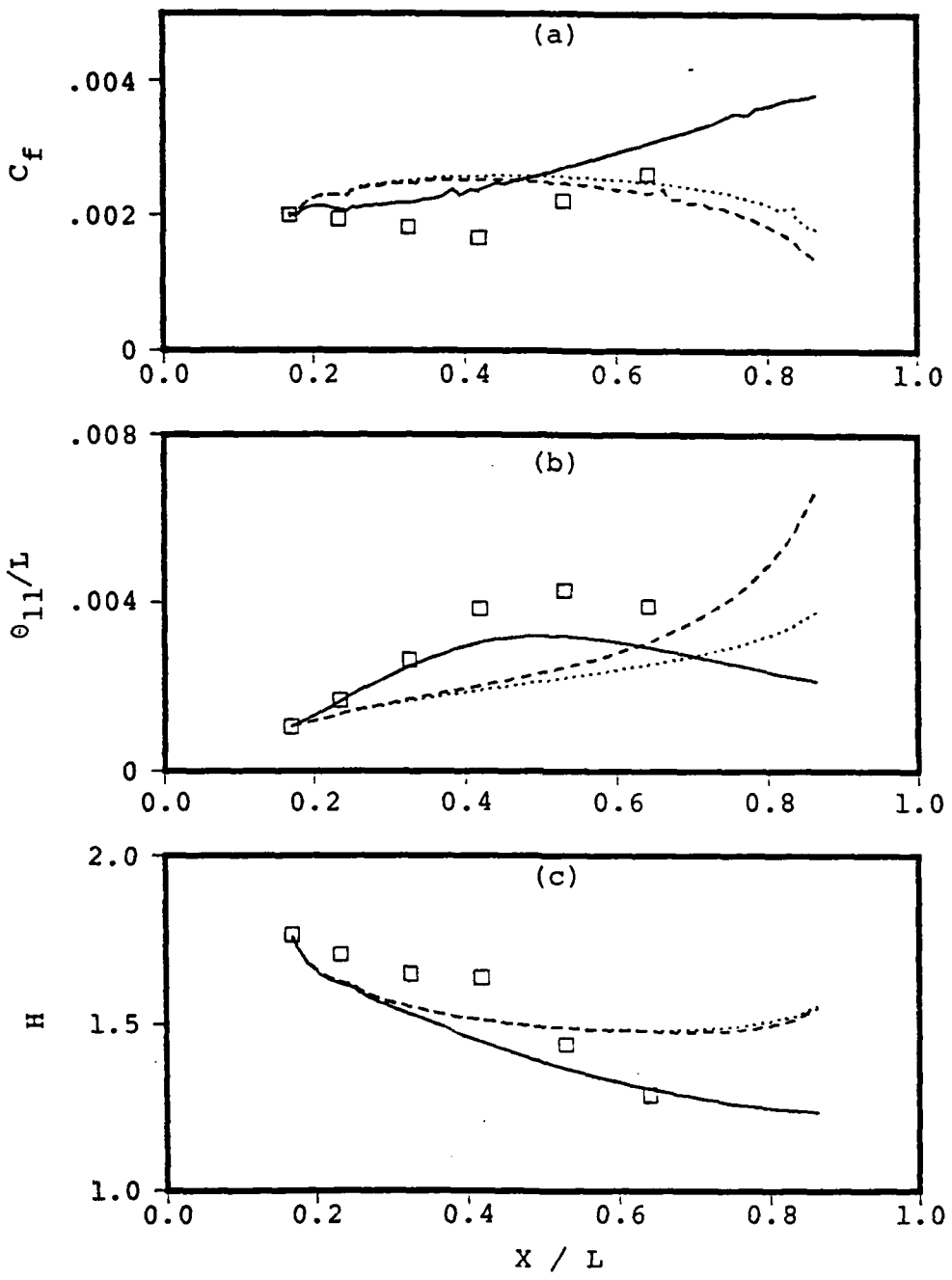

Figure 35. Predicted and measured integral parameters on the leeward plane of the combination body. □ measurement, —— plane of symmetry flow, ... 2-D flow, --- axisymmetric flow.

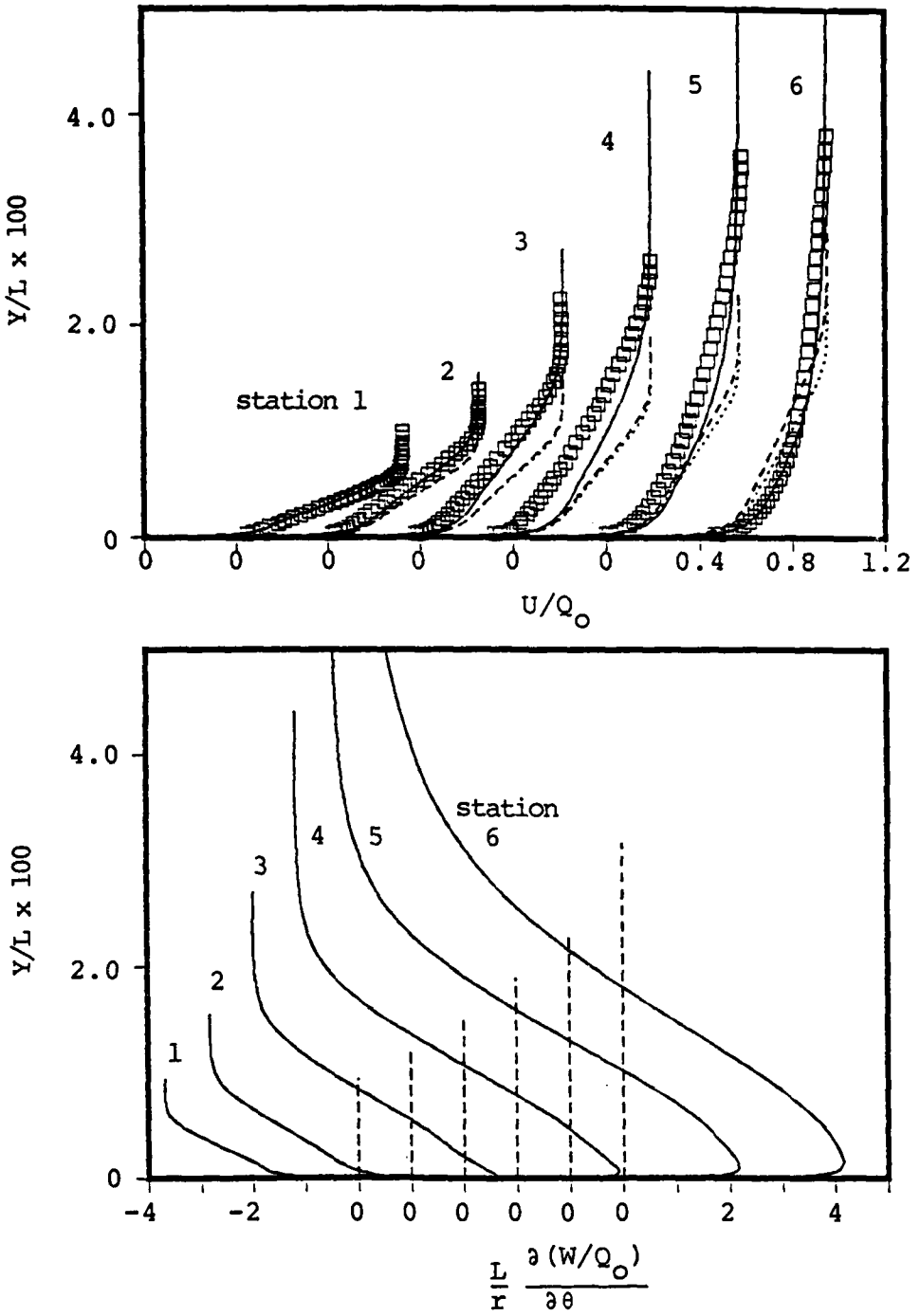

Figure 36. Velocity profiles on the leeward plane of the combination body. Yaw-probe measurement, □ measurement, —— plane of symmetry flow, ... 2-D flow, --- axisymmetric flow.

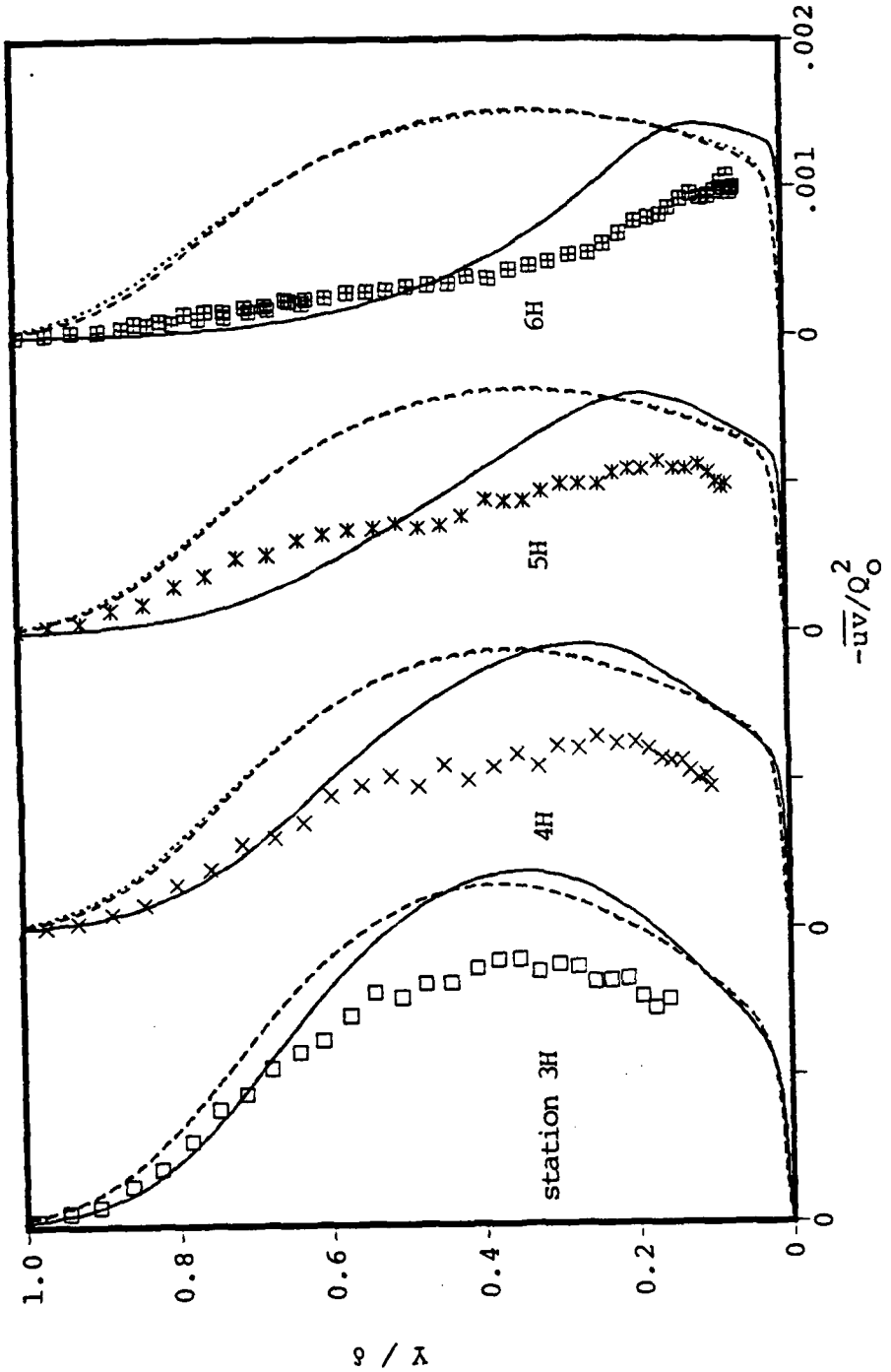

Figure 37. Reynolds stress profiles on the leeward plane of the combination body. symbols;experiment, ——;plane of symmetry flow, ...;2-D flow, --;axisymmetric flow.

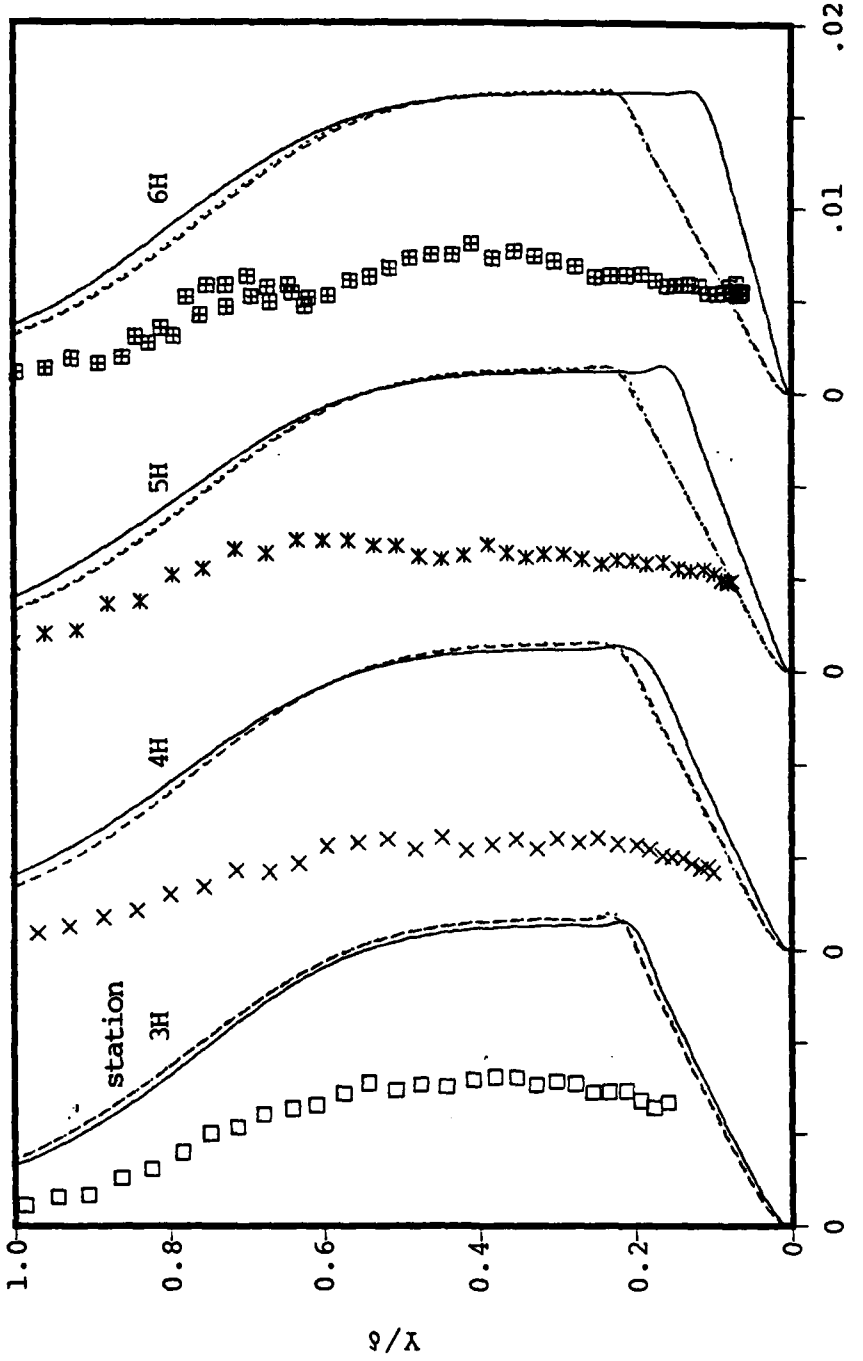

Figure 38. Eddy-viscosity profiles on the leeward plane of the combination body. symbols;measurement, ——;plane of symmetry flow, ····;2-D flow, – – –;axisymmetric flow (using Cebeci's model)

END

FILMED

10-84

DTIC